

## Short communication

# Selective deficits in attentional set-shifting in mice induced by maternal immune activation with poly(I:C)

Kristyna Maleninska<sup>a,b,d,1</sup>, Martina Janikova<sup>a,c,1</sup>, Dominika Radostova<sup>a</sup>, Iveta Vojtechova<sup>a,d</sup>, Tomas Petrasek<sup>a,d</sup>, Denisa Kirdajova<sup>e</sup>, Miroslava Anderova<sup>e</sup>, Jan Svoboda<sup>a</sup>, Ales Stuchlik<sup>a,\*</sup>

<sup>a</sup> Laboratory of the Neurophysiology of Memory, Institute of Physiology of the Czech Academy of Sciences, Videnska 1083, Prague 14220, Czech Republic

<sup>b</sup> Faculty of Science, Charles University, Prague, Czech Republic

<sup>c</sup> First Faculty of Medicine, Charles University, Prague, Czech Republic

<sup>d</sup> National Institute of Mental Health, Topolova 748, Klecany, Czech Republic

<sup>e</sup> Institute of Experimental Medicine of the Czech Academy of Sciences, Videnska 1083, Prague 14220, Czech Republic

## ARTICLE INFO

## Keywords:

Immunochallenge

Poly(I:C)

Maternal immune activation

Cognitive deficit

Schizophrenia

Behavioral tests

Mouse

Interneurons

Prenatal infection

## ABSTRACT

Maternal immune activation has been identified as a significant risk factor for schizophrenia. Using rodent models, past work has demonstrated various behavioral and brain impairments in offspring after immune-activating events. We applied 5 mg/kg of poly(I:C) on gestation day 9 to pregnant mouse dams, whose offspring were then stressed during puberty. We show impairments in attentional set-shifting in a T-maze, and a decreased number of parvalbumin-positive interneurons in the hippocampus as a result of peripubertal stress specifically in females.

## 1. Introduction

**Prenatal exposure to maternal infection** is a risk factor of neurodevelopmental diseases such as schizophrenia [1]. Based on epidemiological studies, maternal immune activation (MIA), sometimes combined with genetic [2] or environmental factors [3], has been established as an animal model of neurodevelopmental disorders [4]. Polyinosinic:polycytidylic acid – or poly(I:C) – is a synthetic analog of double-stranded RNA mimicking viral infection. When administered to pregnant rodent dams, it causes the release of pro-inflammatory cytokines (e.g. interleukin-6; IL-6; reviewed in [4]). The cytokine imbalance then induces maternal inflammation, followed by postnatal brain and behavior pathologies in the offspring. The offspring of poly(I:C)-exposed mothers develop a spectrum of behavioral symptoms, including deficits in sensorimotor gating, latent inhibition and social interaction, and an increased sensitivity to amphetamine (reviewed in [4]). However, some studies have not observed all these behavioral changes (e.g. [5]). Differences in timing and duration of MIA exposure, dose, caging and other factors alter the experiment outcomes and manifestation of different

symptoms (reviewed in [6]). We predicted that tests of executive functions such as attentional set-shifting would show higher sensitivity than less complex tasks such as simple working memory tests. Notably, in schizophrenia patients, set-shifting deficits are one of the most consistent findings [7]. Cortical GABAergic interneurons support cognitive processes including attentional set-shifting (e.g. [8]). Attentional set-shifting is known to heavily rely on correct hippocampal-prefrontal communication [9]. In schizophrenia, the population of interneurons expressing parvalbumin; PV (parvalbumin-positive interneurons; PVIs) exhibits many abnormalities [10]. PVI alterations have been found in adult poly(I:C) offspring mainly in the hippocampus [11].

Our study tested attentional set-shifting performance and other behavioral alterations and changes in the numbers of PVIs related to the MIA model induced by poly(I:C) in C57BL/6N mice. In addition to the prenatal immunochallenge, we exposed the offspring to periadolescent stress, forming a two-hit model as proposed by Giovanoli [3,11]. Such a model has never been tested in an attentional set-shifting task.

\* Correspondence to: Institute of Physiology of the Czech Academy of Sciences, Videnska 1083, Prague 14220, Czech Republic.

E-mail address: [Ales.Stuchlik@fgu.cas.cz](mailto:Ales.Stuchlik@fgu.cas.cz) (A. Stuchlik).

<sup>1</sup> First two authors (K.M. and M.J.) contributed equally.

## 2. Materials and methods

C57BL/6N (Charles River) mice were housed in pairs or triplets in individually-ventilated cages (IVC, 39.1 × 19.9 × 16 cm) in an animal room with stable temperature, humidity and 12/12 cycle (light off at 6AM). After ten days of acclimatization, female mice (N = 16) were timed-mated, and at gestational day (GD) 9 subjected to a single subcutaneous application of poly(I:C) (potassium salt, Tocris) at a dose of 5 mg/kg (injection volume of 1 ml/kg) or vehicle control (sterile 0.9% NaCl, 1 ml/kg). Offspring were weaned and sexed at postnatal day (PD) 21. They were kept in the IVC system until adulthood (approximately 60 days of age) and transferred to standard open cages (26 × 20.5 × 13.5 cm) one week before the start of behavioral testing. Both male (N = 15) and female (N = 21) offspring were used for behavioral experiments and quantification of PVIs in the hippocampus. All experiments were approved by local Animal Care Committees (Projects of Experiments No. 87/2019; 50/2017; 80/2016) and complied with the Animal Protection Code of the Czech Republic and with EU legislation (2010/63/EU).

### 2.1. Verification of cytokines (IL-6)

IL-6 levels were measured in six non-pregnant female mice sacrificed 3 h after the application of poly(I:C) (5 mg/kg) or saline (controls). Mice were anesthetized with isoflurane and blood was collected by cardiac puncture into an anticoagulant-containing tube. Samples were centrifuged at 2500 g, 4 °C for 10 min and separated plasma was used for further analysis. A mouse IL-6 ELISA kit (Sigma-Aldrich, RAB0308) was performed according to the manufacturers' instructions.

### 2.2. Peripubertal stress

Half of the pups (N = 19) underwent mild chronic stress every other day between PD 30 and 40 according to the protocol described in [3]. Briefly, five different stressors were used: three mild shocks (0.3 mA, PD 30), restraint stress for 45 min (PD 32), water deprivation for 16 h (PD 34), two one-minute long forced swimming sessions (PD36) and repeated changes of home cages during the dark phase of the light/dark cycle (PD38). Mice in the control group (N = 17), which did not undergo the stress protocol, were taken out of the cage and briefly handled (15 s) by the same experimenter.

### 2.3. Elevated plus maze

An elevated plus maze (EPM) was used for the assessment of anxiety according to a previously described protocol [12]. The behavior of mice was recorded for 5 min by a camera mounted above the maze. Videos were analyzed manually in BORIS software. The number of entries and total time spent in open arms, closed arms and the central area were calculated.

### 2.4. Open field and sensitivity to amphetamine

We then subjected the mice to testing of spontaneous activity and locomotor sensitization to amphetamine. Mice were tested in a square white Plexiglas apparatus (50 × 50 cm) in two daily sessions. On the first day, mice were injected with saline solution and placed into the maze for 30 min to assess locomotion. 24 h later, they were injected with amphetamine (D-amphetamine sulfate, Sigma-Aldrich; 2.5 mg/kg, subcutaneously) and immediately placed into an open-field arena (90 min) to monitor the locomotor response to amphetamine. Both sessions were recorded and analyzed with an Ethovision system (Noldus, Wageningen, The Netherlands).

### 2.5. Set-shifting task

Set-shifting was tested in a non-transparent, white plus maze with

enclosed arms and one arm blocked by a removable wall, creating a T-maze with the possibility to block different arms across trials. Mice underwent a spatial version of set-shifting based on switching between egocentric and allocentric navigation, as described in [13]. Prior to the experiment, animals were food restricted and kept at 95% of their original body weight until the last experimental session. Condensed milk in water (50:50) was used as a reward and mice were familiarized with this before the experiment. The whole procedure consisted of one habituation session and 10 experimental sessions: five sessions of learning in the egocentric condition and five sessions of the allocentric condition (with a switch on day 6). During the habituation session, small plastic containers with condensed milk were placed in each arm and animals were allowed to freely explore the whole maze for 15 min. The first experimental session started the next day. Colorful geometrical shapes that served as visual cues were attached above each arm and arms were marked according to cardinal points (N = north, S = south, E = east, W = west) (Fig. 1). Each session consisted of 20 trials. In the egocentric condition, mice were placed into the S-arm and the N-arm in a pseudorandom order, and trained to make a left turn to find a reward hidden at the end of the E or the W arms. In the allocentric condition, mice again started from the S and the N arms, but the reward was always hidden in the E-arm. In order to avoid the possibility of mice navigating by the aroma of the milk, we put a small drop of condensed milk on the wall of both correct and incorrect arms. The results were calculated as the % of incorrect trials from each session for both parts. For the second part, never-reinforced (old information) and perseverative (new information) errors were also calculated, because one of the allocentric conditions required the animal to turn left as in the egocentric part (never-reinforced errors) and the other one demanded turning to the right (perseverative errors).

### 2.6. Prepulse inhibition

Prepulse inhibition of the startle reflex (PPI) is considered to be a measure of sensorimotor gating and early information processing, and its impairment has been repeatedly described in schizophrenia [14]. In our study, we adapted the protocol described in [15]. Animals were tested in an acoustic startle response chamber (Coulbourn Habitest, Pennsylvania, USA). The percent difference between prepulse-pulse and pulse-alone trials was counted for each animal and each intensity according to the formula: (startle response to pulse alone – startle response to prepulse-pulse)/startle response to pulse-alone) × 100.

### 2.7. Immunohistochemistry

Immunohistochemistry and brain preparations were done as described earlier in [16]. A rabbit PV antibody (1:1000, Abcam, ab11427) was used as the primary antibody and an Alexa Fluor Plus 555 antibody (1:1000, Invitrogen, A32732) as a secondary antibody. PVIs in the CA1, CA2, CA3 and dentate gyrus of the hippocampus were counted, and the size of the areas measured on a BX53 microscope (Olympus, Japan). Analyzed sections ranged from –1.36 to –2.36 relative to bregma.

## 3. Statistical analyses

All data were analyzed in IBM SPSS software. IL-6 plasma concentrations were analyzed with an independent samples *t*-test. A general linear model (GLM) with repeated measures (RM) was used for the set-shifting task data, with day, treatment, stress and sex as factors. Next, a two-way RM ANOVA and the independent samples *t*-test (new *p*-value after Bonferroni correction = 0.0125) were used. The EPM and open-field test were analyzed with three-way ANOVA. MANOVA and two- or three-way ANOVA were used for data from PPI and the number of PVIs.

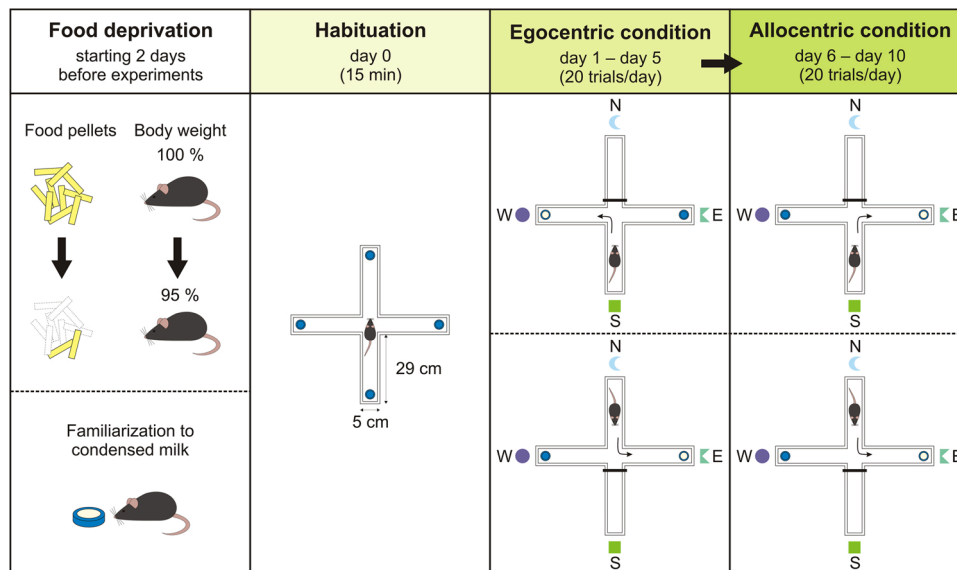


Fig. 1. Schematic illustration of set-shifting procedure and apparatus.

## 4. Results

### 4.1. IL-6 verification

IL-6 levels were high in mice injected with poly(I:C) but below detection levels in controls ( $t(5) = 34.7$ ,  $p < 0.001$ , saline: mean =  $-3.25$ , poly(I:C): mean =  $228$  pg/ml). See Fig. S1 in Supplementary Results.

### 4.2. Behavioral tasks

In the set-shifting test, GLM with RM revealed a significant interaction of day and group in the first, egocentric condition ( $p = 0.03$ ). The subsequent independent samples  $t$ -test showed significantly better performance of the control group compared to the poly(I:C) group on day 4 ( $p = 0.008$ ). In the second, allocentric part of the set-shifting test, GLM with RM revealed a significantly lower number of errors during re-learning of the condition for all animals ( $p < 0.001$ ). Next, we compared interactions of day, group, sex and stress for the never-reinforced errors on day 6 to day 10. GLM with RM showed a significant interaction of day, group and sex ( $p = 0.006$ ). Two-way RM ANOVA revealed a significant interaction for day and group for both males ( $p = 0.004$ ) and females ( $p = 0.006$ ). However, only poly(I:C) males had significantly more never-reinforced errors on day 6 (independent samples test;  $p = 0.001$ ). Lastly, we compared interactions of day, group, sex and stress for the perseverative errors on day 6 to day 10. GLM with RM revealed a significant interaction of day and group ( $p = 0.003$ ). On day 6, poly(I:C) animals were significantly worse than the control group (independent samples test;  $p < 0.001$ ). For complete results see Fig. 2 and Tables S1 and S2 in Supplementary Results. In the elevated plus maze test, open field test with amphetamine challenge and PPI, we found no effects of treatment, stress, sex or their interaction. For complete results see Tables S3–S6 in Supplementary Results.

### 4.3. Immunohistochemistry

Regarding the numbers of PVIs, we found significant effects of stress ( $p = 0.026$ ), sex ( $p = 0.007$ ) and their interaction ( $p = 0.002$ ) on the number of PVIs in the dorsal hippocampus. Further analysis confirmed the significant effects of sex ( $p = 0.003$ ), stress ( $p = 0.012$ ), the treatment\*stress interaction ( $p = 0.03$ ) and the sex\*stress interaction ( $p = 0.005$ ) in CA1, significant effect of sex in CA3 ( $p = 0.047$ ) and the

sex\*stress interaction in CA2 ( $p = 0.023$ ). However, post hoc comparisons of sex and stress in CA2 have shown no significant effect. Next, a significant effect of stress ( $p = 0.048$ ) was found in female, but not in male mice. Female mice stressed in periadolescence had significantly lower numbers of PVIs in CA1 compared to non-stressed female mice ( $p = 0.003$ ). This suggests that control female mice had higher numbers of PVIs than stressed females, while males showed similar numbers of PVIs as stressed females. The effect of poly(I:C) treatment was not significant and the size of hippocampus fields did not differ between groups. For complete results see Fig. 3 and Tables S7–S11 in Supplementary Results.

## 5. Discussion

This study examined the two-hit model proposed by Giovanoli et al. [3,11] in a behavioral battery followed by immunohistochemical staining of PVIs. Impaired set-shifting in mice offspring whose mothers underwent treatment with 5 mg/kg poly(I:C) on GD 9 was found with no other behavioral deficits. On the last day (day 5) of the egocentric condition, we found no between-group differences. Contrary to this finding, on the first day (day 6) of the allocentric condition (i.e. the re-learning condition) we observed significantly fewer perseverative errors (new information) in poly(I:C) offspring and a higher number of never-reinforced (old information) errors in poly(I:C) males compared to control animals. This is in line with the repeatedly-described alterations in cognitive flexibility in schizophrenia patients [17]. While we are the first to show effects of neurodevelopmental poly(I:C) on set-shifting in mice, a few studies have been conducted on rats, but with rather inconsistent results. Poly(I:C) rats were initially found to either commit more perseverative [18] or regressive (late perseverative) errors [19]. Recently, this was questioned in [20], as they reported more regressive errors in controls than poly(I:C) rats. However, no rat study has found a deteriorating effect on never-reinforced errors. In terms of sex, our results correspond with the data in [18] where altered executive functions emerged mainly in males. Similarly in another study [21], male rats prenatally exposed to poly(I:C) had less correct responses in trial-unique nonmatching to location (TUNL) task (described in [22]), but no such deterioration was observed in female rats. Also, male rats had overall better performance in training phase of TUNL, but performed worse on reversal task compared to female rats [21]. It is therefore possible, that male rodents in MIA models are more susceptible to alterations in executive functions. However, the sex differences in

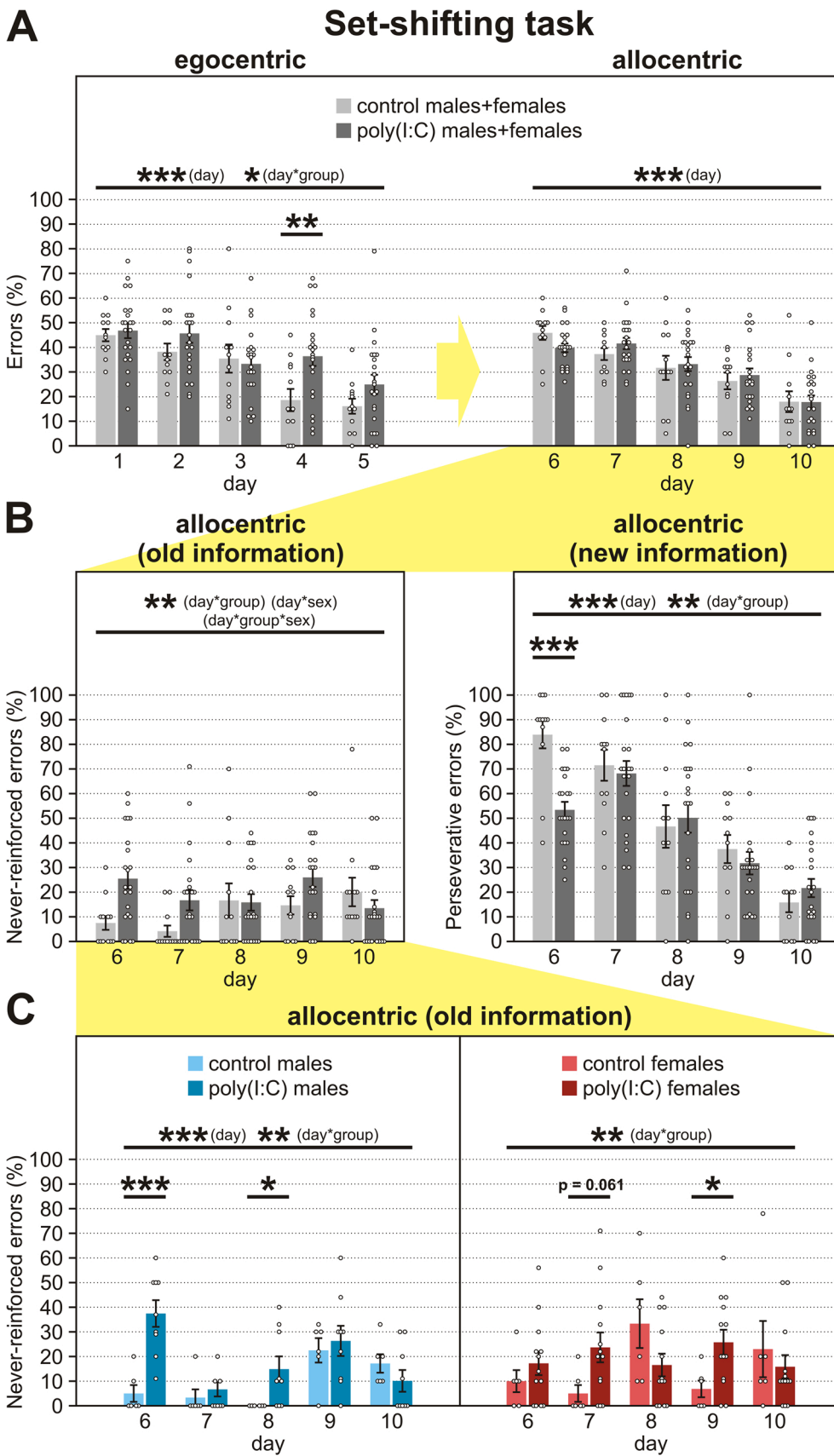


**Fig. 2.** Results from attentional set-shifting. A. Mice in the poly(I:C) group had significantly more errors on the 4th day of the egocentric condition. B. Mice in the control group had significantly more perseverative errors on the 1st day of the allocentric condition (6th day of experiment). C. Male mice in the poly(I:C) group had significantly more never-reinforced errors compared to the control group on the 1st and 3rd day of the allocentric condition (6th and 8th day of experiment). Female mice in the poly(I:C) group had significantly more never-reinforced errors on the 4th day of the allocentric condition (9th day of experiment). All data are presented as mean  $\pm$  SEM, \* $p < 0.05$ ; \*\* $p < 0.01$ ; \*\*\* $p < 0.001$ .



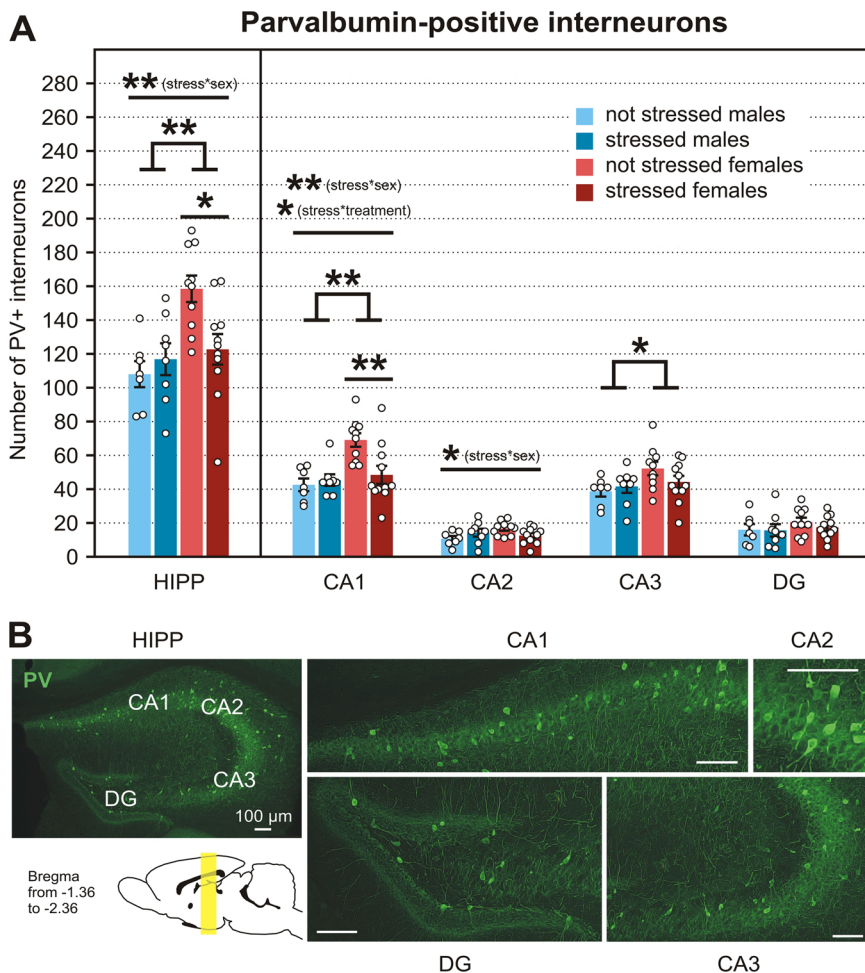


**Fig. 3.** Parvalbumin-positive interneurons (PVIs) in the dorsal hippocampus of adult mice. **A.** Non-stressed female mice in the control group had the highest number of PVIs. Particularly, female mice had significantly higher number of PVIs in the CA1 and CA3 regions compared to male mice. In the CA1 region, non-stressed female mice had significantly more PVIs compared to stressed female mice regardless of treatment group. **B.** Immunohistochemically stained PVIs in the hippocampus. Scale bars (for all images) = 100  $\mu\text{m}$ . CA = *Cornu Ammonis*; DG = dentate gyrus; HIPP = hippocampus; PV = parvalbumin. All data are presented as mean  $\pm$  SEM, \* $p < 0.05$ , \*\* $p < 0.01$ .

MIA models differs with diverse experimental design.

Surprisingly, we found no deficit in PPI, and no group differences in EPM, locomotion or amphetamine sensitivity in an open-field test. Although some authors have reported no changes in PPI [23], the majority have found decreased PPI in the offspring of poly(I:C) exposed mothers [24]. Similarly, elevated amphetamine sensitivity has often been described in the poly(I:C) group (reviewed in [15]), which corresponds to schizophrenia-related phenotype. We also found no significant effect of sex. Deficit in male, but not in female rats prenatally exposed to poly(I:C) has been described in PPI [25,26], while female rats had higher locomotion after acute sensitization with amphetamine [25]. The lack of significant differences between groups in our study might be mediated by housing conditions. Mice were housed in IVC until adulthood, which has been previously shown to mask behavioral changes in a genetic model of schizophrenia [27]. Mueller et al. [5] explored the difference between open caging and IVC systems directly in the poly(I:C) model. Poly(I:C) at a dose of 5 mg/kg caused a high number of abortions, and at a dose of 1 mg/kg no behavioral disruptions in IVC mice, while equal doses in open-cage-housed animals resulted in behavioral alterations. Since we only found a between-group difference in set-shifting, we hypothesize that set-shifting is a highly sensitive task with regards to prefrontal alterations and can uncover even subtle neurobiological disruptions.

We also found a significant effect of stress in females on the numbers of PVIs in the CA1 and CA3 regions of the hippocampus, but no effect of poly(I:C). This is in line with a study describing the effect of chronic stress on PVIs in all areas of the dorsal hippocampus, although in this case rats were subjected to stress for nine weeks [28]. In contrast, Giovanoli et al. (2013, [3]) found no effect of prenatal immune activation,

stress or their combination on the number of PVIs in the dorsal hippocampus. However, they used a 1 mg/kg dose of poly(I:C). Also, sex differences in the number of PVIs as a result of stress in periadolescence, may be underlined by the previously described role of sex steroid hormones and differential developmental trajectory of PVIs in the hippocampus of male and female mice [29].

To summarize, in a two-hit neurodevelopmental model of schizophrenia we found a selective deficit in an attentional set-shifting task, specifically in the first day after shifting the condition. The number of PVIs in the dorsal hippocampus was higher mainly in unstressed female mice compared to male and stressed female mice. Our results corroborate the face validity of this two-hit model in mice in the sense of set-shifting deficits. They also highlight the importance of factors such as caging and the timing of applications that can modify model outcomes.

#### CRediT authorship contribution statement

AS, MA, JS, MJ and KM conceived and designed the study. AS and MA obtained the financial support. KM, MJ, DR and DK performed the experiments. MJ and KM analyzed the data. IV prepared the figures. All authors actively participated on the manuscript preparation. All authors agreed on the final version of the manuscript.

#### Declaration of Competing Interest

The authors declare that they have no known competing financial interests or personal relationships that could have appeared to influence the work reported in this paper.

## Acknowledgments

The study was supported exclusively by the Czech Science Foundation (GACR) grant 19-03016S. We thank the Department of Auditory Neuroscience of the Institute of Experimental Medicine, for providing apparatus and custom made software for recording of PPI of ASR. We also thank Peter Ergang for assistance with IL-6 measurements, and Michaela Radostna and Jindrich Kalvoda for technical support.

## Appendix A. Supporting information

Supplementary data associated with this article can be found in the online version at [doi:10.1016/j.bbr.2021.113678](https://doi.org/10.1016/j.bbr.2021.113678).

## References

- [1] A.S. Brown, E.J. Derkits, Prenatal infection and schizophrenia: a review of epidemiologic and translational studies, *Am. J. Psychiatry* 167 (2010) 261–280, <https://doi.org/10.1176/appi.ajp.2009.09030361>.
- [2] T.V. Lipina, C. Zai, D. Hlousek, J.C. Roder, A.H.C. Wong, Maternal immune activation during gestation interacts with Disc1 point mutation to exacerbate schizophrenia-related behaviors in mice, *J. Neurosci.* 33 (2013) 54–7666, <https://doi.org/10.1523/JNEUROSCI.0091-13.2013>.
- [3] S. Giovanoli, H. Engler, A. Engler, J. Richetto, M. Voget, R. Willi, C. Winter, M. A. Riva, P.B. Mortensen, J. Feldon, M. Schedlowski, U. Meyer, Stress in puberty unmasks latent neuropathological consequences of prenatal immune activation in mice, *Science* 339 (2013) 1100–1102, <https://doi.org/10.1126/science.1228261>.
- [4] U. Meyer, Prenatal Poly (i:C) exposure and other developmental immune activation models in rodent systems, *Biol. Psychiatry* 75 (2014) 307–315, <https://doi.org/10.1016/j.biopsych.2013.07.011>.
- [5] F.S. Mueller, M. Poesel, J. Richetto, U. Meyer, U. Weber-Stadlbauer, Mouse models of maternal immune activation: mind your caging system, *Brain Behav. Immun.* 73 (2018) 643–660, <https://doi.org/10.1016/j.bbi.2018.07.014>.
- [6] U. Meyer, Neurodevelopmental resilience and susceptibility to maternal immune activation, *Trends Neurosci.* 42 (2019) 793–806, <https://doi.org/10.1016/j.tins.2019.08.001>.
- [7] K. Fleming, T.E. Goldberg, J.M. Gold, D.R. Weinberger, Verbal working memory dysfunction in schizophrenia: use of a Brown-Peterson paradigm, *Psychiatry Res.* 56 (1995) 155–161, [https://doi.org/10.1016/0165-1781\(95\)02589-3](https://doi.org/10.1016/0165-1781(95)02589-3).
- [8] K.K. Cho, R. Hoch, A.T. Lee, T. Patel, J.L. Rubenstein, V.S. Sohal, Gamma rhythms link prefrontal interneuron dysfunction with cognitive inflexibility in *dlx5/6+/-* mice, *Neuron* 85 (2015) 1332–1343, <https://doi.org/10.1016/j.neuron.2015.02.019>.
- [9] S.B. Floresco, Y. Zhang, T. Enomoto, Neural circuits subserving behavioral flexibility and their relevance to schizophrenia, *Behav. Brain Res.* 204 (2009) 396–409, <https://doi.org/10.1016/j.bbr.2008.12.001>.
- [10] Z.J. Zhang, G.P. Reynolds, A selective decrease in the relative density of parvalbumin-immunoreactive neurons in the hippocampus in schizophrenia, *Schizophr. Res.* 55 (2002) 1–10, [https://doi.org/10.1016/S0920-9964\(01\)00188-8](https://doi.org/10.1016/S0920-9964(01)00188-8).
- [11] S. Giovanoli, L. Weber, U. Meyer, Single and combined effects of prenatal immune activation and peripubertal stress on parvalbumin and reelin expression in the hippocampal formation, *Brain Behav. Immun.* 40 (2014) 48–54, <https://doi.org/10.1016/j.bbi.2014.04.005>.
- [12] A.A. Walf, C.A. Frye, The use of the elevated plus maze as an assay of anxiety-related behavior in rodents, *Nat. Protoc.* 2 (2007) 322–328, <https://doi.org/10.1038/nprot.2007.44>.
- [13] A. Torres-Berrío, V. Vargas-López, M. López-Canul, The ventral hippocampus is required for behavioral flexibility but not for allocentric/egocentric learning, *Brain Res. Bull.* 146 (2019) 40–50, <https://doi.org/10.1016/j.brainresbull.2018.12.011>.
- [14] R. San-Martin, L.A. Castro, P.R. Menezes, F.J. Fraga, P.W. Simões, C. Salum, Meta-analysis of sensorimotor gating deficits in patients with Schizophrenia evaluated by prepulse inhibition test, *Schizophr. Bull.* 46 (2020) 1482–1497, <https://doi.org/10.1093/schbul/sbaa059>.
- [15] U. Meyer, J. Feldon, M. Schedlowski, B.K. Yee, Towards an immuno-precipitated neurodevelopmental animal model of schizophrenia, *Neurosci. Biobehav. Rev.* 29 (2005) 913–947, <https://doi.org/10.1016/j.neubiorev.2004.10.012>.
- [16] H. Brozka, A. Pistikova, D. Radostova, K. Vales, J. Svoboda, A.N. Grzyb, A. Stuchlik, Adult neurogenesis reduction by a cyostatic treatment improves spatial reversal learning in rats, *Neurobiol. Learn. Mem.* 141 (2017) 93–100, <https://doi.org/10.1016/j.nlm.2017.03.018>.
- [17] C.R. Bowie, P.D. Harvey, Cognition in schizophrenia: Impairments, determinants, and functional importance, *Psychiatr. Clin. North Am.* 28 (2005) 613–633, <https://doi.org/10.1016/j.psc.2005.05.004>.
- [18] Y. Zhang, B.N. Cazakoff, C.A. Thai, J.G. Howland, Prenatal exposure to a viral mimetic alters behavioural flexibility in male, but not female, rats, *Neuropharmacology* 62 (2012) 1299–1307, <https://doi.org/10.1016/j.neuropharm.2011.02.022>.
- [19] S.A. Ballentine, Q. Greba, W. Dawicki, X. Zhang, J.R. Gordon, J.G. Howland, Behavioral alterations in rat offspring following maternal immune activation and ELR-CXC chemokine receptor antagonism during pregnancy: implications for neurodevelopmental psychiatric disorders, *Prog. Neuro-Psychopharmacol. Biol. Psychiatry* 57 (2015) 155–165, <https://doi.org/10.1016/j.pnpbp.2014.11.002>.
- [20] B.R. Lins, J.L. Hurlbise, A.J. Roebuck, W.N. Marks, N.K. Zabder, G.A. Scott, Q. Greba, W. Dawicki, X. Zhang, C.D. Rudulier, J.R. Gordon, J.G. Howland, Prospective analysis of the effects of maternal immune activation on rat cytokines during pregnancy and behavior of the male offspring relevant to Schizophrenia, *eNeuro* 5 (2018), <https://doi.org/10.1523/ENEURO.0249-18.2018>.
- [21] A. Gogos, A. Sbsa, D. Witkamp, M. van den Buuse, Sex differences in the effect of maternal immune activation on cognitive and psychosis-like behavior in Long Evans rats, *EJN* 52 (2020) 2614–2626, <https://doi.org/10.1111/ejn.14671>.
- [22] J.C. Talpos, S.M. McTighe, R. Dias, L.M. Saksida, T.J. Bussey, Trial-unique, delayed nonmatching-to-location (TUNL): a novel, highly hippocampus-dependent automated touchscreen test of location memory and pattern separation, *Neurobiol. Learn. Mem.* 94 (2010) 341–352, <https://doi.org/10.1016/j.nlm.2010.07.006>.
- [23] A.R. Deane, N. Potemkin, R.D. Ward, Mitogen-activated protein kinase (MAPK) signalling corresponds with distinct behavioural profiles in a rat model of maternal immune activation, *Behav. Brain Res.* 396 (2021), 112876, <https://doi.org/10.1016/j.bbr.2020.112876>.
- [24] F.L. Haddad, S.V. Patel, S. Schmid, Maternal immune activation by poly I:C as a preclinical model for neurodevelopmental disorders: a focus on Autism and Schizophrenia, *Neurosci. Biobehav. Rev.* 113 (2020) 546–567, <https://doi.org/10.1016/j.neubiorev.2020.04.012>.
- [25] C. Meehan, L. Harms, J.D. Frost, R. Barreto, J. Todd, U. Schall, C. Shannon Weickert, K. Zavitsanou, P.T. Michie, D.M. Hodgson, Effects of immune activation during early or late gestation on schizophrenia-related behaviour in adult rat offspring, *Brain, Behav., Immun.* 63 (2017) 8–20, <https://doi.org/10.1016/j.bbi.2016.07.144>.
- [26] C.W. Hui, A. St-Pierre, H.El Hajji, Y. Remy, S.S. Hébert, G.N. Luheshi, L. K. Srivastava, M.É. Tremblay, Prenatal immune challenge in mice leads to partly sex-dependent behavioral, microglial, and molecular abnormalities associated with Schizophrenia, *Front. Mol. Neurosci.* 11 (2018) 13, <https://doi.org/10.3389/fnmol.2018.00013>.
- [27] W. Logge, J. Kingham, T. Karl, Do individually ventilated cage systems generate a problem for genetic mouse model research? *Genes. Brain Behav.* 13 (2014) 713–720, <https://doi.org/10.1111/gbb.12149>.
- [28] B. Czéh, Z. Varga, K. Henningsen, G.L. Kovács, A. Miseta, O. Wiborg, Chronic stress reduces the number of GABAergic interneurons in the adult rat hippocampus, dorsal-ventral and region-specific differences, *Hippocampus* 25 (2015) 393–405, <https://doi.org/10.1002/hipo.22382>.
- [29] J.W.C. Wu, X. Du, M. van den Buuse, R.A. Hill, Sex differences in the adolescent developmental trajectory of parvalbumin interneurons in the hippocampus: a role for estradiol, *Psychoneuroendocrinology* 45 (2014) 167–178, <https://doi.org/10.1016/j.psyneuen.2014.03.016>.



# No effect of riluzole and memantine on learning deficit following quinpirole sensitization - An animal model of obsessive-compulsive disorder



Martina Janikova\*, Hana Brozka, Dominika Radostova, Jan Svoboda, Ales Stuchlik\*

Institute of Physiology, Czech Academy of Sciences, Prague, Czech Republic

## ARTICLE INFO

### Keywords:

Quinpirole  
Memantine  
Riluzole  
Obsessive-compulsive disorder  
Active allothetic place avoidance task

## ABSTRACT

**Rationale:** Chronic quinpirole (QNP) sensitization is an established animal model relevant to obsessive-compulsive disorder (OCD) that has been previously shown to induce several OCD-like behavioral patterns, such as compulsive-like checking and increased locomotion.

**Objectives:** In current study we explored the effect of ant glutamatergic drugs, memantine and riluzole, on cognitive and behavioral performance of QNP sensitized rats.

**Methods:** During habituation phase, the rats ( $N = 56$ ) were injected with QNP (0.25 mg/kg) or saline solution (every other day up to 10 injections) and placed into rotating arena without foot shocks for 50-min exploration. Active place avoidance task in rotating arena with unmarked to-be-avoided shock sector was used during acquisition phase. Rats were injected with memantine (1 mg/kg or 5 mg/kg), riluzole (1 mg/kg or 5 mg/kg) or saline solution 30 min before the trial and with QNP (0.25 mg/kg) or saline right before they were placed inside the rotating arena with 60° unmarked shock sector. Locomotion and number of entrances into the shock sector were recorded.

**Results:** QNP sensitization led to a robust deficit in place learning. However, neither memantine nor riluzole did reverse or alleviate the deficit induced by QNP. Contrarily, memantine significantly aggravated QNP induced deficit.

**Conclusions:** The exacerbation of cognitive deficit following ant glutamatergic agents could be mediated by decreased glutamate concentration in nucleus accumbens and decreased hippocampal activation in the QNP sensitization model.

## 1. Introduction

Quinpirole (QNP) sensitization model is considered a valid animal model relevant to Obsessive-Compulsive Disorder (OCD; for review see [46]). Its validity is supported by a striking similarity in the temporal-spatial structure of behavior performed by rats sensitized to quinpirole and the compulsive behavior of patients with OCD [47]. In short, repeated injection of QNP – a D2/D3 agonist results in stereotyped checking behavior in an open-field arena with 4 foreign objects in it. Preference of locales (objects and corners) remains stable between sessions (Brozka et al., unpublished results), paralleling patients' compulsive behavioral patterns which do not vary much over time [52]. Rigidity of behavior is also manifested as a deficit of spontaneous alteration in T-maze [11]. Moreover, in our lab we discovered a robust deficit in reversal learning in rats sensitized to QNP [22,23]. Observed reversal learning deficit was improved only by co-application of clomipramine and risperidone [23], a treatment strategy effective in

alleviating OCD symptoms in a subpopulation of OCD patients [8]. Importantly, cognitive flexibility deficits are considered an endophenotype of many OCD subtypes [2–4] and have been proposed to mediate compulsive symptoms in OCD patients [3]. Focus on improving cognitive capabilities is therefore of utmost importance in OCD treatment.

There are many ‘competing’ hypotheses of OCD pathophysiology (reviewed in [19]). These hypotheses usually consider a malfunction of one of the main neurotransmitter/modulator systems as a putative cause of OCD [19]. The most popular is a serotonin hypothesis, which is based on effectiveness of SSRIs in OCD treatment [26]. Yet, only around 40–86% of patients respond to established treatments or their combinations and treatment response is often incomplete [14]. These facts suggest possible role of other neurotransmitter systems in pathophysiology of OCD. Beneficial effects of supplemental antipsychotic medication point towards involvement of dopaminergic system in OCD [24]. Increasing evidence is also gathered on disruption of glutamatergic

\* Corresponding authors at: Institute of Physiology of the Czech Academy of Sciences, Videnska 1083, 142 20 Prague, Czech Republic.

E-mail addresses: [martina.janikova@fgu.cas.cz](mailto:martina.janikova@fgu.cas.cz) (M. Janikova), [ales.stuchlik@fgu.cas.cz](mailto:ales.stuchlik@fgu.cas.cz) (A. Stuchlik).

<https://doi.org/10.1016/j.physbeh.2019.01.013>

Received 7 December 2018; Received in revised form 15 January 2019; Accepted 16 January 2019

Available online 28 February 2019

0031-9384/ © 2019 Published by Elsevier Inc.



neurotransmission in patients with OCD [54].

Although ‘dopamine hypothesis’ is not currently a leading one in OCD-etiology research, ‘dopamine animal models’ produce strikingly similar behavioral patterns to OCD [47]. Moreover, alterations in dopaminergic system are often intertwined with changes in glutamate system [18,50]. Glutamate is a most common excitatory neurotransmitter that is implicated in many neuropsychiatric disorders. Glutamate aberration is either primary, such as is implicated in schizophrenia [29,33], or it can be secondary to changes in other neuromodulator system, as is implicated in OCD ([39], but see [40]). Glutamatergic synapses are influenced by neuromodulation, including neuromodulation by dopamine [41]. Moreover, alteration to dopamine system can well explain alterations of cortico-striatal circuits - a finding most replicated in OCD patients in functional imaging studies [9,21,25]. Functional glutamatergic hyperactivity at rest in OCD patients have been found especially in areas of orbitofrontal cortex, anterior cingulate cortex and caudate nucleus [30,31], while hypoactivity has been found in nucleus accumbens [13]. These findings can be explained by hyperactivity of direct and hypoactivity of indirect pathway of cortico-striatal circuits [30]. In parallel, administration of QNP, an agonist of D2/D3 receptors, seems to produce similar neurobiological changes in rats as found in OCD patients. Administration of QNP through microdialysis probe has been found to increase extracellular levels of glutamate in the substantia nigra [1] and Escobar et al. [12] found significantly lower extracellular concentrations of glutamate in the nucleus accumbens in QNP sensitized rats. Similarly, in the study by Krügel et al. [27] the basal glutamate concentration in nucleus accumbens was decreased in rats perfused with QNP. It is of question if glutamatergic agents, novel drugs used in OCD treatment [20,37], are capable to normalize animal phenotype after insult into integrity of dopamine system.

In the current study we aimed at testing the effect of glutamatergic agents, memantine and riluzole, in QNP animal model of OCD. Memantine is a non-competitive low-affinity NMDA receptor antagonist used mainly in treatment of Alzheimer's disease. It has been shown to successfully block the NMDA glutamate receptors and therefore normalize the glutamatergic system when over-activated [34] such as is observed in substantia nigra in QNP sensitized rats [1]. Another anti-glutamatergic agent, riluzole, which is currently used in treatment of amyotrophic lateral sclerosis, inhibits glutamate release and potentiates reuptake of extrasynaptic glutamate [15,16].

The present study was aimed to replicate the previous findings [22,23] of a QNP-induced reversal deficit in an active place avoidance task. In addition, the current study aimed to evaluate the effect of memantine and riluzole, agents decreasing glutamatergic neurotransmission, on this deficit. We hypothesized that based on the evidence of their efficiency in clinical OCD; these drugs will alleviate the QNP-induced cognitive deficit.

## 2. Materials and methods

### 2.1. Animals

Fifty-six male Long-Evans rats from the breeding colony of Institute of Physiology (CAS, Czech Republic) were used. Rats were 3–4 months old at the start of experiment and weighed 400–500 g. Rats were housed in pairs in 43x28x25 cm plastic boxes in an animal room with stable temperature and 12/12 light/dark cycle. Water and food were available ad libitum. The experiment was preceded by ten days of handling and habituation in experimental apparatuses. All rat manipulations complied with the Animal Protection Code of the Czech Republic and a corresponding directive of the European Community Council on the use of laboratory animals (2010/63/EU).

### 2.2. Drugs and design

There were two phases to the experiment: a habituation phase and an acquisition phase. For the habituation phase, right before being placed into the apparatus, rats were injected subcutaneously with QNP ( $N = 46$ ; 0.25 mg/kg) or saline ( $N = 10$ ). For the acquisition phase, the QNP-treated rats were randomly assigned into five groups: a QNP-treated control group ( $N = 10$ ); groups that received QNP and either riluzole 1 mg/kg ( $N = 10$ ) or 5 mg/kg ( $N = 8$ ); and groups that received QNP and either memantine 1 mg/kg ( $N = 10$ ) or 5 mg/kg ( $N = 8$ ). The saline-treated rats continued to receive saline and served as the saline control group ( $N = 10$ ). QNP hydrochloride (Sigma-Aldrich, Czech Republic, Cat. No. Q102), memantine hydrochloride (Sigma-Aldrich, Czech Republic, Cat. No. M9292) and riluzole (Sigma-Aldrich, Czech Republic, Cat. No. R116) were dissolved in saline solution (0.9% NaCl) to achieve required concentration.

### 2.3. Behavioral procedure and apparatus

#### 2.3.1. Carousel maze

Because impaired cognitive flexibility together with spatial working memory deficits has been found in OCD patients, [2–4,51], active allothetic place avoidance task (AAPA) on a rotating arena (Carousel maze) has been used in this study (Fig. 1). It has been successfully employed in previous studies on spatial memory, learning deficits, cognitive coordination and cognitive flexibility in various animal models (for review see Stuchlik et al. [46]). In active place avoidance, the animal has to learn to coordinate arena and room frames and use only extra-maze cues (e.g. posters on the wall, door, etc.) to navigate in the maze and successfully solve the task. AAPA is therefore quite demanding procedure and it is the tasks with high workload in which the OCD patients has shown spatial working memory performance deficits [51].

Carousel maze consists of an elevated metallic disc surrounded by a transparent plastic wall. The maze rotates clockwise at one rotation per min. Unmarked 60° to-be-avoided sector is defined inside the arena, where rats receive mild foot-shocks at intervals of 1200 ms until they leave the sector. The to-be-avoided sector is visually imperceptible and is fixed to stable location relative to the room frame (independent on the arena rotation). The animals should learn the position of the shock sector using the extra-maze cues and avoid it. The intensity of foot-shocks is adjusted individually (0.2–0.6 mA) to elicit escape response



Fig. 1. An original photograph of the Carousel arena.



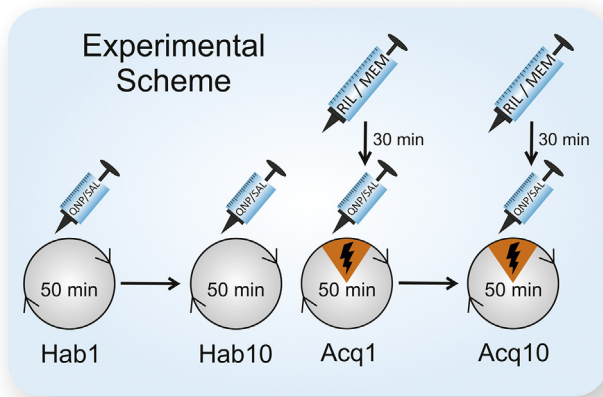


**Fig. 2.** Design of the study. Schematic illustration of habituation and acquisition experimental design. Arena always rotated clockwise.

and motivate the animal to learn the sector position. To prevent freezing, we kept the foot-shocks on minimal possible level. The foot-shocks are administered through a cable attached to a harness on the back of the rat and connected to the conductive subcutaneous implant. An overhead camera was used to monitor the rat, which had an infrared light-emitting diode (LED) attached to its back with a rubber harness. A software program detects movements of the rat by monitoring the  $x$ ,  $y$  coordinates of the LED.

### 2.3.2. QNP sensitization and habituation

The habituation phase served also to induce sensitization to QNP. Rats received repeated injections of QNP (0.25 mg/kg) or saline solution every other day (up to 10 injections). All animals were injected subcutaneously every other day up to the total of 10 injections. Immediately after the injection, the animals were placed onto the rotating Carousel apparatus for 50-min exploration without foot-shocks (Fig. 2). The dose of QNP (0.25 mg/kg) has been shown to be the lowest dose successfully producing sensitization [48] and inter-injection interval every other day was chosen with respect to previously applied protocol in our lab [22,23].

### 2.3.3. Acquisition testing

The acquisition phase (ACQ) started two days after the end of habituation phase. Before the acquisition procedure, rats were subcutaneously implanted with a hypodermic needle; the needle was connected to a current source through which electric shocks were delivered. Again, all animals were tested every other day (up to 10 injections). Rats were retrieved from their home cage 30 min before each trial, injected with memantine (1 mg/kg or 5 mg/kg), riluzole (1 mg/kg or 5 mg/kg) or saline solution and returned back to their cage. Right before the trial, rats were injected with QNP (0.25 mg/kg) or saline solution and placed onto the Carousel maze on the opposite side from the shock sector. From start to the end of the trial, the arena rotated at a constant speed of 1 rotation/min (Fig. 2). Since we observed a strong deficit in QNP-treated animals in acquisition we did not proceed to testing reversal learning.

## 2.4. Data analysis and statistics

### 2.4.1. Measured parameters and statistical analysis

Main parameters measured were number of entrances (measured as number of entrances into the to-be-avoided sector) and level of locomotion (measured as the distance walked during the whole session in meters). Low number of entrances represents good learning (low errors), unimpaired memory and an efficient avoiding strategy. In analysis, each session was binned into five consecutive 10-min intervals, to

assess within the session learning. Three way-repeated-measure ANOVA (sessions  $\times$  interval  $\times$  treatment) was used to compare all treatment groups in acquisition phase. Tukey's HSD test was used when appropriate. Statistical analysis was done using SPSS software (IBM SPSS, version 23 USA).

## 3. Results

### 3.1. QNP sensitization and habituation

To assess if sensitization with quinpirole was successful, we compared locomotion between saline treated and QNP-sensitized animals during habituation sessions. We used three-way repeated-measures-ANOVA (session  $\times$  interval  $\times$  treatment) with day of habituation session (hab01-hab10) and time interval (0–10 min - 40–50 min) as repeated measure factors and treatment (QNP or saline) as a between group factor. Also, we specifically compared locomotion between two groups in last day of habituation to confirm sensitization [49]. The analysis was conducted on 39 rats in the quinpirole group and 8 rats in the saline group, 9 rats were rejected from analysis due to missing data.

#### 3.1.1. Main effects

Data met parametric assumptions and so we proceeded with parametric procedure. However, assumption of sphericity was not met for repeated measure ( $p < .001$ ), thus Greenhouse-Geisser correction was applied. There was a main effect of session [ $F(9,405) = 4220$ ,  $p < .001$ ,  $\eta^2 = 0.083$ ], of treatment [ $F(1,45) = 20,824$ ,  $p < .001$ ,  $\eta^2 = 0.316$ ] and also of interval [ $F(4,180) = 8322$ ,  $p = .001$ ,  $\eta^2 = 0.156$ ]. Main effects will be interpreted along with interaction interpretations.

#### 3.1.2. Interaction effect of session $\times$ treatment

Moreover, we observed a significant interaction between habituation session and treatment [session  $\times$  treatment:  $F(9,405) = 3.805$ ,  $p = .001$ ,  $\eta^2 = 0.078$ ]. This is due to gradual increase of locomotion in QNP groups, as significantly higher locomotion in QNP group compared to saline group has been found from 2th session onward. In the last day of habituation significant difference was accompanied by two-fold increase of locomotion in QNP sensitized group (QNP =  $112 \pm 33$  m; saline =  $53 \pm 19$  m). Data is visualized in the Fig. 3a and Fig. 3c.

#### 3.1.3. Interaction effect interval $\times$ treatment

Furthermore, interval  $\times$  treatment interaction was also significant [ $F(4, 180) = 107.951$ ,  $p < .001$ ,  $\eta^2 = 0.706$ ], suggesting different pattern of locomotion levels in the course of a session between saline and QNP groups. Rats in saline group moved significantly more in the first 10 min of session and their locomotion decreased in later intervals, while locomotion of rats in QNP group was lower than locomotion of saline group in first interval but was increasing in later intervals, greatly surpassing locomotion of saline controls. Data is visualized in the Fig. 3b.

## 3.2. Acquisition testing

Numbers of entrances into to-be-avoided sector were not normally distributed; therefore, we used a logarithmic transformation. Also, assumption of sphericity was not met for repeated measures ( $p < .001$ ) and so  $p$ -values are reported using Greenhouse-Geisser correction. Three-way repeated-measure-ANOVA (session  $\times$  interval  $\times$  treatment) was performed on total 43 animals (8 rats in QNP-SAL group, 7 rats in both QNP-MEM groups, 7 rats in QNP-RIL 1 mg/kg, 6 rats in QNP-RIL 5 mg/kg and 8 rats in saline group). 13 rats, randomly distributed between groups, were rejected from analysis due to missing data.

### 3.2.1. Effect of session

The three-way repeated measures ANOVA (with treatment as a

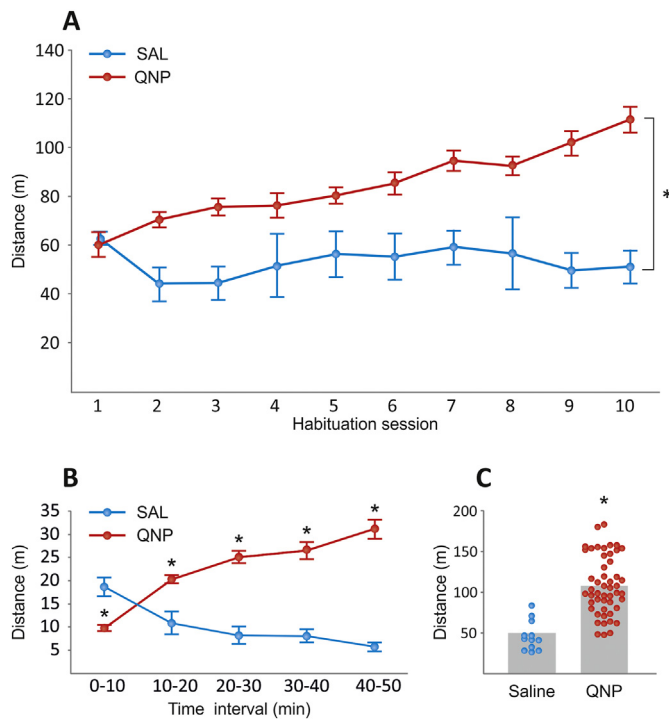


**Fig. 3.** Results from habituation. Data are presented as mean values  $\pm$  SEM. (A) Locomotion (meters/50 min) of QNP sensitized animals and control group during all sessions. In the last day of habituation there was two-fold increase of locomotion in QNP group (QNP =  $112 \pm 33$  m; SAL =  $53 \pm 19$  m). (B) Mean changes in locomotion of QNP and saline groups during the course of the 10th session. Control group locomoted significantly more in the first 10-min interval and their locomotion continued to decrease during whole session, while locomotion of QNP group continued to increase. Differences between both groups were significant in each time interval ( $p \leq .001$ ). (C) Significant difference between locomotion of QNP and saline group on the 10th day of habituation ( $p < .001$ ).

between the subject factor and session and time interval as a within the subject factor) showed a significant effect of session [ $F(9, 333) = 11,367, p < .001, \eta^2 = 0.235$ ] on number of entrances. Simple planned contrasts were used to dissect effect of session. Contrasts revealed that, overall, animals made significantly more errors on the first five sessions compared to the last session [Session 1:  $F(1, 37) = 36.024, p < .001, \eta^2 = 0.493$ ; Session 2:  $F(1, 37) = 31.813, p < .001, \eta^2 = 0.462$ ; Session 3:  $F(1, 37) = 16.582, p < .001, \eta^2 = 0.313$ ; Session 4:  $F(1, 37) = 12.064, p < .05, \eta^2 = 0.246$ ; Session 5:  $F(1, 37) = 9.472, p < .05, \eta^2 = 0.204$ ]. Differences between all other sessions and the last session were not significant. This suggests that prolonged arena exposure (fifth and later sessions) does not lead to improved performance.

### 3.2.2. Effect of treatment

Next, the three-way ANOVA showed a significant main effect of treatment [ $F(5, 37) = 21,399, p < .001, \eta^2 = 0.743$ ]. Tukey's HSD test was used to specify differences between treatment groups. It revealed that all groups made significantly more entrances into to-be avoided sector compared to saline group ( $p < .01$ ). Moreover, QNP-memantine 5 mg/kg group made significantly more entrances than QNP-saline group ( $p < .05$ ). QNP-memantine 5 mg/kg treated group made the highest number of entrances overall (see the Fig. 4).

### 3.2.3. Effect of interval

Next, main effect of time interval was found significant [ $F(4, 148) = 22.080, p < .001, \eta^2 = 0.374$ ]. This indicates that entrances are not homogeneously distributed across the length of a session. We

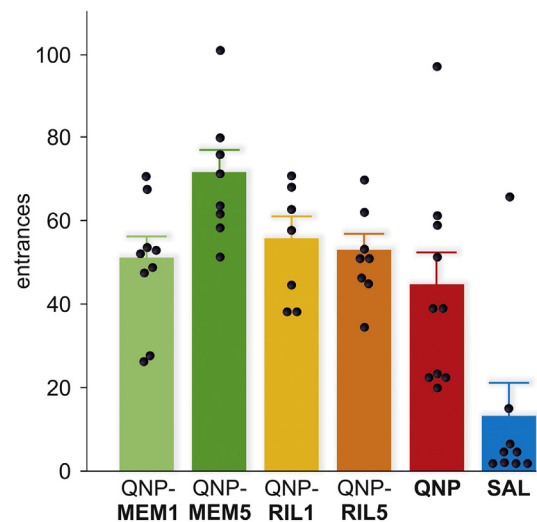


**Fig. 4.** Results from acquisition. Number of entrances into to-be-avoided sector of all treatment groups compared to QNP-saline and saline control group. Data are presented as average number of errors  $\pm$  SEM. All groups made significantly more errors than control group ( $p < .01$ ). QNP-memantine 5 mg/kg group made the highest number of errors, even significantly more than QNP-saline group ( $p < .05$ ). \* denotes a significant difference from the control group at  $p < .01$ . # denotes a significant difference from the QNP-saline group at  $p < .05$ .

used repeated planned contrasts to compare each 10-min interval to the consecutive one. Animals made significantly less errors in the second 10-min interval compared to the first 10-min interval and third 10-min interval compared to the second interval ( $p < .5$ ). Also, rats made fewer errors during last 10-min interval compared to previous 10-min interval ( $p < 0.001$ ). This indicated that 50-min session is of adequate length to maximize learning.

### 3.2.4. Interaction effect of session $\times$ interval $\times$ treatment

Importantly, 3-way interaction of session  $\times$  interval  $\times$  treatment was significant [ $F(180, 1332) = 1.683, p < .05, \eta^2 = 0.185$ ]. Further analysis showed significant session  $\times$  interval interaction in all treatment groups [QNP-SAL:  $F(36, 288) = 1.642, p = .015, \eta^2 = 0.170$ ; QNP-MEM1:  $F(36, 216) = 1.658, p = .015, \eta^2 = 0.217$ ; QNP-MEM5:  $F(36, 216) = 1.639, p = .017, \eta^2 = 0.215$ ; QNP-RIL1:  $F(36, 216) = 1.781, p = .007, \eta^2 = 0.229$ ; QNP-RIL5:  $F(36, 180) = 1.638, p = .019, \eta^2 = 0.247$ ; SALINE:  $F(36, 216) = 2.056, p = .001, \eta^2 = 0.225$ ]. Results imply different behavioral pattern of individual treatment groups during sessions and time intervals. While performance of saline group generally improved between first and second time interval between second and third session and then continued to be almost stably good, performance of QNP-saline, QNP riluzole 1 mg/kg and QNP-memantine 1 mg/kg was significantly worse in the beginning but continued to improve during the whole session. This may imply impaired long-term memory in these treatment groups. Although performance of QNP-memantine 5 mg/kg and QNP/riluzole 5 mg/kg also improved during the course of each session, they still made higher number of errors overall. This implies possible role of different drug doses on learning and behavior of rats, when lower doses may result into more positive outcomes. Results are visualized in Fig. 5.

### 3.3. Locomotion and entrances correlations

Additionally, we correlated locomotion and number of entrances to assess if hyper-locomotion, observed during QNP sensitization, was related to the cognitive performance. First, we averaged number of entrances and locomotion separately for each animal (an average of all sessions). Pearson's correlation was used. There was a significant

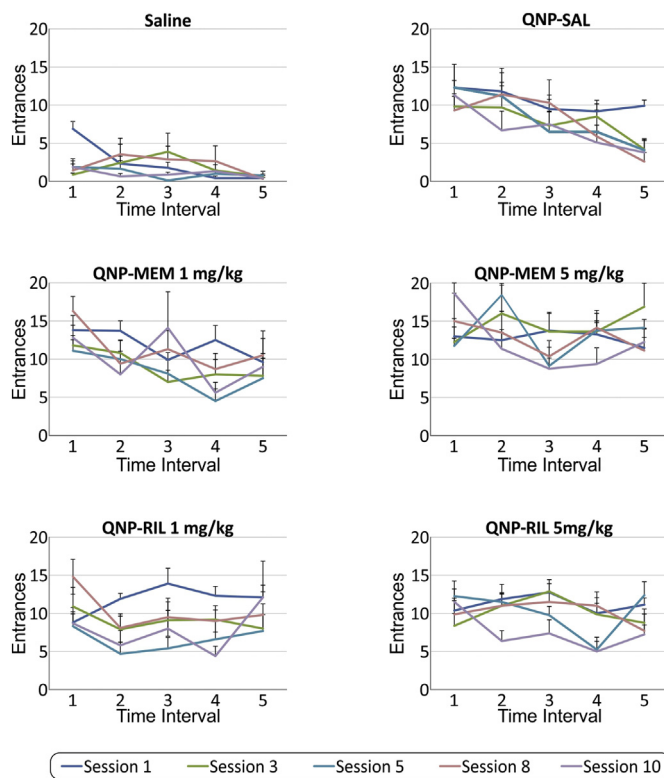


**Fig. 5.** Results from acquisition. Significant three-way interaction (time interval  $\times$  session  $\times$  treatment). Each treatment group behaved distinctively in different time segments ( $p < .05$ ). Data are presented as average number of errors + SEM.

positive correlation between number of entrances and walked distance only in group treated with QNP and riluzole 1 mg/kg ( $r = 0.669$ ,  $p = .034$ ,  $R^2 = 0.45$ ). In no other group there was a significant correlation between number of entrances and distance walked (see Fig. 6 in Supplementary material). Moreover, we analyzed correlation for each interval within each session for each treatment groups and correlation between entrances and distance emerged relatively rarely (see Table 1 in Supplementary material). Interestingly, positive correlation was observed for all groups treated with QNP, while negative correlation emerged in some intervals for saline treated animals. However, we can conclude that there is no overt link between locomotion and number of entrances in this task.

#### 4. Discussion

The present study tested the effect of glutamatergic agents on cognitive deficit in a QNP animal model of OCD. Testing of effects of memantine and riluzole was based on indications of elevated glutamate levels in OCD [30,31]. Our hypothesis predicted that the effects of QNP would be alleviated by concurrent administration of antiglutamatergic drugs memantine and riluzole.

##### 4.1. A deficit in spatial learning induced by QNP sensitization model

First, we detected that repeated QNP (0.25 mg/kg) injection given immediately before 50-min exposure to a rotating carousel arena produced a strong hyperlocomotion along with an inability to acquire the active place avoidance task in the Carousel. This result seemingly contradicts our previous results where rats pretreated chronically with higher dose of QNP (0.5 mg/kg) did not show a QNP-induced deficit in acquisition or reversal learning in the Carousel paradigm, although trends for a deficit were present [22,23]. In current study, a lower dose

(0.25 mg/kg) induced an impairment of initial learning of the active place avoidance. However, in addition to the lower dose of QNP, there is another difference which may help to explain the discrepancy observed. The present study, contrarily to the previous ones, involved exposing the rats to the rotating arena immediately after injection of QNP, while the previous studies employed a protocol, in which the rats were introduced into the environment after 30 min. Conceivably, having the entire sensitizing experience in a novel environment may be detrimental to new learning under QNP in that environment.

Additionally, as shown by lack of significant correlation between locomotion and number of errors with exception of QNP-riluzole 1 mg/kg group, we propose that the cognitive effects of QNP upon learning of the active place avoidance task are independent of the QNP-induced hyperactivity. This prediction is in agreement with previous studies, specifically the one that showed a deficit in spontaneous alternation in QNP-treated rats having been independent on the hyperactivity [11], as well as our previous reports [22,23].

##### 4.2. No beneficial effect of memantine and riluzole on the QNP-induced learning deficit

The second principal finding of the present study is that administration of drugs decreasing glutamatergic neurotransmission did not reverse or even alleviate the deficit induced by QNP. In fact, memantine (5 mg/kg) significantly potentiated this deficit. Contrarily to our findings, augmentation therapy with glutamatergic agents, like memantine, riluzole or amantadine, has been found effective in improvement of OCD symptoms in humans [17,35,38,44]. Modarresi et al. [32] found that 73,3% of 32 studied SSRI-refractory OCD patients achieved treatment response on memantine augmentation therapy. Similar results have been achieved with riluzole. In an open-label study, Coric et al. [5] recruited 13 treatment-resistant OCD patients, who received riluzole 50 mg twice a day during 12 weeks trial additionally to their current medication. Out of 13 patients, seven patients demonstrated at least 35% reduction of symptoms according to Yale-Brown Obsessive-Compulsive Scale scores and 5 were categorized as treatment responders. Pittenger et al. [36] have shown very similar results. Approximately half of the treatment-refractory OCD patients exhibited significant improvement that lasted over several months during which records were available [36].

One possible explanation of the present findings lays in the glutamatergic effect of QNP on different brain structures. While QNP was found to increase levels of glutamate in substantia nigra [1] and striatum [28], it was also shown to decrease glutamate concentration in nucleus accumbens (NAc) [12,27]. Lesion of NAc has been found to result in stereotypical behavior [10]. Moreover, NAc is essential structure for normal declarative memory formation [7] and reversal learning [6], suggesting that hypoactivity of NAc may mediate both acquisition and reversal deficit. Therefore, anti-glutamatergic agents may not only normalize glutamate levels in areas with its higher concentration, but also contribute to further decrease of glutamate levels in regions with already low levels, like NAc, leading to disruption of the system in opposite direction. Moreover, both memantine and riluzole has been found effective only in augmentation therapy together with other, typically SSRI, medication [17,32,35,38,44]. Moreover, as shown in the study by Modarresi et al. [32], at least 12 weeks of memantine augmentation therapy was necessary for the treatment response to occur, suggesting that 20 days of acquisition treatment period may have been short time for significant improvement. Notably, Vlček et al. [53] proposed glutamatergic treatments may be especially effective in specific subtypes of patients with specific cognitive deficits and maladaptive compensatory memory processes such as checkers. Our data, however, do not support this view, because the QNP sensitization models specifically the compulsive checking and no positive effect of memantine and riluzole was seen in this model. Interestingly, Servaes et al. [42] used molecular imaging by positron-emission tomography of



mGluR 5 receptor availability in the QNP-sensitization model and found increased availability of these receptors in multiple structures, including the hippocampus and entorhinal cortex. The authors proposed that removal of dopamine D2-like receptor inhibition of glutamate release may have mediated this effect, leading to enhanced glutamate release. This view is further supported by another finding of Servaes et al. [43] which found a decrease of radioactively-labeled fluorodeoxyglucose uptake in the hippocampus in the model of OCD based on QNP sensitization. It is therefore possible that decreased activation of the hippocampus mediates the acquisition deficit and further deactivation of this structure by agents decreasing glutamatergic transmission may lead even to further disruption of cognitive deficit.

## 5. Conclusions

The present study shows that QNP sensitization can lead to deficits in place learning in a task requiring segregation of mutually discordant spatial reference frames. We also show that drugs interfering with glutamatergic neurotransmission, memantine and riluzole do not alleviate or reverse a place learning deficit in active place avoidance task induced by QNP sensitization. Since the model based on QNP sensitization was shown to produce compulsive-like checking in open-field arena with objects, these data provide evidence of limited predictive validity of QNP sensitization in relation to antiglutamatergic agents, although such a conclusion would need support from findings using antiglutamatergic agents in an augmentation paradigm. This effect might be mediated by decreased glutamate concentration in nucleus accumbens and decreased hippocampal neuronal activation in the QNP sensitization model, which is further compromised by decreasing glutamate neurotransmission.

Supplementary data to this article can be found online at <https://doi.org/10.1016/j.physbeh.2019.01.013>.

## Acknowledgements

This work was supported by GACR grant 17-04047S and AZV grant 15-34524A. Institutional support for IPHYS was provided by RVO:67985823.

## References




- [1] J. Abarca, K. Gysling, R.H. Roth, G. Bustos, Changes in extracellular levels of glutamate and aspartate in rat substantia nigra induced by dopamine receptor ligands: in vivo microdialysis studies, *Neurochem. Res.* 20 (2) (1995) 159–169.
- [2] S.R. Chamberlain, A.D. Blackwell, N.A. Fineberg, T.W. Robbins, B.J. Sahakian, The neuropsychology of obsessive compulsive disorder: the importance of failures in cognitive and behavioural inhibition as candidate endophenotypic markers, *Neurosci. Behav. Rev.* 29 (2005) 399–419.
- [3] S.R. Chamberlain, N.A. Fineberg, A.D. Blackwell, T.W. Robbins, B.J. Sahakian, Motor inhibition and cognitive flexibility in obsessive-compulsive disorder and trichotillomania, *Am. J. Psychiatr.* 163 (2006) 1282–1284.
- [4] S.R. Chamberlain, N.A. Fineberg, L.A. Menzies, A.D. Blackwell, E.T. Bullmore, T.W. Robbins, B.J. Sahakian, Impaired cognitive flexibility and motor inhibition in unaffected first-degree relatives of patients with obsessive-compulsive disorder, *Am. J. Psychiatr.* 154 (2) (2007) 335–338.
- [5] V. Coric, S. Taskiran, C. Pittenger, S. Wasylink, D.H. Mathalon, G. Valentine, et al., Riluzole augmentation in treatment-resistant obsessive-compulsive disorder: an open-label trial, *Biol. Psychiatry* 58 (5) (2005) 424–428.
- [6] R. Cools, M.J. Frank, S.E. Gibbs, A. Miyakawa, W. Jagust, M. D'Esposito, Striatal dopamine predicts outcome-specific reversal learning and its sensitivity to dopaminergic drug administration, *J. Neurosci.* 29 (5) (2009) 1538–1542.
- [7] J.J. Day, M.F. Roitman, M. Wightman, R.M. Carelli, Associative learning mediates dynamic shifts in dopamine signaling in the nucleus accumbens, *Nat. Neurosci.* 10 (8) (2007) 1020–1028.
- [8] E.H. Declodt, D.S. Stein, Current trends in drug treatment of obsessive-compulsive disorder, *Neuropsychiatr. Dis. Treat.* 6 (2010) 233–242.
- [9] K. Dunlop, B. Woodside, M. Olmsted, P. Colton, P. Giacobbe, J. Downar, Reductions in cortico-striatal hyperconnectivity accompany successful treatment of obsessive-compulsive disorder with dorsomedial prefrontal rTMS, *Neuropsychopharmacology* 41 (5) (2016) 1395–1403.
- [10] A. Dvorkin, C. Silva, T. McMurran, L. Bisnaire, J. Foster, H. Szechtman, Features of compulsive checking behavior mediated by nucleus accumbens and orbital frontal cortex, *Eur. J. Neurosci.* 32 (9) (2010) 1552–1563.
- [11] H. Einat, H. Szechtman, Perseveration without hyperlocomotion in a spontaneous alternation task in rats sensitized to the dopamine agonist quinpirole, *Physiol. Behav.* 57 (1) (1995) 55–59.
- [12] A. Escobar, F.A. Cornejo, M. Olivares-Costa, M. Gonzáles, J.A. Fuentealba, K. Gysling, R.A. España, M.E. Andrés, Reduced dopamine and glutamate neurotransmission in the nucleus accumbens of quinpirole-sensitized rats hints at inhibitory D2 autoreceptor function, *J. Neurochem.* 134 (2015) 1081–1090.
- [13] M. Figeo, M. Vink, F. de Geus, N. Vulink, D.J. Veltman, H. Westenberg, D. Denys, Dysfunctional reward circuitry in obsessive-compulsive disorder, *Biol. Psychiatry* 69 (9) (2011) 867–874.
- [14] E.B. Foa, M.R. Liebowitz, M.J. Kozak, S. Davies, R. Campeas, M.F. Franklin, J.D. Huppert, K. Kjernisted, V. Rowan, A. Schmidt, B. Simpson, T. Xin, Randomized, placebo-controlled trial of exposure and ritual prevention, Clomipramine and their combination in the treatment of obsessive-compulsive disorder, *Am. J. Psychiatr.* 162 (2005) 151–161.
- [15] M.E. Frizzo, L.P. Dall'Onder, K.B. Dalcin, D.O. Souza, Riluzole enhances glutamate uptake in rat astrocyte cultures, *Cell. Mol. Neurobiol.* 24 (1) (2004) 123–128.
- [16] E. Fumagalli, M. Funicello, T. Rauen, M. Gobbi, T. Mennini, Riluzole enhances the activity of glutamate transporters GLAST, GLT1 and EAAC1, *Eur. J. Pharmacol.* 578 (2–3) (2008) 171–176.
- [17] A. Ghaleiha, N. Entezari, A. Modabbernia, B. Najand, N. Askari, M. Tabrizi, M. Ashrafi, R. Hajiaghaee, S. Ahondzadeh, Memantine add-on in moderate to severe obsessive-compulsive disorder: randomized double-blind placebo controlled study, *J. Psychiatr. Res.* 47 (2012) 175–180.
- [18] T. Gleich, L. Deserno, R.C. Lorenz, R. Boehme, A. Pankow, R. Buchret, S. Kuhn, A. Heinz, F. Schlagenhaut, J. Gallinat, Prefrontal and striatal glutamate differently relate to striatal dopamine: potential regulatory mechanisms of striatal presynaptic dopamine function? *J. Neurosci.* 35 (26) (2015) 9615–9621.
- [19] W.K. Goodman, D. Grice, K.A.B. Lapidus, B. Coffey, Obsessive-compulsive disorder, *Psychiatr. Clin. North Am.* 37 (3) (2014) 257–267.
- [20] A. Häge, T. Banaschewski, J.K. Buiteller, R.M. Dijkhuizen, B. Franke, D.J. Lythgoe, K. Mechler, S.C.R. Williams, R.W. Dittmann, et al., Glutamatergic medication in the treatment of obsessive compulsive disorder (OCD) and autism spectrum disorder (ASD) – study protocol for a randomized controlled trial, *Trials* 17 (2016) 141.
- [21] B.J. Harrison, C. Soriano-Mas, J. Pujol, et al., Altered corticostriatal functional connectivity in obsessive-compulsive disorder, *Arch. Gen. Psychiatry* 66 (11) (2009) 1189–1200.
- [22] H. Hatalova, D. Radostova, A. Pistikova, K. Vales, A. Stuchlik, Spatial reversal learning in chronically sensitized rats and in undrugged sensitized rats with dopamine D2-like receptor agonist quinpirole, *Front. Behav. Neurosci.* 8 (122) (2014) 1–13.
- [23] H. Hatalova, D. Radostova, A. Pistikova, K. Vales, A. Stuchlik, Detrimental effect of clomipramine on hippocampus-dependent learning in an animal model of obsessive-compulsive disorder induced by sensitization with d2/d3 agonist quinpirole, *Behav. Brain Res.* 317 (2017) 210–217.
- [24] M.A. Jenike, Obsessive-compulsive disorder, *N. Engl. J. Med.* 350 (2004) 259–265.
- [25] W.H. Jung, D.-H. Kang, E. Kim, K.S. Shin, J.H. Jang, J.S. Kwon, Abnormal corticostriatal-limbic functional connectivity in obsessive-compulsive disorder during reward processing and resting-state, *Neuroimage* 3 (2013) 27–38.
- [26] M. Kellner, Drug treatment of obsessive-compulsive disorder, *Dialogues Clin. Neurosci.* 12 (2) (2010) 187–197.
- [27] U. Krügel, T. Schraft, R. Regenthal, P. Illes, H. Kittner, Purinergic modulation of extracellular glutamate levels in the nucleus accumbens in vivo, *Int. J. Dev. Neurosci.* 22 (2004) 565–570.
- [28] N. Laprade, J.-J. Soghomonian, Differential regulation of mRNA levels encoding for the two isoforms of glutamate decarboxylase (GAD65 and GAD67) by dopamine receptors in the rat striatum, *Mol. Brain Res.* 34 (1) (1995) 65–74.
- [29] J.A. Lieberman, R.R. Grigis, G. Brucato, H. Moore, F. Provenzano, L. Kegeles, D. Javitt, J. Kantrowitz, M.M. Wall, M.C. Corcoran, S.A. Schobel, S.A. Small, Hippocampal dysfunction in the pathophysiology of schizophrenia: a selective review and hypothesis for early detection and intervention, *Mol. Psychiatry* 00 (2017) 1–9.
- [30] T.V. Maia, R.E. Cooney, B.S. Peterson, The neural bases of obsessive-compulsive disorder in children and adults, *Dev. Psychopathol.* 20 (4) (2008) 1251–1283.
- [31] L. Menzies, S.R. Chamberlain, A.R. Laird, S.M. Thelen, B.J. Sahakian, E.T. Bullmore, Integrating evidence from neuroimaging and neuropsychological studies of obsessive-compulsive disorder: the orbitofronto-striatal model revisited, *Neurosci. Biobehav. Rev.* 32 (3) (2008) 525–549.
- [32] A. Modarresi, M. Sayyah, S. Razooghi, K. Eslami, M. Javadi, L. Kouti, Memantine augmentation improves symptoms in serotonin reuptake inhibitor-refractory obsessive-compulsive disorder: a randomized controlled trial, *Pharmacopsychiatry* 51 (6) (2017) 263–269.
- [33] B. Moghaddam, D. Javitt, From revolution to evolution: the glutamate hypothesis of schizophrenia and its implication for treatment, *Neuropsychopharmacology* 37 (1) (2012) 4–15.
- [34] D. Olivares, V.K. Desphande, Y. Shi, D.K. Lahiri, N.H. Greig, J.T. Rogers, X. Huang, N-methyl D-aspartate (NMDA) receptor antagonists and memantine treatment for Alzheimer's disease, vascular dementia and Parkinson's disease, *Curr. Alzheimer Res.* 9 (6) (2012) 746–758.
- [35] M. Pasquini, M. Biondi, Memantine augmentation for refractory obsessive-compulsive disorder, *Prog. Neuro-Psychopharmacol. Biol. Psychiatry* 30 (2006) 1173–1175.
- [36] C. Pittenger, B. Kelmendi, S. Wasylink, M.H. Bloch, V. Coric, Riluzole augmentation in treatment-refractory obsessive-compulsive disorder: a series of 13 cases, with long-term follow-up, *J. Clin. Psychopharmacol.* 28 (3) (2008) 363–367.
- [37] C. Pittenger, Glutamatergic agents for OCD and related disorders, *Curr. Treat.*



- Option. *Psychiatry* 2 (3) (2015) 271–283.
- [38] M. Poyurovsky, R. Weizman, A. Weizman, L. Koran, Memantine for treatment-resistant OCD, *Am. J. Psychiatry* 162 (11) (2005) 2191–2192.
- [39] D.R. Rosenberg, S.N. MacMillan, G.J. Moore, Brain anatomy and chemistry may predict treatment response in paediatric obsessive-compulsive disorder, *Int. J. Neuropsychopharmacol.* 4 (2) (2001) 179–190.
- [40] J.Y. Rotge, B. Auouizerate, J. Tignol, B. Bioulac, P. Burbaud, D. Guehl, The glutamate-based genetic immune hypothesis in obsessive-compulsive disorder. An integrative approach from genes to symptoms, *Neuroscience* 165 (2) (2010) 408–417.
- [41] S.R. Seasack, D.B. Carr, N. Omelchenko, A. Pinto, Anatomical substrates for glutamate-dopamine interactions: evidence for specificity of connections and extra-synaptic actions, *Ann. New York Acad. Sci.* 1003 (2003) 36–52.
- [42] S. Servaes, D. Glorie, J. Verhaeghe, S. Stroobants, S. Staelens, Preclinical molecular imaging of glutamatergic and dopaminergic neuroreceptor kinetics in obsessive compulsive disorder, *Prog. Neuro-Psychopharmacol. Biol. Psychiatry* 77 (2017) 90–98.
- [43] S. Servaes, D. Glorie, J. Verhaeghe, L. Wyffels, S. Stroobants, S. Staelens, [18F]-FDG PET neuroimaging in rats with quinpirole-induced checking behavior as a model for obsessive compulsive disorder, *Psychiatry Res.* 257 (2016) 31–38.
- [44] S.E. Stewart, E.A. Jenike, D.M. Hezel, D.E. Stack, N.H. Dodman, L. Shuster, et al., A single-blinded case-control study of memantine in severe obsessive-compulsive disorder, *J. Clin. Psychopharmacol.* 30 (1) (2010) 34–39.
- [45] A. Stuchlik, D. Radostova, H. Hatalova, K. Vales, T. Nekovarova, J. Koprivova, J. Svoboda, J. Horacek, Validity of quinpirole sensitization rat model of OCD: linking evidence from animal and clinical studies, *Front. Behav. Neurosci.* 10 (2016) 1–7.
- [46] H. Szechtman, W. Sulis, D. Eilam, Quinpirole induces compulsive checking behavior in rats: a potential animal model of obsessive-compulsive disorder (OCD), *Behav. Neurosci.* 112 (6) (1998) 1475–1485.
- [47] H. Szechtman, H. Dai, S. Mustafa, H. Einat, R.M. Sullivan, Effects of dose and inter-dose interval on locomotor sensitization to the dopamine agonist quinpirole, *Pharmacol. Biochem. Behav.* 48 (4) (1994) 921–928.
- [48] H. Szechtman, H. Talangbavan, D. Eilam, Environmental and behavioral components of sensitization induced by the dopamine agonist quinpirole, *Behav. Pharmacol.* 4 (4) (1993) 405–410.
- [49] K.Y. Tseng, P. O'Donnell, Dopamine-glutamate interactions controlling prefrontal cortical pyramidal cell excitability involve multiple signaling mechanism, *J. Neurosci.* 24 (22) (2004) 5131–5139.
- [50] N.J.A. van der Wee, N.F. Ramsey, J.M. Jansma, D.A. Denys, H.J.G.M. van Meegen, H.M.G. Westenberg, R.S. Kahn, Spatial working memory deficits in obsessive compulsive disorder are associated with excessive engagement of the medial frontal cortex, *NeuroImage* 20 (2003) 2271–2280.
- [51] D. Veale, A. Roberts, Obsessive-compulsive disorder, *BMJ* 348 (2014) 31–37.
- [52] P. Vlček, J. Polák, M. Brunovský, J. Horáček, Role of glutamatergic system in obsessive-compulsive disorder with possible therapeutic implications, *Pharmacopsychiatry* 51 (6) (2018) 229–242 (01/02(51)).
- [53] K. Wu, G.L. Hanna, D.R. Rosenberg, P.D. Arnold, The role of glutamate signaling in the pathogenesis and treatment of obsessive-compulsive disorder, *Pharmacol. Biochem. Behav.* 100 (4) (2012) 726–735.

## Article

# Memantine and Riluzole Exacerbate, Rather Than Ameliorate Behavioral Deficits Induced by 8-OH-DPAT Sensitization in a Spatial Task

Martina Janikova<sup>1,2,\*,†</sup>, Karolina Mainerova<sup>1,†</sup>, Iveta Vojtechova<sup>1,2,3</sup> , Tomas Petrasek<sup>1,3</sup>, Jan Svoboda<sup>1</sup>   
and Ales Stuchlik<sup>1,\*</sup> 

<sup>1</sup> Institute of Physiology of the Czech Academy of Sciences, Videnska 1083, 142 20 Prague, Czech Republic; karolinamainerova@gmail.com (K.M.); Iveta.Vojtechova@nudz.cz (I.V.); Tomas.Petrasek@nudz.cz (T.P.); jan.svoboda@fgu.cas.cz (J.S.)

<sup>2</sup> First Faculty of Medicine, Charles University, Katerinska 1660/12, 121 08 Prague, Czech Republic

<sup>3</sup> National Institute of Mental Health, Topolova 748, 250 67 Klecany, Czech Republic

\* Correspondence: martina.janikova@fgu.cas.cz (M.J.); ales.stuchlik@fgu.cas.cz (A.S.)

† These authors contributed equally to this work.

**Abstract:** Chronic sensitization to serotonin 1A and 7 receptors agonist 8-OH-DPAT induces compulsive checking and perseverative behavior. As such, it has been used to model obsessive-compulsive disorder (OCD)-like behavior in mice and rats. In this study, we tested spatial learning in the 8-OH-DPAT model of OCD and the effect of co-administration of memantine and riluzole—glutamate-modulating agents that have been shown to be effective in several clinical trials. Rats were tested in the active place avoidance task in the Carousel maze, where they learned to avoid the visually imperceptible shock sector. All rats were subcutaneously injected with 8-OH-DPAT (0.25 mg/kg) or saline (control group) during habituation. During acquisition, they were pretreated with riluzole (1 mg/kg), memantine (1 mg/kg), or saline solution 30 min before each session and injected with 8-OH-DPAT (“OH” groups) or saline (“saline” groups) right before the experiment. We found that repeated application of 8-OH-DPAT during both habituation and acquisition significantly increased locomotion, but it impaired the ability to avoid the shock sector. However, the application of 8-OH-DPAT in habituation had no impact on the learning process if discontinued in acquisition. Similarly, memantine and riluzole did not affect the measured parameters in the “saline” groups, but in the “OH” groups, they significantly increased locomotion. In addition, riluzole increased the number of entrances and decreased the maximum time avoided of the shock sector. We conclude that monotherapy with glutamate-modulating agents does not reduce but exacerbates cognitive symptoms in the animal model of OCD.

**Keywords:** obsessive-compulsive disorder; 8-OH-DPAT; memantine; riluzole; spatial learning; memory



**Citation:** Janikova, M.; Mainerova, K.; Vojtechova, I.; Petrasek, T.; Svoboda, J.; Stuchlik, A. Memantine and Riluzole Exacerbate, Rather Than Ameliorate Behavioral Deficits Induced by 8-OH-DPAT Sensitization in a Spatial Task. *Biomolecules* **2021**, *11*, 1007. <https://doi.org/10.3390/biom11071007>

Academic Editors: Alexander V. Kulikov and Salvatore Cuzzocrea

Received: 2 April 2021

Accepted: 6 July 2021

Published: 9 July 2021

**Publisher's Note:** MDPI stays neutral with regard to jurisdictional claims in published maps and institutional affiliations.



**Copyright:** © 2021 by the authors. Licensee MDPI, Basel, Switzerland. This article is an open access article distributed under the terms and conditions of the Creative Commons Attribution (CC BY) license (<https://creativecommons.org/licenses/by/4.0/>).

## 1. Introduction

Obsessive-compulsive disorder (OCD) is a severe neuropsychiatric disorder affecting 1–3% of the population worldwide [1]. It is often chronic and can be very debilitating. Patients with OCD suffer from obsessions, which are recurring intrusive thoughts, and compulsions, which are ritualized stereotypic behaviors usually driven by the anxiety arising from the obsessions [2]. Patients describe the mechanism of OCD as anxiety created by obsessions being released with compulsions. This cycle is often very time and resource consuming and can destroy one's ability to concentrate or perform basic daily tasks [2]. Apart from the core symptoms of OCD—obsessions and compulsions—deficits in executive functions and other cognitive domains have been described [3,4]. Patients with OCD have decreased cognitive flexibility measured in different set-shifting tasks [4] and also worse results in spatial cognitive flexibility tasks in virtual reality [5–7].

Disruption of neurotransmitter systems is considered to play a role in the pathophysiology of OCD (for a review, see Goodman et al. [8]). The hypothesis of the involvement of serotonin in the pathophysiology of OCD is popular, mainly due to the effectiveness of selective serotonin reuptake inhibitors (SSRIs) in the treatment of OCD. Additionally, an association of OCD with genes coding components of the serotonin system, such as monoamine oxidase A, or genes encoding the serotonin receptors has been shown (reviewed by Derksen et al. [9]). Moreover, agonizing serotonin receptors with meta-chlorophenyl piperazine (mCPP) and antagonizing serotonin 2A and 2C receptors with ritanserin exacerbates OCD symptoms in humans, as well as in animal models [10,11]. Contrarily, agonizing serotonin 1A/2A/2C receptors with psilocybin reduces OCD symptoms [12]. The specificity of serotonin involvement in OCD is not clear yet. It is possible that other neurotransmitter systems, such as the glutamate system, are involved, and this can be underlined by the fact that approximately 10% to 60% of patients still do not fully respond to SSRIs [13]. Glutamate is the primary excitatory neurotransmitter in the brain, and its function seems disrupted in patients with OCD [14]. Higher glutamate concentrations were found in patients with OCD in the cerebrospinal fluid [15], the orbitofrontal cortex [16], and caudate nucleus [17], and lower in the anterior cingulate cortex [17]. Therefore, there have been attempts to study glutamate-modulating agents as a possible treatment of OCD. Drugs with different mechanisms of action have been tested, such as N-methyl-D-aspartate (NMDA) receptor antagonist amantadine, a partial agonist of NMDA receptor D-cycloserine, or NMDA receptor antagonist ketamine [18–20]. Several clinical trials and case reports suggested the efficiency of memantine (a non-competitive low-affinity NMDA receptor antagonist) and riluzole (a drug that decreases presynaptic glutamate release by blocking sodium channels). Riluzole is an anticonvulsant drug, nowadays officially used for the treatment of amyotrophic lateral sclerosis, and off-label, it is used for the treatment of some psychiatric conditions, including OCD [21,22]. Memantine is now used for the treatment of severe Alzheimer's disease. Several case studies have reported its efficacy for patients with treatment-refractory OCD [23,24]. In a meta-analysis of double-blinded, placebo-controlled, randomized studies made by Kishi et al. [25], memantine was valued as a valid treatment for patients with SSRI-refractory OCD symptoms. Adding memantine to the SSRIs significantly improved symptoms of OCD in patients [26].

Animal models of OCD are important tools to study this disorder with yet unknown pathophysiology. They also serve for designing and validating possible treatments. One of the pharmacological animal models of OCD is the chronic sensitization to 8-OH-DPAT, an agonist of serotonin 1A and 7 receptors. Application of this drug induces behavioral sensitization, which leads to perseverative and compulsive behaviors [27,28]. Both rats and mice treated with 8-OH-DPAT exhibit perseverative behavior and decreased spontaneous alternation in Y-maze and T-maze [29,30] and repetitive stereotypical behavior in an open-field arena [27]. In this study, we aimed to test the effects of riluzole and memantine on locomotor activity and spatial learning in the 8-OH-DPAT model of OCD. We tested these domains in chronically sensitized rats after acute administration of 8-OH-DPAT and also in chronically sensitized rats, but not after acute administration of 8-OH-DPAT. We used an acquisition configuration in the active place avoidance task on a rotating arena (Carousel maze), which is a well-established task for rats and mice, allowing simultaneous assessment of spatial learning and locomotor stimulation [31,32] (for a review, see Stuchlík et al. [33]).

## 2. Materials and Methods

### 2.1. Animals

Adult (4–5 months old) male Long–Evans rats from the breeding colony of the Institute of Physiology of the Czech Academy of Sciences were used in this experiment (98 animals in total). At the beginning of the experiment, they weighed approximately 400–500 g. Rats were housed in pairs in an animal room with a stable temperature and 12/12 light/dark cycle, with food and water always freely available. The acquisition testing was preceded

by 5 days of handling and 10 sessions of habituation to the experimental arena, during which sensitization to the drugs took place.

## 2.2. Drugs and Design

8-OH-DPAT (Sigma-Aldrich, Prague, Czech Republic, Cat. No. H8520), Memantine hydrochloride (Sigma-Aldrich, Prague, Czech Republic, Cat. No. M9292), and riluzole (Sigma-Aldrich, Prague, Czech Republic, Cat. No. R116) were dissolved in sterile saline (0.9% NaCl) at concentrations of 0.25 mg/mL, 1 mg/mL, and 1 mg/mL, respectively. The experiment consisted of a habituation phase and an acquisition phase. In the habituation phase, subcutaneous injection of 8-OH-DPAT (N = 84, 0.25 mg/kg; 1 mL/kg) or sterile saline (N = 14; 1 mL/kg) was given to the animals immediately before they were placed onto the rotating arena without any shocks (see Section 2.3). In the acquisition phase, the 8-OH-DPAT group was randomly divided into six groups according to the treatment plan, which proceeded as follows: 30 min before being put into the apparatus, animals received subcutaneous injections of either saline (1 mL/kg), riluzole (1 mg/kg; 1 mL/kg), or memantine (1 mg/kg; 1 mL/kg). The dose of 1 mg/kg was chosen based on the results of our previous study [34], where a higher dose (5 mg/kg) had a detrimental effect on learning and locomotion in quinpirole-treated rats. Furthermore, the therapeutic effect of riluzole in the dose of 1 mg/kg has been described [35], and subcutaneous application of memantine (1 mg/kg) leads to a similar plasmatic concentration (1  $\mu$ M) in rats as found in patients treated with a standard dose of 20 mg/daily [36]. Immediately before placement into the apparatus, animals received a subcutaneous injection of saline (“saline” groups) or 8-OH-DPAT (“OH” groups) at a dose of 0.25 mg/kg, which has previously been described as an effective dose [27]. The design of the treatment groups can be seen in Table 1.

**Table 1.** The design of the treatment groups.

Habituation	N	Acquisition		N	Group	Description
		30 min before the Test	Before the Test			
Saline	14	Saline	Saline	14	SAL-SAL <sup>a</sup>	Global controls
8-OH-DPAT	84	Saline	Saline	14	OH-SAL <sup>a</sup>	Sensitized/undrugged/untreated
8-OH-DPAT		Memantine	Saline	14	MEM-SAL <sup>a</sup>	Sensitized/undrugged/memantine treated
8-OH-DPAT		Riluzole	Saline	14	RIL-SAL <sup>a</sup>	Sensitized/undrugged/riluzole treated
8-OH-DPAT		Saline	8-OH-DPAT	14	OH-OH <sup>b</sup>	Sensitized/drugged/untreated
8-OH-DPAT		Memantine	8-OH-DPAT	14	MEM-OH <sup>b</sup>	Sensitized/drugged/memantine treated
8-OH-DPAT		Riluzole	8-OH-DPAT	14	RIL-OH <sup>b</sup>	Sensitized/drugged/riluzole treated

<sup>a</sup> All groups that received saline during acquisition are referred to as “saline” groups. <sup>b</sup> All groups that received 8-OH-DPAT during acquisition are referred to as “OH” groups.

## 2.3. Apparatus and Behavioral Procedures

### 2.3.1. Active Place Avoidance Task in Carousel Maze

All experiments were conducted on a rotating arena (Carousel maze) (Figure 1A). The Carousel maze was a smooth metallic disk of a circular shape (diameter of 82 cm) enclosed by a 60 cm high transparent polyacrylic wall in a conical shape (to prevent reflections to the camera). The arena rotated clockwise (1 revolution per min) and was elevated 1 m above the floor. An unmarked to-be-avoided sector (60 degrees) was stable and defined in room-frame coordinates during the acquisition testing. In the sector, animals received a mild, 500 ms long electric shock through a subcutaneous needle implanted between their shoulders. Rats received shocks in 1800 ms intervals until they left the sector. The foot shocks were kept at the lowest possible level (0.2–0.6 mA) and were titrated for each subject, so they would be unpleasant but not painful and hence would not produce freezing in the animals (for a protocol, see Willis et al. [37]). To monitor the animals in the apparatus, they wore a small rubber jacket on their back with an infrared light-emitting diode (LED) attached. Another LED was mounted on the arena periphery and monitored the rotation, allowing the reconstructions of trajectories in the coordinate frames of the arena and room.



Signals from both LEDs were captured by an analog overhead camera (Figure 1B), digitized by the DT-3155 card (Data Translation, Marlborough, MA, USA), and recorded on a PC located in an adjacent room (Figure 1C) with an online tracking program (Tracker, BioSignal Group, New York, NY, USA). An open-source software, Carousel Maze Manager [38], was used to analyze the trajectories offline and extract the evaluated parameters.

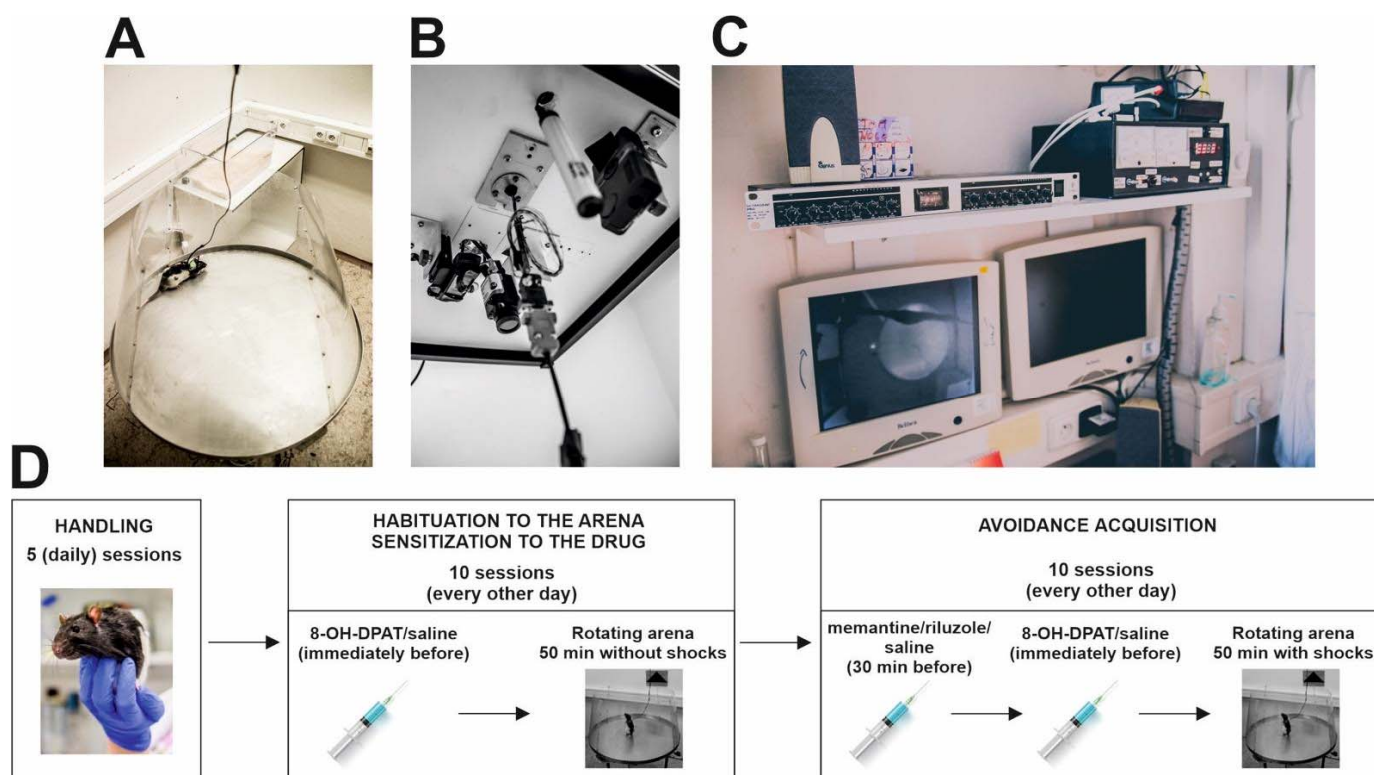


**Figure 1.** Experimental setup and design. (A) Rotating Carousel maze. (B) Camera recording the movement of experimental rats and cable with an infrared light-emitting diode attached to the ceiling above the Carousel maze. (C) Experiments were monitored on computers from an adjacent room. (D) Design of the experiment.

### 2.3.2. 8-OH-DPAT Sensitization and Habituation to the Arena

The sensitization to 8-OH-DPAT was performed during the ten-session habituation to the arena (10 injections every other day), providing the chronic model. The rats were injected with 8-OH-DPAT (0.25 mg/kg) or saline (1 mL/kg). Immediately after the injection, the rats were put into the rotating Carousel maze without the activated shock sector, so they could explore freely and habituate to the rotating arena for 50 min.

### 2.3.3. Acquisition Testing

Before the acquisition phase, conscious animals were gently implanted with a subcutaneous needle piercing the rats' skin between their shoulders. The sharp end of the needle was cut and bent to form a small loop, which was connected to a source for the mild electric shocks via an alligator clip. In the acquisition phase, active place avoidance testing was conducted. The animals were tested every other day with a total of 10 days/10 injections. Rats were injected with riluzole, memantine (both at a dose of 1 mg/kg), or saline, 30 min before each trial. Immediately before the session, rats were injected with saline again or with 8-OH-DPAT (0.25 mg/kg, Figure 1D). Subsequently, they were placed into the maze to the side opposite the shock sector. The arena rotated for the whole 50 min of the trial at a speed of 1 revolution per minute. As the position of the "to-be-avoided" sector was not marked, animals had to use stable extra maze cues (e.g., door, shelves, windows, posters on the wall) to avoid the sector.

## 2.4. Data Analysis and Statistics

The main parameters measured were locomotion (measured as the total distance walked during the whole session (m)), the number of errors/entrances (measured as the number of entrances into the to-be-avoided sector), maximum time avoided (measuring maximum interval without entrance to the to-be-avoided sector in a given session (s)), and median speed after shock (measuring the angular velocity (deg/s)). A low number of entrances represents good learning (low errors), unimpaired memory, and an efficient avoiding strategy. Furthermore, the first and the last sessions were dissected into five consecutive 10 min intervals to assess the within-session learning (Supplementary Figure S1). An independent *t*-test was used to test between-group differences on the first and the last day of habituation. Mixed-effect regression was further used to compare all treatment groups in the acquisition phase. Analysis of all parameters, with the exception of locomotion, was performed on root transformed data in SPSS (IBM SPSS, version 23, Chicago, IL, USA) and jamovi (version 1.1.9.0) software. One rat was excluded from the final analysis due to technical problems during the acquisition phase.

## 3. Results

### 3.1. Habituation

To assess whether successful sensitization to 8-OH-DPAT took place, we first compared the locomotion of rats from the 8-OH-DPAT and saline groups on the last day of habituation. Animals in the 8-OH-DPAT group had significantly higher locomotion in comparison to the saline group  $t(83) = -8.54, p < 0.001, 95\% \text{ CI} = [-317, 197]$ . Interestingly, rats sensitized with 8-OH-DPAT had significantly higher locomotion even from the first day of habituation  $t(789.3) = 3.44, p < 0.001, 95\% \text{ CI} = [35.48, 129.2]$ , which shows the acute effect of the drug (Figure 2).

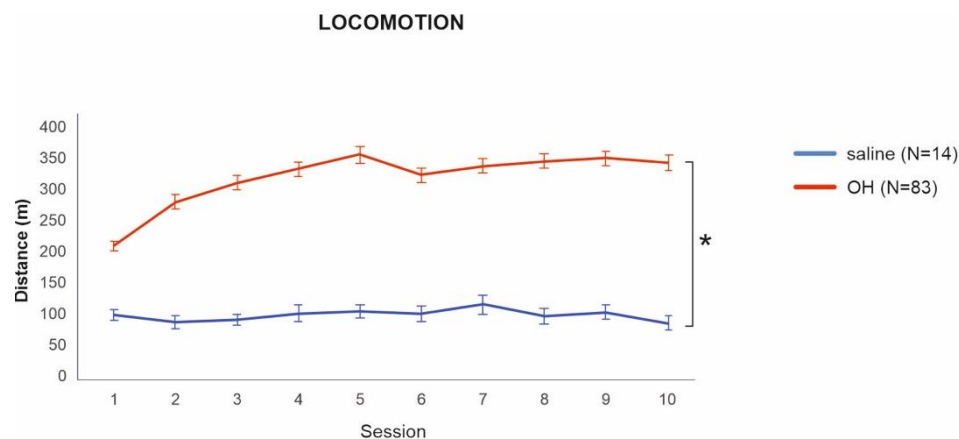


**Figure 2.** Locomotion of the 8-OH-DPAT and saline groups during habituation. Locomotion in the 8-OH-DPAT group was significantly higher from the first day of sensitization/habituation throughout all 10 sessions. \* denotes a significant difference at  $p = 0.001$ . Data are presented as mean values  $\pm$  SEM.

### 3.2. Acquisition

#### 3.2.1. Locomotion

Table 1 shows the group design. Acute treatment with 8-OH-DPAT caused significantly higher locomotion in all the “OH” groups compared to the “saline” groups that received 8-OH-DPAT only during habituation. Both riluzole and memantine in the RIL-OH and MEM-OH groups further aggravated the hyperlocomotion compared to the OH-OH group. Memantine and riluzole had, however, no effect in the “saline” groups. The “saline” groups did not significantly differ from each other

The locomotion significantly differed between groups [ $F(6, 90) = 35.58, p < 0.001$ ], but not between sessions, as reflected by an absence of the main effect of session [ $F(9, 809) = 1.65,$

$p = 0.098$ ] or group\*session interaction [ $F(54, 809) = 1.11, p = 0.273$ ]. Simple and repeated planned contrasts showed that the OH-OH group had significantly higher locomotion than the OH-SAL and SAL-SAL groups ( $p < 0.001$ ). On the other hand, the OH-SAL group did not significantly differ from the SAL-SAL group. The MEM-SAL and RIL-SAL groups also did not have different locomotion from the SAL-SAL group, the OH-SAL group, or from each other. Importantly, the MEM-OH and RIL-OH groups had significantly higher locomotion than the OH-OH group ( $p < 0.001$  or  $p = 0.020$ , respectively), but not from one another ( $p = 0.123$ ). For results, see Table 2 and Figure 3A.

**Table 2.** Simple and repeated planned contrast results of the between-group difference in the locomotion.

Parameter	Treatment Group Differences	df	t	p	95% CI
Locomotion	SAL-SAL * OH-SAL	90	0.164	0.870	−37.08, 43.860
	SAL-SAL * MEM-SAL	90	0.664	0.509	−27.27, 55.206
	SAL-SAL * RIL-SAL	90	0.368	0.714	−32.86, 48,073
	OH-SAL * MEM-SAL	90	0.503	0.616	−30.66, 51.814
	OH-SAL * RIL-SAL	90	0.204	0.839	−36.255, 44.681
	MEM-SAL * RIL-SAL	90	0.302	0.764	−32.86, 48.073
	OH-OH * SAL-SAL	90	−5.819	<0.001	−160.63, 79.687
	OH-OH * OH-SAL	90	−5.655	<0.001	−157.24, −76.295
	OH-OH * MEM-OH	90.1	3.919	<0.001	40.45, 121.408
	OH-OH * RIL-OH	90	2.363	0.020	8.33, 89.271
	MEM-OH * RIL-OH	90	−1.556	0.123	−72.61, 8.341

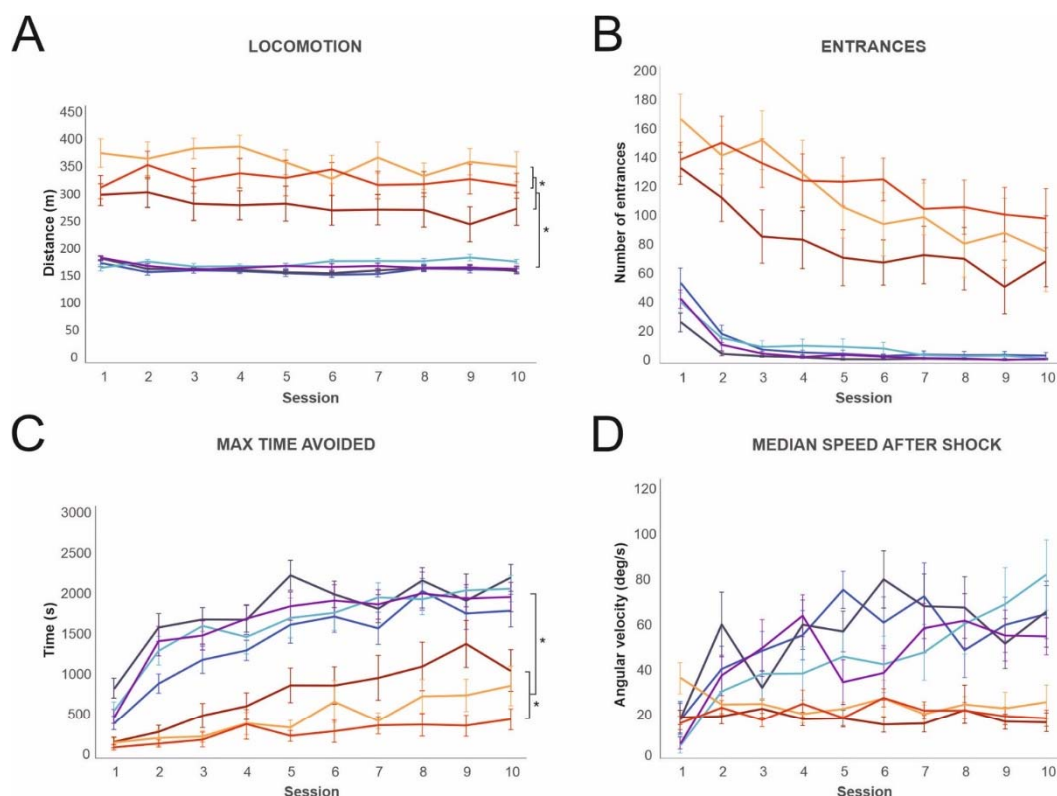


**Figure 3.** Cont.

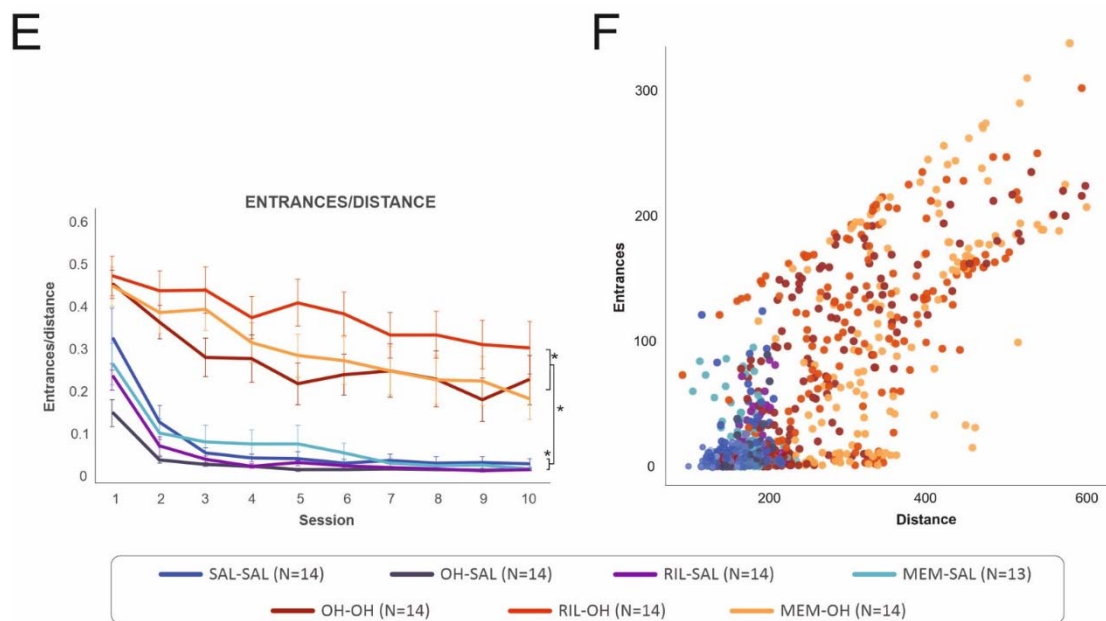


**Figure 3.** The behavior of all treatment groups during the 10 acquisition sessions in the five measured parameters. (A) Locomotion was stable during all 10 sessions for each group, although it was significantly higher in the “OH” compared to the “saline” groups. The MEM-OH and RIL-OH groups had significantly higher locomotion compared to the OH-OH group. (B) The number of entrances to the shock sector decreased across sessions, but it was significantly higher in the “OH” groups compared to the “saline” groups during all 10 sessions. The RIL-OH and MEM-OH groups had the highest number of entrances to the shock sector. (C) Maximum time avoided increased from the first to the last session and was significantly higher in the “saline” groups than in the “OH” groups. (D) Median speed after shock did not change in the “OH” groups and only slightly increased in the “saline” groups, but with noticeable variation across sessions. (E) The entrances/distance parameter showed that the “OH” groups had a higher number of entrances compared to the “saline” groups, and the RIL-OH group had the highest number of entrances even when controlled for locomotion. The OH-SAL and RIL-SAL groups had the lowest number of entrances per distance. (F) Correlation of locomotion and number of entrances. A higher number of entrances correlated with hyperlocomotion in some animals from the “OH” groups. \* denotes a significant difference at  $p = 0.05$ . Data are presented as mean values  $\pm$  SEM with exception of Figure 3F, which presents each trial for each animal.

### 3.2.2. Entrances to the Shock Sector

The “OH” groups had a significantly higher number of entrances to the shock sector compared to the “saline” groups, suggesting decreased spatial learning ability after acute treatment with 8-OH-DPAT. Learning deficit was further exacerbated by memantine in the MEM-OH group (although not significantly) and riluzole in the RIL-OH group (significantly). There was no significant difference between the “saline” groups (Figure 3B). For a graphical illustration of typical trajectories of all treatment groups, see Figure 4.

Analysis showed significant main effects of group [ $F(6, 91) = 32.35, p < 0.001$ ], session [ $F(9, 818) = 63.84, p < 0.001$ ], and group\*session interaction [ $F(54, 818) = 1.87, p < 0.001$ ]. Simple and repeated planned contrasts further revealed that the OH-OH group had a significantly higher number of entrances than the OH-SAL and SAL-SAL groups ( $p < 0.001$ ). The OH-SAL, MEM-SAL, and RIL-SAL groups did not have a significantly different number of entrances to the shock sector than the SAL-SAL group; the MEM-SAL and RIL-SAL groups also did not differ from each other or the OH-SAL group. While the MEM-OH group showed only a trend toward an increased number of entrances in comparison to the OH-OH group ( $p = 0.072$ ), the RIL-OH group had a significantly higher number of entrances than the OH-OH group ( $p = 0.007$ ). The MEM-OH group did not differ from the RIL-OH group in the number of entrances (for results, see Table 3). Rats had also a significantly lower number of entrances between the first and second sessions ( $p < 0.001$ ) and the second and third sessions ( $p = 0.002$ ). The difference between the third and fourth



sessions was close to the significance level ( $p = 0.051$ ). However, planned contrasts showed almost no significant difference in group\*session interaction. The significance was probably caused by the difference between the “saline” and “OH” groups. The “saline” groups had an almost stable number of entrances from the third day on, while the number of entrances in the “OH” groups continuously decreased from the first to late acquisition sessions, although remaining very high on the last day.

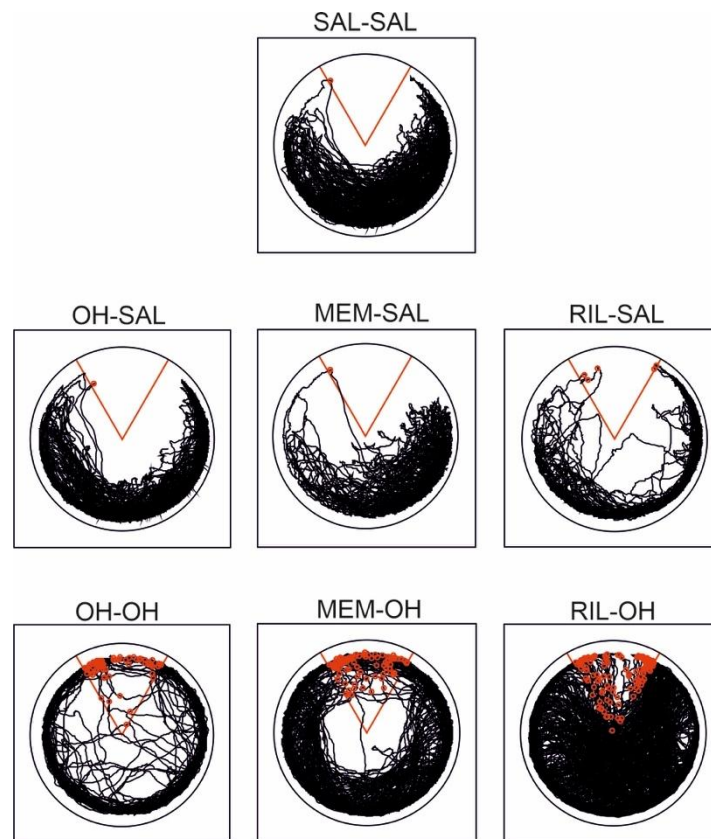


**Figure 4.** Typical trajectories of treatment groups on the 10th day of acquisition. The “to-be-avoided” sector is marked in red, and shocks received are marked as red circles. The SAL-SAL (control group) and OH-SAL groups avoided the sector well. Similarly, the MEM-SAL and RIL-SAL groups had a comparably good performance. All groups that received 8-OH-DPAT also during acquisition were more active, and they did not avoid the shock sector efficiently. The RIL-OH group had the highest locomotion and number of entrances to the to-be-avoided sector.

**Table 3.** Simple and repeated planned contrast results of the between-group difference in the number of entrances.

Parameter	Treatment Group Differences	df	t	p	95% CI
Entrances	SAL-SAL * OH-SAL	90	−0.839	0.404	−2.635, 1.06
	SAL-SAL * MEM-SAL	90	−0.009	0.992	−1.890, 1.87
	SAL-SAL * RIL-SAL	90	−0.413	0.681	−2.234, 1.46
	OH-SAL * MEM-SAL	90	−0.944	0.348	−2.734, 0.957
	OH-SAL * RIL-SAL	90	0.814	0.418	−1.099, 2.661
	MEM-SAL * RIL-SAL	90	0.395	0.694	−1.501, 2.260
	OH-OH * SAL-SAL	90	5.529	<0.001	3.360, 7.05
	OH-OH * OH-SAL	90	−6.368	<0.001	−7.84, 4.150
	OH-OH * MEM-OH	90	−1.82	0.072	−3.56, 0.13
	OH-OH * RIL-OH	90	2.767	0.007	0.76, 4.45
	MEM-OH * RIL-OH	90	0.944	0.348	−2.734, 0.957

### 3.2.3. Maximum Time Avoided

Groups acutely treated with 8-OH-DPAT had a significantly lower maximum time avoided compared to the “saline” groups. Riluzole in the RIL-OH group significantly worsened the performance, leading to the RIL-OH group having a significantly lower maximum time avoided than the OH-OH group. Similarly, the MEM-OH group had a considerably, but not significantly, lower maximum time avoided compared to the OH-OH group. There was no significant difference between the “saline” groups (Figure 3C).

A main effect of group [ $F(6, 90) = 28.05, p < 0.001$ ], session [ $F(9, 809) = 69.04, p < 0.001$ ], and group\*session interaction [ $F(54, 809) = 1.97, p < 0.001$ ] was found. As shown by simple and repeated planned contrasts, rats in the OH-OH group were able to avoid the shock sector for a significantly shorter maximum time between two shocks than rats in the OH-SAL and SAL-SAL groups ( $p < 0.001$ ). Again, the MEM-SAL and RIL-SAL groups did not differ from the SAL-SAL and OH-SAL groups and each other. Contrarily, the RIL-OH group had a significantly shorter maximum time avoided than the OH-OH group ( $p = 0.002$ ), and the MEM-OH group had a substantially, although not significantly, shorter maximum time avoided than the OH-OH group ( $p = 0.054$ ). Again, the MEM-OH and RIL-OH groups did not differ from each other (for results, see Table 4). There was also a significant difference between the first and second ( $p < 0.001$ ), second and third ( $p = 0.008$ ), fourth and fifth ( $p = 0.020$ ), and the seventh and eighth sessions ( $p = 0.007$ ), suggesting a slow increase of maximum time avoided in all groups during the whole acquisition training.

**Table 4.** Simple and repeated planned contrast results of the between-group difference in the maximum time avoided of the shock sector.

Parameter	Treatment Group Differences	df	t	p	95% CI
Max time avoided	SAL-SAL * OH-SAL	90	1.858	0.067	−0.307, 11.430
	SAL-SAL * MEM-SAL	90	0.93	0.355	−3.14, 8.82
	SAL-SAL * RIL-SAL	90	1.155	0.251	−2.411, 9.326
	OH-SAL * MEM-SAL	90	−0.892	0.375	−8.702, 3.258
	OH-SAL * RIL-SAL	90	−0.703	0.484	−7.97, 3.765
	MEM-SAL * RIL-SAL	90	−0.203	0.840	−6.598, 5.362
	OH-OH * SAL-SAL	90	−3.696	<0.001	−995.5, −305.5
	OH-OH * OH-SAL	90	5.926	<0.001	11.875, 23.61
	OH-OH * MEM-OH	90	1.955	0.054	−0.0014, 11.725
	OH-OH * RIL-OH	90	−3.11	0.002	−15.184, −3.45
	MEM-OH * RIL-OH	90	1.155	0.251	−2.41, 9.330

### 3.2.4. Median Speed after Shock

Increased locomotor speed after shock, as well as visual observation of the animals, showed that all animals were able to perceive the shock and react to it. However, the “OH” groups had slower escape reactions than the “saline” groups (Figure 3D). We found significant main effects of group [ $F(6, 88.4) = 8.93, p < 0.001$ ], session [ $F(9, 768) = 8.71, p < 0.001$ ], and group\*session interaction [ $F(54, 767.8) = 2.63, p < 0.001$ ]. Simple and repeated planned contrasts revealed that the OH-OH group had a significantly lower median speed after shock than the OH-SAL and SAL-SAL groups ( $p < 0.001$ ). The OH-SAL and SAL-SAL groups were not significantly different in median speed after shock, and the MEM-SAL and RIL-SAL groups did not differ from the SAL-SAL and OH-SAL groups or from each other. Similarly, the MEM-OH and RIL-OH groups were not significantly different from the OH-OH group or from each other (for results, see Table 5). Furthermore, there was a significant difference between the first and second sessions ( $p < 0.001$ ). For significant interaction results, see interaction Table S1 in the Supplementary Materials.

**Table 5.** Simple and repeated planned contrast results of the between-group difference in the median speed after shock.

Parameter	Treatment Group Differences	df	t	p	95% CI
Median speed after shock	SAL-SAL * OH-SAL	90	0.119	0.906	−1.019, 1.150
	SAL-SAL * MEM-SAL	90	−1.3996	0.165	−1.897, 0.316
	SAL-SAL * RIL-SAL	90	−1.365	0.176	−1.838, 0.329
	OH-SAL * MEM-SAL	90	0.3999	0.689	−1.987, 3.006
	OH-SAL * RIL-SAL	90	−0.021	0.983	−2.476, 2.424
	MEM-SAL * RIL-SAL	90	−0.4204	0.674	−3.032, 1.961
	OH-OH * SAL-SAL	90	4.954	<0.001	1.653, 3.817
	OH-OH * OH-SAL	90	5.0849	<0.001	1.721, 3.880
	OH-OH * MEM-OH	90	1.089	0.279	−0.478, 1.673
	OH-OH * RIL-OH	90	0.554	0.581	−0.770, 1.378
	MEM-OH * RIL-OH	90	−0.537	0.593	−1.366, 0.778

### 3.2.5. Entrances/Distance

The number of entrances is strongly influenced by locomotion (see Figure 3F), as hyperactive animals are more likely to enter the sector by chance. To exclude the possibility that the differences in the number of errors were only driven by locomotor activity, we calculated the ratio of the number of entrances to the walked distance for each animal and each session. Statistical analysis of this parameter showed that the “OH” groups had more entrances per unit of distance, suggesting an impairment of their ability to avoid the sector which was independent of elevated locomotion (Figure 3E).

Analysis showed a significant effect of group [ $F(6, 606) = 125.562, p < 0.001$ ] and session [ $F(9, 833) = 20.729, p < 0.001$ ]. Group\*session interaction was not significant [ $F(54, 833) = 0.687, p = 0.958$ ]. Simple and repeated planned contrasts revealed that the OH-OH group had a significantly higher number of entrances per walked distance compared to the OH-SAL and SAL-SAL groups ( $p < 0.001$ ). Interestingly, the OH-SAL group was not significantly different from the RIL-SAL group, but both groups had a significantly lower entrances/distance parameter compared to the SAL-SAL ( $p < 0.001$  or  $p = 0.014$ , respectively) and MEM-SAL groups ( $p = 0.001$  or  $p = 0.030$ , respectively), suggesting the OH-SAL and RIL-SAL groups had a slightly lower number of entrances per similar distance than the MEM-SAL and SAL-SAL groups. Similarly, the MEM-OH group was not significantly different from the OH-OH group, but the RIL-OH had a significantly higher number of entrances per distance compared to the OH-OH ( $p < 0.001$ ) and MEM-OH groups ( $p = 0.003$ ) (for results, see Table 6). A significant difference was also between the first and second sessions ( $p < 0.001$ ), and the difference between the second and third sessions was approaching significance ( $p = 0.053$ ).

**Table 6.** Simple and repeated planned contrast results of the between-group difference in the number of entrances per unit of distance.

Parameter	Treatment Group Differences	df	t	p	95% CI
Entrances/distance	SAL-SAL * OH-SAL	346.8	3.36	<0.001	0.034, 0.1141
	SAL-SAL * MEM-SAL	606.9	−0.4557	0.649	−0.048, 0.0299
	SAL-SAL * RIL-SAL	443.6	2.463	0.014	0.0105, 0.0920
	OH-SAL * MEM-SAL	550.3	3.297	0.001	0.0264, 0.1037
	OH-SAL * RIL-SAL	529.5	1.151	0.250	−0.0161, 0.0618
	MEM-SAL * RIL-SAL	819.5	2.1692	0.030	0.0041, 0.0803
	OH-OH * SAL-SAL	440.3	−9.714	<0.001	−0.2381, −0.1581
	OH-OH * OH-SAL	405.3	−13.552	<0.001	−0.312, −0.233
	OH-OH * MEM-OH	777.2	1.1267	0.260	−0.0157, 0.0581
	OH-OH * RIL-OH	782.3	4.321	<0.001	0.0437, 0.1164
	MEM-OH * RIL-OH	731.5	2.995	0.003	0.0203, 0.0974

#### 4. Discussion

We found that acute systemic administration of 8-OH-DPAT (0.25 mg/kg) to rats immediately before the 50 min session in the arena elicited a strong hyperlocomotion and impaired learning and avoidance of the shock sector. In addition, rats that received 8-OH-DPAT did not accelerate the escape reaction throughout training as did the control groups. Visual inspection of their reaction revealed they preserved the responsiveness to electrical shocks, but their escape route was less spatially organized to effectively leave the “to-be-avoided” sector, suggesting poor spatial knowledge of the environment. Contrary to hyperlocomotion we observed after acute administration of 8-OH-DPAT, in another study, authors described a decrease in locomotor activity and also a perseverative behavior and learning deficit [29]. However, they tested mice in a different task (non-aversive T-maze) and used higher doses of 8-OH-DPAT (1 or 2 mg/kg) than we did. It could indicate a dose-dependent effect on animal behavior with the lower doses stimulating and higher doses inhibiting impact. Alternatively, animals after 8-OH-DPAT application may react differently when solving the task under stress with an aversive motivation compared to non-aversive tasks.

We also observed only the acute effect of 8-OH-DPAT. Only the “OH” groups injected with 8-OH-DPAT (0.25 mg/kg) during habituation/sensitization and subsequently in the acquisition had higher locomotion. If the drug application was discontinued after the end of the habituation phase, sensitization to 8-OH-DPAT during habituation had no effect on spatial performance and locomotion during acquisition. Contrarily, Johnson and Szechtman [39] found that chronic administration of 8-OH-DPAT at low doses (0.0625, 0.125 mg/kg) per 8 days produced hyperlocomotion and compulsive checking even when tested after several days without the 8-OH-DPAT. However, it should be noted that the difference between spontaneous behavior (open field) and motivated behavior (carousel maze) might add up to the divergence of results. Furthermore, we tested the locomotion and cognitive skills, not the manifestation of the compulsion-like behavior per se (checking).

Memantine and riluzole significantly increased locomotion in rats acutely treated with 8-OHDPAT, even above the OH-OH group level. In the case of memantine, this effect could have been induced by the stimulatory effect of memantine itself, as it was found to produce hyperlocomotion in higher doses (5 mg/kg) [40] and dose-dependent (from 3 mg/kg) decrease of impulsivity [41]. Regarding riluzole, a previous study showed decreased behavioral and motor activity, as well as an analgesic effect, albeit at a dose four times higher (4 mg/kg) than we used in the present study [42]. At our doses (1 mg/kg), there was no effect of memantine or riluzole in the “saline” groups.

Interestingly, the learning deficit was further aggravated with the application of memantine or riluzole (1 mg/kg), and the RIL-OH group had the overall highest number of entrances to the shock sector. The RIL-OH and MEM-OH groups had only a very slight improvement over the whole acquisition testing (Figure 3B) and no improvement within a session (Supplementary Figure S1B). This is in agreement with the previously shown lack of any beneficial effect of memantine and riluzole on the quinpirole model of cognitive deficit related to OCD [34], but contrasts the positive memantine’s effect in relieving serotonin-induced compulsive scratching behavior in mice (however, in this case, at a ten-times higher dose, 10 mg/kg, and added to fluoxetine) [43]. In a marble-burying model of compulsive behavior, memantine (10 mg/kg) was effective in suppressing the marble-burying behavior in rats without affecting locomotion. Riluzole (10 mg/kg) was not effective in alleviating marble-burying behavior at all, although it decreased motor behavior [44].

One of the possible explanations for our observed results showing the potentiation of the 8-OH-DPAT effect with memantine and riluzole may be their action upon different brain structures. 8-OH-DPAT presynaptically blocks AMPA receptors and glutamate release through activation of 5-HT<sub>1A</sub> receptors. Nevertheless, as a 5-HT<sub>7</sub> receptor agonist, it also enhances AMPA activity postsynaptically and CA3-CA1 synaptic transmission in the hippocampus [45]. Additionally, 8-OH-DPAT modulates glutamate transmission induced



by exogenous AMPA administration [43]. Together with 8-OH-DPAT inhibiting LTP by 5-HT<sub>1A</sub>, memantine and riluzole can disturb learning and memory by further decreasing the glutamate levels. Besides the hippocampus, 8-OH-DPAT reduces excitation in the entorhinal cortex [46]. 5-HT<sub>1A</sub> and 5-HT<sub>7</sub> receptors inhibit glutamate transmission in the frontal cortex and also in the cerebellum and many other structures involved in the motor and affective behavior (for a review, see Ciranna et al. [47]).

Our results are analogous to those of our laboratory's previous study, which showed that riluzole and memantine exerted similar exacerbating effects in an animal model of OCD induced by dopamine receptor agonist quinpirole [34]. This shows that quinpirole and 8-OH-DPAT models might not respond well to anti-glutamatergic monotherapy by riluzole or memantine at lower doses. Possibly, higher doses of memantine or riluzole are needed to affect symptoms of quinpirole and 8-OH-DPAT animal models of OCD. However, such doses are often accompanied by side effects, such as motor inhibition or analgesia. In human studies, riluzole and memantine were effective as augmentation therapy of treatment-refractory OCD [21]. However, they did not work for all of the patients, and studies done with riluzole are limited by their small sizes. Memantine was effective in several case studies [23,24], as well as in one randomized study [25]. However, both memantine and riluzole were effective only when given together with existing treatment with SSRIs, and they were not examined alone [25,48,49]. Importantly, we measured the effect of memantine and riluzole on cognitive deficit rather than on OCD-like symptoms, which is the main focus of before mentioned human studies. Our results imply that the use of glutamate-modulating drugs in monotherapy might not be a viable treatment option for cognitive deficits induced in pharmacological animal models of OCD, although they may still work for obsessive-compulsive symptoms. It might be worth examining other doses of memantine and riluzole in future research.

**Supplementary Materials:** The following materials are available online at <https://www.mdpi.com/article/10.3390/biom11071007/s1>, Figure S1: Behavior of all treatment groups during the first and the last acquisition sessions dissected in five 10 min intervals, Table S1: Significant interactions.

**Author Contributions:** M.J.: investigation, data analysis and visualization, writing—original draft preparation; K.M.: investigation, data analysis and visualization, writing—original draft preparation; I.V.: writing and editing; T.P.: writing and editing; J.S.: supervision and editing; A.S.: conceptualization and methodology, supervision, writing and editing. All authors have read and agreed to the published version of the manuscript.

**Funding:** The study was supported mainly by the Czech Health Research Council (AZV), Grant NU20-04-00147. The institution and infrastructure support was provided by the ERDF project, OPVK Microscopic System CZ.2.16/3.1.00/28034, ERDF OPVK BrainView CZ.2.16/3.1.00/21544, and MEYS (LM2015062) Czech-BioImaging.

**Institutional Review Board Statement:** All animal manipulations complied with the Animal Protection Code of the Czech Republic and a corresponding directive of the European Community Council on the use of laboratory animals (2010/63/EU) and were approved by the Local and the Ministry's Animal Care Committees (Project of Experiments, No. 50/2016, 80/2016).

**Informed Consent Statement:** Not applicable.

**Data Availability Statement:** The data presented in this study are available upon request from the corresponding authors.

**Acknowledgments:** We thank Michaela Radostna for assistance with the behavioral experimentation and lab managing support and Stepan Bahník for consultation on data analysis.

**Conflicts of Interest:** All authors declare no conflict of interest.



## References

1. Stein, D.J.; Denys, D.; Gloster, A.T.; Hollander, E.; Leckman, J.F.; Rauch, S.L.; Phillips, K.A. Obsessive-compulsive Disorder: Diagnostic and Treatment Issues. *Psychiatr. Clin. N. Am.* **2009**, *32*, 665–685. [[CrossRef](#)]
2. Jenike, M.A. Obsessive—Compulsive Disorder. *N. Engl. J. Med.* **2004**, *203*, 259–265. [[CrossRef](#)]

3. Shin, N.Y.; Lee, T.Y.; Kim, E.; Kwon, J.S. Cognitive functioning in obsessive compulsive disorder: A meta-analysis. *Psychol. Med.* **2004**, *44*, 1121–1130. [[CrossRef](#)]
4. Snyder, H.R.; Kaiser, R.H.; Warren, S.L.; Heller, W. Obsessive-compulsive disorder is associated with broad impairments in executive function: A metaanalysis. *Clin. Psychol. Sci. J. Assoc. Psychol. Sci.* **2015**, *3*, 301–330. [[CrossRef](#)] [[PubMed](#)]
5. Han, K.; Young Kim, I.; Kim, J.-J. Assessment of cognitive flexibility in real life using virtual reality: A comparison of healthy individuals and schizophrenia patients. *Comput. Biol. Med.* **2015**, *42*, 841–847. [[CrossRef](#)] [[PubMed](#)]
6. La Paglia, F.; la cascina, C.; Rizzo, R.; Riva, G.; La Barbera, D. Assessment of Executive Functions in Patients with Obsessive Compulsive Disorder by NeuroVR. *Stud. Health Technol. Inform.* **2015**, *181*, 98–102. [[CrossRef](#)]
7. Delahaye, M.; Lemoine, P.; Cartwright, S.; Deuring, G.; Beck, J.; Pflueger, M.; Graf, M.; Hachtel, H. Learning aptitude, spatial orientation and cognitive flexibility tested in a virtual labyrinth after virtual stress induction. *BMC Psychol.* **2015**, *3*, 22. [[CrossRef](#)] [[PubMed](#)]
8. Goodman, W.K.; Grice, D.E.; Lapidus, K.A.B.; Coffey, B.J. Obsessive-compulsive disorder. *Psychiatr. Clin. N. Am.* **2014**, *37*, 257–267. [[CrossRef](#)] [[PubMed](#)]
9. Derksen, M.; Feenstra, M.; Willuhn, I.; Denys, D. The serotonergic system in obsessive-compulsive disorder. *Handb. Behav. Neurosci.* **2020**, *31*, 865–891. [[CrossRef](#)]
10. Marazziti, D.; Hollander, E.; Lensi, P.; Ravagli, S.; Cassano, G.B. Peripheral markers of serotonin and dopamine function in obsessive-compulsive disorder. *Psychiatry Res.* **1992**, *42*, 41–51. [[CrossRef](#)]
11. Erzegovesi, S.; Ronchi, P.; Smeraldi, E. 5HT-2 receptor and fluvoxamine effect in obsessive-compulsive disorder. *Hum. Psychopharmacol. Clin. Exp.* **1992**, *7*, 287–289. [[CrossRef](#)]
12. Moreno, F.A.; Wiegand, C.B.; Taitano, E.K.; Delgado, P.L. Safety, tolerability, and efficacy of psilocybin in 9 patients with obsessive-compulsive disorder. *J. Clin. Psychiatry* **2006**, *67*, 1735–1740. [[CrossRef](#)]
13. Kotapati, V.P.; Khan, A.M.; Dar, S.; Begum, G.; Bachu, R.; Adnan, M.; Zubair, A.; Ahmed, R.A. The Effectiveness of Selective Serotonin Reuptake Inhibitors for Treatment of Obsessive-Compulsive Disorder in Adolescents and Children: A Systematic Review and Meta-Analysis. *Front. Psychiatry* **2019**, *10*. [[CrossRef](#)]
14. Rotge, J.Y.; Aouizerate, B.; Tignol, J.; Bioulac, B.; Burbaud, P.; Guehl, D. The glutamate-based genetic immune hypothesis in obsessive-compulsive disorder. An integrative approach from genes to symptoms. *Neuroscience* **2010**, *165*, 408–417. [[CrossRef](#)] [[PubMed](#)]
15. Chakrabarty, K.; Bhattacharyya, S.; Christopher, R.; Khanna, S. Glutamatergic dysfunction in OCD. *Neuropsychopharmacology* **2005**, *30*, 1735–1740. [[CrossRef](#)] [[PubMed](#)]
16. Whiteside, S.P.; Port, J.D.; Deacon, B.J.; Abramowitz, J.S. A magnetic resonance spectroscopy investigation of obsessive-compulsive disorder and anxiety. *Psychiatry Res. Neuroimaging* **2006**, *146*, 137–147. [[CrossRef](#)] [[PubMed](#)]
17. Rosenberg, D.R.; Macmaster, F.P.; Keshavan, M.S.; Fitzgerald, K.D.; Stewart, C.M.; Moore, G.J. Decrease in caudate glutamatergic concentrations in pediatric obsessive-compulsive disorder patients taking paroxetine. *J. Am. Acad. Child Adolesc. Psychiatry* **2000**, *39*, 1096–1103. [[CrossRef](#)]
18. Kushner, M.G.; Kim, S.W.; Donahue, C.; Thuras, P.; Adson, D.; Kotlyar, M.; McCabe, J.; Peterson, J.; Foa, E.B. D-Cycloserine Augmented Exposure Therapy for Obsessive-Compulsive Disorder. *Biol. Psychiatry* **2007**, *62*, 835–838. [[CrossRef](#)]
19. Norberg, M.M.; Krystal, J.H.; Tolin, D.F. A Meta-Analysis of D-Cycloserine and the Facilitation of Fear Extinction and Exposure Therapy. *Biol. Psychiatry* **2008**, *63*, 1118–1126. [[CrossRef](#)]
20. Rodriguez, C.I.; Kegeles, L.S.; Levinson, A.; Feng, T.; Marcus, S.M.; Vermes, D.; Flood, P.; Simpson, H.B. Randomized Controlled Crossover Trial of Ketamine in Obsessive-Compulsive Disorder: Proof-of-Concept. *Neuropsychopharmacology* **2013**, *38*, 2475–2483. [[CrossRef](#)]
21. Grant, P.; Song, J.Y.; Swedo, S.E. Review of the use of the glutamate antagonist riluzole in psychiatric disorders and a description of recent use in childhood obsessive-compulsive disorder. *J. Child. Adolesc. Psychopharmacol.* **2010**, *20*, 309–315. [[CrossRef](#)] [[PubMed](#)]
22. Emamzadehfard, S.; Kamaloo, A.; Paydary, K.; Ahmadipour, A.; Zeinoddini, A.; Ghaleiha, A.; Mohammadinejad, P.; Zeinoddini, A.; Akhondzadeh, S. Riluzole in augmentation of fluvoxamine for moderate to severe obsessive-compulsive disorder: Randomized, double-blind, placebo-controlled study. *Psychiatry Clin. Neurosci.* **2010**, *70*, 332–341. [[CrossRef](#)] [[PubMed](#)]
23. Pasquini, M.; Biondi, M. Memantine augmentation for refractory obsessive-compulsive disorder. *Prog. Neuro-Psychopharmacol. Biol. Psychiatry* **2006**, *30*, 1173–1175. [[CrossRef](#)]
24. Poyurovsky, M.; Weizman, R.; Weizman, A.; Koran, L. Memantine for treatment-resistant OCD. *Am. J. Psychiatry* **2005**, *162*, 2191–2192. [[CrossRef](#)]
25. Kishi, T.; Matsuda, Y.; Iwata, N. Combination Therapy of Serotonin Reuptake Inhibitors and Memantine for Obsessive-Compulsive Disorder: A Meta-Analysis of Double-Blind, Randomized, Placebo-Controlled Trials. *J. Alzheimer's Dis.* **2018**, *64*, 43–48. [[CrossRef](#)] [[PubMed](#)]
26. Modarresi, A.; Sayyah, M.; Razooghi, S.; Eslami, K.; Javadi, M.; Kouti, L. Memantine Augmentation Improves Symptoms in Serotonin Reuptake Inhibitor-Refractory Obsessive-Compulsive Disorder: A Randomized Controlled Trial. *Pharmacopsychiatry* **2018**, *51*, 263–269. [[CrossRef](#)]
27. Alkhatib, A.H.; Dvorkin-Gheva, A.; Szechtman, H. Quinpirole and 8-OH-DPAT induce compulsive checking behavior in male rats by acting on different functional parts of an OCD neurocircuit. *Behav. Pharmacol.* **2013**, *24*, 65–73. [[CrossRef](#)]

28. Monteiro, P.; Feng, G. Learning from animal models of obsessive-compulsive disorder. *In Biol. Psychiatry* **2016**, *79*, 7–16. [[CrossRef](#)]
29. Odland, A.U.; Jessen, L.; Fitzpatrick, C.M.; Andreasen, J.T. 8-OH-DPAT Induces Compulsive-like Deficit in Spontaneous Alternation Behavior: Reversal by MDMA but Not Citalopram. *ACS Chem. Neurosci.* **2019**, *10*, 3094–3100. [[CrossRef](#)]
30. Yadin, E.; Friedman, E.; Bridger, W.H. Spontaneous alternation behavior: An animal model for obsessive-compulsive disorder? *Pharmacol. Biochem. Behav.* **1991**, *40*, 311–315. [[CrossRef](#)]
31. Bures, J.; Fenton, A.A.; Kaminsky, Y.; Zinyuk, L. Place cells and place navigation. *Proc. Natl. Acad. Sci. USA* **1997**, *94*, 343–350. [[CrossRef](#)]
32. Bures, J.; Fenton, A.A.; Kaminsky, Y.; Wesierska, M.; Zahalka, A. Rodent navigation after dissociation of the allocentric and idiothetic representations of space. *Neuropharmacology* **1998**, *37*, 689–699. [[CrossRef](#)]
33. Stuchlík, A.; Petrášek, T.; Prokopová, I.; Holubová, K.; Hatalová, H.; Valeš, K.; Kubík, Š.; Dockery, C.; Wesierska, M. Place Avoidance Tasks as Tools in the Behavioral Neuroscience of Learning and Memory Origin of place avoidance tasks. *Physiol. Res.* **2013**, *62*, 1–19. [[CrossRef](#)]
34. Janikova, M.; Brozka, H.; Radostova, D.; Svoboda, J.; Stuchlik, A. No effect of riluzole and memantine on learning deficit following quinpirole sensitization—An animal model of obsessive-compulsive disorder. *Physiol. Behav.* **2019**, *204*, 241–247. [[CrossRef](#)] [[PubMed](#)]
35. Sugiyama, A.; Saitoh, A.; Iwai, T.; Takahashi, K.; Yamada, M.; Sasaki-Hamada, S.; Oka, J.; Inagaki, M.; Yamada, M. Riluzole produces distinct anxiolytic-like effects in rats without the adverse effects associated with benzodiazepines. *Neuropharmacology* **2012**, *62*, 2489–2498. [[CrossRef](#)]
36. Beconi, M.G.; Howland, D.; Park, L.; Lyons, K.; Giuliano, J.; Dominguez, C.; Munoz-Sanjuan, I.; Pacifici, R. Pharmacokinetics of memantine in rats and mice. *PLoS Curr. Huntingt. Dis.* **2012**, *1*, 1–15. [[CrossRef](#)] [[PubMed](#)]
37. Willis, E.F.; Bartlett, P.F.; Vukovic, J. Protocol for Short- and Longer-term Spatial Learning and Memory in Mice. *Front. Behav. Neurosci.* **2017**, *11*, 197. [[CrossRef](#)] [[PubMed](#)]
38. Bahnik, S. Carousel Maze Manager. Version 0.4.0. 2014. Available online: [https://github.com/bahniks/CM\\_Manager\\_0\\_4\\_0](https://github.com/bahniks/CM_Manager_0_4_0) (accessed on 21 September 2020).
39. Johnson, E.F.; Szechtman, H. A dose-response study of separate and combined effects of the serotonin agonist 8-OH-DPAT and the dopamine agonist quinpirole on locomotor sensitization, /cross-sensitization, and conditioned activity. *Behav. Pharmacol.* **2016**, *27*, 439–450. [[CrossRef](#)]
40. Réus, G.Z.; Valvassori, S.S.; Machado, R.A.; Martins, M.R.; Gavioli, E.C.; Quevedo, J. Acute treatment with low doses of memantine does not impair aversive, non-associative and recognition memory in rats. *Naunyn-Schmiedeberg's Arch. Pharmacol.* **2008**, *376*, 295–300. [[CrossRef](#)] [[PubMed](#)]
41. Sukhanov, I.M.; Zakharova, E.S.; Danysz, W.; Bepalov, A.Y. Effects of NMDA receptor channel blockers, MK-801 and memantine, on locomotor activity and tolerance to delay of reward in Wistar-Kyoto and spontaneously hypertensive rats. *Behav. Pharmacol.* **2004**, *15*, 263–271. [[CrossRef](#)] [[PubMed](#)]
42. Kretschmer, B.D.; Kratzer, U.; Schmidt, W.J. Riluzole, a glutamate release inhibitor, and motor behavior. *Naunyn-Schmiedeberg's Arch. Pharmacol.* **1998**, *358*, 181–190. [[CrossRef](#)]
43. Wald, R.; Dodman, N.; Shuster, L. The Combined Effects of Memantine and Fluoxetine on an Animal Model of Obsessive Compulsive Disorder. *Exp. Clin. Psychopharmacol.* **2009**, *17*, 191–197. [[CrossRef](#)]
44. Egashira, N.; Okuno, R.; Harada, S.; Matsushita, M.; Mishima, K.; Iwasaki, K.; Fujiwara, M. Effects of glutamate-related drugs on marble-burying behavior in mice: Implications for obsessive-compulsive disorder. *Eur. J. Pharmacol.* **2008**, *586*, 164–170. [[CrossRef](#)]
45. Costa, L.; Trovato, C.; Musumeci, S.A.; Catania, M.V.; Ciranna, L. 5-HT1A and 5-HT7 receptors differently modulate AMPA receptor-mediated hippocampal synaptic transmission. *Hippocampus* **2012**, *22*, 790–801. [[CrossRef](#)] [[PubMed](#)]
46. Schmitz, D.; Gloveli, T.; Empson, R.M.; Draguhn, A.; Heinemann, U. Serotonin reduces synaptic excitation in the superficial medial entorhinal cortex of the rat via a presynaptic mechanism. *J. Physiol.* **1998**, *508*, 119–129. [[CrossRef](#)] [[PubMed](#)]
47. Ciranna, L. Serotonin as a Modulator of Glutamate- and GABA-Mediated Neurotransmission: Implications in Physiological Functions and in Pathology. *Curr. Neuropharmacol.* **2006**, *4*, 101–114. [[CrossRef](#)] [[PubMed](#)]
48. Aboujaoude, E.; Barry, J.J.; Gamel, N. Memantine augmentation in treatment-resistant obsessive-compulsive disorder: An open-label trial. *J. Clin. Psychopharmacol.* **2009**, *29*, 51–55. [[CrossRef](#)]
49. Pittenger, C.; Kelmendi, B.; Wasyluk, S.; Bloch, M.H.; Coric, V. Riluzole augmentation in treatment-refractory obsessive-compulsive disorder: A series of 13 cases, with long-term follow-up. *J. Clin. Psychopharmacol.* **2008**, *28*, 363–367. [[CrossRef](#)] [[PubMed](#)]

# CRMP2 mediates Sema3F-dependent axon pruning and dendritic spine remodeling

Jakub Ziak<sup>1,2</sup>, Romana Weissova<sup>1,2,†</sup>, Kateřina Jeřábková<sup>3,†</sup>, Martina Janikova<sup>4</sup>, Roy Maimon<sup>5</sup>, Tomas Petrasek<sup>4</sup>, Barbora Pukajova<sup>1,2</sup>, Marie Kleisnerova<sup>1</sup>, Mengzhe Wang<sup>6</sup>, Monika S Brill<sup>6</sup>, Petr Kasperek<sup>3</sup>, Xunlei Zhou<sup>7</sup>, Gonzalo Alvarez-Bolado<sup>7</sup>, Radislav Sedlacek<sup>3</sup>, Thomas Misgeld<sup>6,8</sup> , Ales Stuchlik<sup>4</sup>, Eran Perlson<sup>5</sup> & Martin Balastik<sup>1,\*</sup> 

## Abstract

Regulation of axon guidance and pruning of inappropriate synapses by class 3 semaphorins are key to the development of neural circuits. Collapsin response mediator protein 2 (CRMP2) has been shown to regulate axon guidance by mediating semaphorin 3A (Sema3A) signaling; however, nothing is known about its role in synapse pruning. Here, using newly generated *crmp2*<sup>-/-</sup> mice we demonstrate that CRMP2 has a moderate effect on Sema3A-dependent axon guidance *in vivo*, and its deficiency leads to a mild defect in axon guidance in peripheral nerves and the corpus callosum. Surprisingly, *crmp2*<sup>-/-</sup> mice display prominent defects in stereotyped axon pruning in hippocampus and visual cortex and altered dendritic spine remodeling, which is consistent with impaired Sema3F signaling and with models of autism spectrum disorder (ASD). We demonstrate that CRMP2 mediates Sema3F signaling in primary neurons and that *crmp2*<sup>-/-</sup> mice display ASD-related social behavior changes in the early postnatal period as well as in adults. Together, we demonstrate that CRMP2 mediates Sema3F-dependent synapse pruning and its dysfunction shares histological and behavioral features of ASD.

**Keywords** axon guidance; collapsin response mediator protein 2; dendritic spines; semaphorins; synapse pruning

**Subject Categories** Cell Adhesion, Polarity & Cytoskeleton; Neuroscience

**DOI** 10.15252/embr.201948512 | Received 17 May 2019 | Revised 11 December 2019 | Accepted 12 December 2019 | Published online 9 January 2020

**EMBO Reports (2020) 21: e48512**

## Introduction

The pattern of axonal connections is established during pre- and postnatal development by a cascade of multiple events. In embryogenesis, axonal growth cones are guided to their targets and multiple axon branches are formed. Since both correct and incorrect projections are formed, the embryonic brain connectome is only transient and the inaccurate connections are eliminated (pruned) in the early postnatal development [1]. Defects in development and maturation of brain circuits have been linked to several neurodevelopmental disorders including autism spectrum disorder (ASD), schizophrenia, or epilepsy [2–4].

Generally, two types of pruning are recognized: (i) small-scale axon pruning, regulated by neural activity or trophic support and (ii) large-scale stereotyped axon pruning, which is genetically predetermined [1,3]. Stereotyped pruning can be further histologically divided into degeneration-like [5] and retraction-like [6], which has been linked to secreted semaphorins and their coreceptors, e.g., plexin-A4 and plexin-A3 [6,7]. Intracellular mediators that transmit signals from plexins in axon pruning are not completely understood. One of the key molecule downstream of semaphorin 3A (Sema3A) signaling that directly interacts with cytoskeleton components is collapsin response mediator protein 2 (CRMP2) [8–10]. In its non-phosphorylated state, CRMP2 binds to tubulin dimers and promotes their polymerization [11]. However, upon phosphorylation, it dissociates from microtubules promoting growth cone collapse [12]. Two splice variants of *Crmp2* have been found that differ at the N-terminus—CRMP2A and CRMP2B [13,14]. CRMP2B is phosphorylated by cyclin-dependent kinase 5 (CDK5) at Ser522, by GSK-3β at Thr509, Thr514, and Ser518, and by Rho kinase at Thr555 [12,15,16]. We have recently shown that CRMP2A is phosphorylated at N-terminal Ser27 by Cdk5,

1 Department of Molecular Neurobiology, Institute of Physiology of the Czech Academy of Sciences, Prague, Czech Republic

2 Faculty of Science, Charles University in Prague, Prague, Czech Republic

3 Department of Transgenic Models of Diseases and Czech Centre for Phenogenomics, Institute of Molecular Genetics of the Czech Academy of Sciences, Prague, Czech Republic

4 Department of Neurophysiology of the Memory, Institute of Physiology of the Czech Academy of Sciences, Prague, Czech Republic

5 Department of Physiology and Pharmacology, Sackler Faculty of Medicine, Tel-Aviv University, Tel-Aviv, Israel

6 Institute of Neuronal Cell Biology, Technical University Munich, Munich, Germany

7 Institute of Anatomy and Cell Biology, Heidelberg University, Heidelberg, Germany

8 German Center for Neurodegenerative Diseases and Munich Cluster for Systems Neurology, Munich, Germany

\*Corresponding author. Tel: +420 241 062 822; E-mail: martin.balastik@fgu.cas.cz

<sup>†</sup>These authors contributed equally to this work



which promotes its interaction and stabilization by prolyl isomerase Pin1 [14]. Recently, CRMP2 deficiency in conditional knockout mice has been linked to schizophrenia due to changes in dendritic morphology (decreased spine number in CA1 neurons and layer 5 cortical neurons), behavioral changes (hyperactivity and social behavior impairment), and prepulse inhibition (PPI) deficit [17,18]. In addition to schizophrenia, deregulation of CRMP2 has been in humans associated with autism spectrum disorder (ASD), mood disorders, epilepsy, or Alzheimer's disease [19–24], (SFARI Gene database). Among these, ASD and schizophrenia are of special interest since their symptomatic proximity but distinct pathogenesis. The exact role of CRMP2 in the development of these conditions has so far been elusive. Although schizophrenia and ASD share some behavioral characteristics (e.g., decreased cognitive functions, impaired social skills, repetitive behavior), they differ in the timing of their onset (early childhood for ASD, late adolescence for schizophrenia) [25] and the nature of the underlying neuronal connectivity disorder. Whereas hypoconnectivity (lower number of dendrites, dendritic spines, general decrease of white matter) is often present in schizophrenia, ASD has been associated with local hyperconnectivity caused by either increased synapse formation or their incomplete pruning [26]. Because CRMP2 is downstream of semaphorin signaling, which controls axonal pruning [6], and it has been linked to both schizophrenia and ASD, it is one of the prime candidates to regulate this process. However, the *in vivo* analysis of both conditional and full CRMP2 knockout mice has to date mainly focused on the dendritic phenotype and associated behavioral aspects. In addition, the role of CRMP2 in class 3 semaphorin signaling (other than Sema3A), which has been previously linked to defects in pruning and ASD (particularly Sema3F), is so far not known.

In order to characterize the function of CRMP2 in axon growth, guidance, and pruning and its role in class 3 semaphorin signaling *in vivo*, we generated CRMP2 full knockout mice (*crmp2*<sup>-/-</sup>). We show that CRMP2 participates in regulation of axon guidance in both central and peripheral nervous systems. In peripheral nervous system, deficiency of CRMP2 leads to mild overgrowth and increased branching of ophthalmic branch of trigeminal nerve and other selected peripheral nerves. In the central nervous system, we detected defects in postnatal callosal axon growth and guidance. Both of these systems are regulated by Sema3A, which was previously shown to induce CRMP2 phosphorylation and signaling *in vitro*. Indeed, we confirm that primary motor and DRG neurons isolated from *crmp2*<sup>-/-</sup> mice have defects mediating Sema3A signaling.

Importantly, we show that CRMP2 is essential also for synaptic refinement as *crmp2*<sup>-/-</sup> mice demonstrate defective stereotyped pruning of axons arising from hippocampus and visual cortex and inadequate elimination of dendritic spines in dentate gyrus (DG). Pruning in both of these systems is dependent on Sema3F rather than Sema3A, and its defect is in accord with ASD rather than schizophrenia-like phenotype. In agreement with this hypothesis, we show that CRMP2 is essential for Sema3F-induced axon retraction and dendritic spine remodeling in primary hippocampal cultures and that *crmp2*<sup>-/-</sup> mice suffer from ultrasonic vocalizations defect in early postnatal stages as well as social behavioral changes in adults linked to ASD.

In summary, we provide evidence that in addition to its role in Sema3A-dependent axon guidance, CRMP2 is a key mediator of Sema3F-dependent axon pruning and dendritic spine remodeling.

Our data highlight the importance of CRMP2 in neural circuit formation and refinement *in vivo* and demonstrate that its deficiency leads to defects in neural development associated with neurodevelopmental disorders, in particular ASD and schizophrenia.

## Results

### Crmp2 deficiency leads to axonal growth defects in peripheral nerves

We used TALEN (transcription activator-like effector nucleases) mutagenesis to delete the second and third exons of the *Crmp2* locus leading to a knockout of both CRMP2 protein isoforms CRMP2A and CRMP2B (Figs 1A and B, and EV1A and B). The knockout mice were viable and fertile, and the size of their brains was similar to the WT littermates (Fig EV1C). In agreement with Ref. [17], we observed ventriculomegaly in the homozygous mice (Fig EV1D and E).

CRMP2 has been shown to mediate Sema3A signaling and regulate axon guidance *in vitro* [8]. To test whether CRMP2 deficiency leads to altered axon growth also *in vivo*, we first analyzed the development of peripheral nerves in E10.5–E12.5 embryos using whole-mount immunohistochemistry (Fig EV2A) as their development is regulated by Sema3A [27–30]. We quantified changes in neuron growth by measuring the area innervated by axons from each given nerve and branching by counting of the total number of branches. The growth and branching of ophthalmic branch of the trigeminal nerve were significantly increased in *crmp2*<sup>-/-</sup> mice at E10.5–E12.5 and similarly increased was the sprouting of the lateral branches of the spinal nerves. (Axon projections from dorsal root ganglions (DRGs) to the spinal cord were not changed in *crmp2*<sup>-/-</sup> mice) (Figs 1C–E, and EV2B and C). Since CRMP2 deficiency *in vivo* led to increased, rather than reduced axon growth, our data indicate that the growth-promoting function of CRMP2 can be compensated *in vivo* at least in the tested neurons, but that its function as a mediator of repulsive axon guidance signals is unique and cannot be fully rescued by other proteins. Since the growth of both ophthalmic branch and the lateral branches of the spinal nerves is negatively regulated by Sema3A [28], our data support the function of CRMP2 as a mediator of Sema3A signaling.

To directly demonstrate that CRMP2 deficiency interferes with Sema3A signaling in peripheral neurons isolated from *crmp2*<sup>-/-</sup> mice, we took an advantage of microfluidic chamber approach for extraaxonal environment manipulation. In this chamber, cell bodies and axons are separated in proximal or distal compartment, respectively [31]. We prepared spinal cord explants from WT and *crmp2*<sup>-/-</sup> E11.5–E12.5 embryos and cultured them for 4–5 days until motor neuron axons crossed to the distal compartment (Fig EV2H). Then, we stained axons with Alexa 647-conjugated cholera toxin subunit B and analyzed their growth by live imaging. Without Sema3A addition, the growth of WT and *crmp2*<sup>-/-</sup> explants and their axons were comparable indicating again that the axon growth-promoting function of CRMP2 is redundant, at least in the tested neurons. When we added Sema3A (5 nM) to the distal (axonal) compartment, we observed decrease in the number of growing WT axons, as expected ( $P < 0.001$ , Fig 1F and G, Movie EV1). However, in *crmp2*<sup>-/-</sup> explants, Sema3A had no significant effect on the number of growing axons ( $P = 0.99$ , Fig 2F and G, Movie EV1). In addition, we

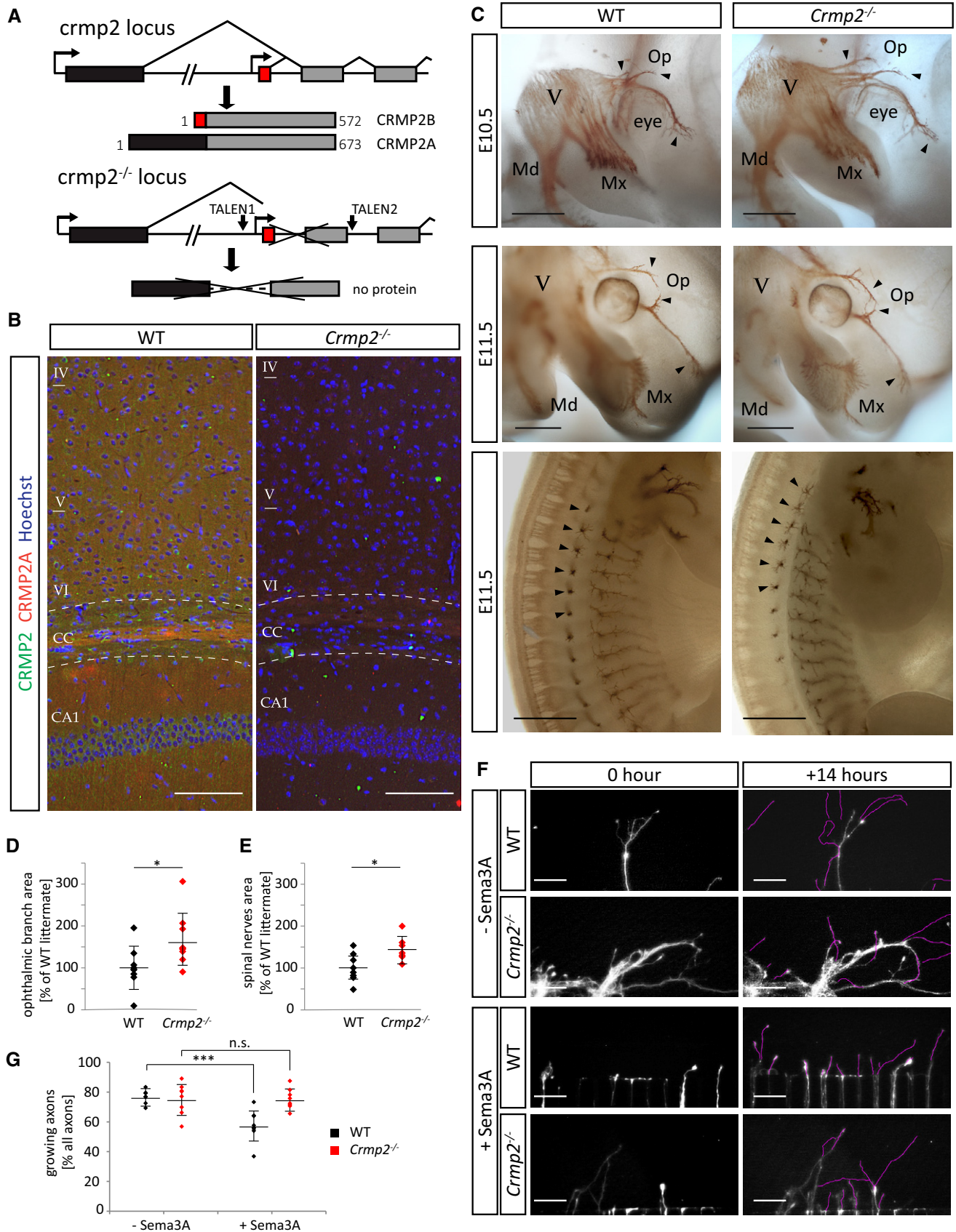


Figure 1.

**Figure 1. CRMP2 deficiency leads to axonal growth defects in peripheral nerves.**

- A Generation of *crmp2* knockout mice by TALEN mutagenesis. Alternative first exons are highlighted in black and red.
- B CRMP2 expression in adult cortex (layers VI–IV), corpus callosum (CC), and hippocampal area CA1. CRMP2 (green) is expressed throughout the cortex and hippocampus, and CRMP2A (red) is particularly strongly expressed in a subset of callosal axons. Nuclei are counterstained with Hoechst 33342. Scale bars: 50  $\mu$ m.
- C Whole-mount immunohistochemistry with anti-neurofilaments antibody for visualization of peripheral nerves. In *crmp2*<sup>-/-</sup> embryos, the growth of ophthalmic branch of the trigeminal nerve is increased and axons are defasciculated (first and second rows, arrowheads). Similarly, we detected increased growth and branching of lateral branches of spinal nerves in *crmp2*<sup>-/-</sup> embryos (third row, arrowheads). Trigeminal nerve (V) and its branches (Op—ophthalmic, Mx—maxillary, Md—mandibular) are indicated. Scale bars: 500  $\mu$ m.
- D, E Quantification of areas innervated by ophthalmic branches of trigeminal ganglion and spinal nerve, normalized to WT littermates (each dot depicts one embryo). Area of ophthalmic branch in *crmp2*<sup>-/-</sup> was increased by 66% ( $P < 0.05$ ,  $n = 10$ , 3 litters). For spinal nerves, total area in knockouts was increased by 45% ( $P < 0.05$ , WT  $n = 8$ , *crmp2*<sup>-/-</sup>  $n = 7$ , 3 litters). Mean  $\pm$  SD, \* $P < 0.05$ ,  $t$ -test.
- F Growth of motor neurons from E11.5–E12.5 WT and *crmp2*<sup>-/-</sup> spinal cord explants in microfluidic chambers. Excerpts from 14-h time-lapse imaging are shown. Upon application of Semaphorin 3A into distal compartment, WT axons tend to stop or slow down their growth unlike *crmp2*<sup>-/-</sup> axons. Purple lines highlight the growth path of individual axons in a distal chamber. Scale bars: 100  $\mu$ m. See also Movie EV1.
- G Quantification of the fraction of growing (> 50  $\mu$ m) axons in one imaging field (WT: control 76.8  $\pm$  5.7%, Semaphorin 3A 57.7  $\pm$  10.6%,  $P < 0.001$ , *crmp2*<sup>-/-</sup>: control 75.4  $\pm$  10.4%, Semaphorin 3A 75.4  $\pm$  6.7%,  $P = 0.99$ ),  $n = 3$  experiments per genotype, 7–8 explants per condition. Mean  $\pm$  SD. \*\*\* $P < 0.001$ , 2-way ANOVA with Bonferroni's multiple comparison test.

analyzed Semaphorin 3A-induced growth cone collapse in E11.5–E12.5 isolated DRGs. Neurons were treated with Semaphorin 3A for 30 min, then fixed, and stained for actin and  $\beta$ 3-tubulin. In *crmp2*<sup>-/-</sup> neurons, responsiveness to Semaphorin 3A was significantly decreased (Fig EV2G) which is in accord with the previously published data [8,32]. Thus, our data demonstrate that CRMP2 mediates Semaphorin 3A signaling *in vitro* and participates in guidance of multiple peripheral nerves in Semaphorin 3A-regulated regions *in vivo*.

### CRMP2 regulates anatomy and axon guidance in corpus callosum

In addition to the peripheral nerves, we analyzed the effect of CRMP2 deficiency on axonal growth also in the central nervous system. We detected anatomical changes in the largest axonal bundle of the brain, the corpus callosum, in *crmp2*<sup>-/-</sup> mice. The length of corpus callosum was significantly reduced in juvenile (-19.2%,  $P < 0.05$ ) as well as adult (-19.5%,  $P < 0.05$ ) knockout mice as can be appreciated in both sagittal and coronal sections (Fig 2A and B). More detailed labeling of the tract with anti-neurofilaments antibody showed that the posterior part of the corpus callosum (splenium) is markedly hypoplastic in *crmp2*<sup>-/-</sup> mice, ending rostrally to the habenular commissure, while the WT splenium is longer, located just above the habenular commissure (Fig 2C).

Callosal axons have been shown to be guided by Semaphorin 3A [33,34]. Thus, we analyzed whether dysgenesis of the corpus callosum we detected in *crmp2*<sup>-/-</sup> mice is also accompanied by defects in callosal axon guidance. We *in utero* electroporated WT and *crmp2*<sup>-/-</sup> embryonic cortices with pCAGGS-EGFP vector at E15.5, which results in labeling of cortical layer 2/3 (i.e., mainly callosal-projecting neurons). The brains were collected at postnatal day 6 (P6), fixed in 4% PFA, and cut coronally to trace callosal axons in a hemisphere contralateral to the electroporation site (Fig 2D and E). At this stage, axons from somatosensory cortex enter the contralateral cortex in WT [35]. Most of the WT axons showed well organized, parallel growth. In contrast, *crmp2*<sup>-/-</sup> axons often failed to grow in an organized, parallel way upon leaving the main callosal tract, their distribution in the cortex seemed uneven. We tracked the electroporated axons after leaving callosal bundle at the contralateral site and quantified their tortuosity (i.e., the ratio of real length of the segment vs. distance of the first and last point of the segment, Fig 2E). We found that tortuosity was significantly higher in *crmp2*<sup>-/-</sup> in comparison with WT ( $P < 0.001$ , Fig 2F).

Importantly, in some coronal sections of *crmp2*<sup>-/-</sup> mice we detected deregulated growth of callosal axons even in the midline. Together with the reduced length of corpus callosum in *crmp2*<sup>-/-</sup> mice in the rostro-caudal axis we detected (Fig 2A–C), it was suggested that CRMP2 deficiency may alter the rostro-caudal guidance of callosal axons in the midline. To test this hypothesis, we traced the callosal axons by injecting Dil into the fixed P9 and adult somatosensory cortices and analyzed organization and fasciculation of the traced axons in the midline (see Materials and Methods). We found that at P9, *crmp2*<sup>-/-</sup> axons were significantly more distorted as seen upon plotting to polar histograms or fan-in diagrams (interval (0°,  $\pm 20^\circ$ ):  $P < 0.05$ , interval ( $\pm 20^\circ$ ,  $\pm 40^\circ$ ):  $P = 0.02$ , Fig 2H–I, Appendix Fig S1A and B).

Together, our results show that CRMP2 regulates growth and guidance of selected axons in both peripheral (PNS) and central nervous system (CNS). In addition, since CRMP2 deficiency in *crmp2*<sup>-/-</sup> mice leads to enhanced, rather than reduced axon growth, our results suggest that in the analyzed PNS and CNS regions, the mediation of the repulsive axon guidance signals by CRMP2 takes precedence over its axon growth-promoting function.

### CRMP2 mediates Semaphorin 3F-driven, but not Semaphorin 3A-driven axon pruning

CRMP2 has been associated with neurodevelopmental disorders like schizophrenia and ASD characterized by altered brain connectivity [36] and defects in postnatal synaptic refinement through axon and dendrite pruning [26,37]. Importantly, in many regions Semaphorin 3F seems to play a more important role in pruning than Semaphorin 3A [6,7]. Therefore, we asked whether CRMP2 regulates axon pruning and if, in this function, it mediates Semaphorin 3A or rather Semaphorin 3F signaling. For this, we analyzed two developing axonal systems showing either Semaphorin 3F-mediated pruning (the infrapyramidal bundle, IPB; [6]) or Semaphorin 3A-mediated pruning (the hippocamposeptal bundle; [6]). First, we analyzed stereotyped pruning of infrapyramidal bundle (IPB) of hippocampal mossy fibers taking place between P20 and P40 and regulated by Semaphorin 3F and its receptor complex (Nrp2/PlxnA3) [6]. At P14 (i.e., before pruning), calbindin immunostaining revealed the presence of IPB in both WT and *crmp2*<sup>-/-</sup> mice (Fig 3A and B). Synapses were formed in both IPB and the main bundles as revealed by VGluT1 staining (Fig 3A and B). In 7-week-old animals, however, when pruning was complete in WT, the IPB remained



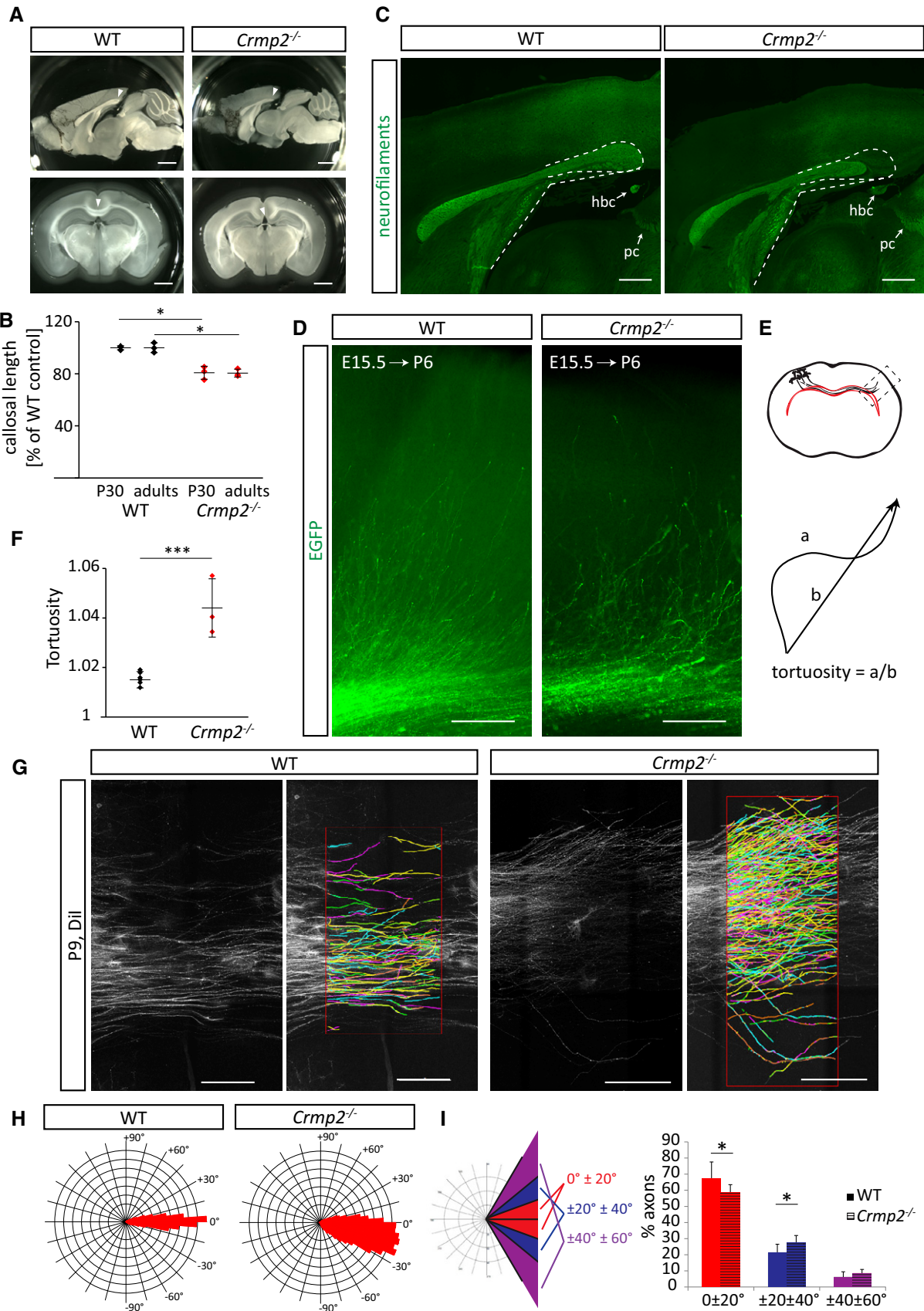


Figure 2.



**Figure 2. CRMP2 regulates postnatal development of corpus callosum.**

- A CRMP2 deficiency leads to callosal hypoplasia. Shortening of corpus callosum (arrowheads) is apparent in both sagittal (first row) and coronal sections (second row) of adult brains. Scale bars: 1 mm.
- B Quantification of callosal length in 30-day-old mice (P30,  $n = 3$ ,  $crmp2^{-/-}$  is  $80.8 \pm 5\%$  of WT,  $P = 0.003$ ) and adult mice ( $n = 3$ ,  $crmp2^{-/-}$  is  $80.5 \pm 3\%$  of WT,  $P = 0.002$ ), mean  $\pm$  SD,  $*P < 0.05$ ,  $t$ -test.
- C Labeling of adult corpus callosum with anti-neurofilaments antibody in sagittal sections. Outline depicts missing posterior part of the tract in  $crmp2^{-/-}$  mice. Caudal part of the corpus callosum in WT is located dorsally above the habenular commissure (hbc), while in  $crmp2^{-/-}$  mice, callosum terminates rostrally before reaching the hbc (arrows). PC indicates posterior commissure. Scale bars: 500  $\mu$ m.
- D The growth of GFP-labeled callosal axons in the contralateral cortex at P6 (embryos were electroporated at E15.5). Note the disorganized paths of  $crmp2^{-/-}$  axons. Scale bars: 200  $\mu$ m.
- E Schematic drawing of the callosal axon path and axonal tortuosity calculation. Pyramidal neurons in layer II/III project their axons into the contralateral cortex [rectangle depicts the area displayed in (D)]. Axonal tortuosity quantification as shown in (F), tortuosity = 1 if  $a = b$ .
- F Quantification of tortuosity of axons (WT  $n = 6$  pups,  $crmp2^{-/-}$   $n = 3$  pups) upon their exit from the callosal tract (WT  $1.016 \pm 0.003$  vs.  $crmp2^{-/-}$   $1.044 \pm 0.012$ ,  $P < 0.001$ ), mean  $\pm$  SD,  $***P < 0.001$ ,  $t$ -test.
- G Dil-labeled callosal axons from P9 oblique brain sections (see the Appendix Fig S1) and their reconstruction in NeuroLucida 360 (WT  $n = 6$ ,  $crmp2^{-/-}$   $n = 9$ ). Scale bars: 200  $\mu$ m.
- H Polar histograms of callosal axons reconstructed in (G). Note the broader range of axon growth angles in  $crmp2^{-/-}$  mice.
- I Left: schematic representation of polar histogram analysis by clustering the traced axons (WT  $n = 6$  pups,  $crmp2^{-/-}$   $n = 9$  pups) into three groups based on the growth angles. Right: proportion of axons growing in selected clusters (WT,  $0^\circ$  to  $\pm 20^\circ$ :  $67.3 \pm 10.3\%$ ;  $\pm 20^\circ$  to  $\pm 40^\circ$ :  $21.2 \pm 5.3\%$ ;  $\pm 40^\circ$  to  $\pm 60^\circ$ :  $6.22 \pm 3.2\%$ ;  $crmp2^{-/-}$ ,  $58.5 \pm 5\%$ ,  $P = 0.047$ ,  $27.7 \pm 4.3\%$ ,  $P = 0.022$ ,  $8.64 \pm 2.25\%$ ,  $P = 0.11$ ), mean  $\pm$  SD,  $*P < 0.05$ ,  $t$ -test.

present in  $crmp2^{-/-}$  mice, and their IPB index (IPB length/main bundle length) was significantly higher than in WT ( $P < 0.001$ , Fig 3C–G). The same pattern of IPB pruning was detected also in sagittal sections (Fig EV3A). To determine the maturity of IPB synapses, we stained adult coronal sections with antibodies against VgluT2 or VgluT1, which are both expressed in developing mossy fibers, but in adult hippocampus only VgluT1 is present [38]. We found VgluT1 in the main bundles of WT and  $crmp2^{-/-}$  mice, as well as in the unpruned IPBs of  $crmp2^{-/-}$  (Fig 3E and F). We did not detect the immature VgluT2 signal (Fig 3C and D). Thus, the IPB axons formed during postnatal development persist in  $crmp2^{-/-}$  mice into adulthood and form mature synapses. These results demonstrate that IPB pruning is defective in  $crmp2^{-/-}$  mice (as is the case in  $Sema3F^{-/-}$ ,  $Nrp2^{-/-}$ , and  $PlxnA3^{-/-}$  mice) [6].

We next tested whether stereotyped pruning of a different group of axons arising from hippocampus—the hippocamposeptal axons of CA1 pyramidal neurons—is also affected in  $crmp2^{-/-}$  mice. CA1 neurons send their axons into medial and lateral septum at P0–1. However, at P8, only the axons projecting to the lateral septum persist, while the ones projecting into the medial septum are pruned [39]. In this system, the pruning is mediated by *Sema3A* and not *Sema3F* [6]. Our analysis of the development of the CA1 hippocamposeptal axons in  $crmp2^{-/-}$  mouse brains by retrograde Dil tracing (Fig EV3B) showed no change in these brains as compared to WT brains at P0 or P8, indicating that the *Sema3A*-mediated pruning of hippocamposeptal axons is not affected in  $crmp2^{-/-}$  mice.

To further support the role of CRMP2 as a mediator of *Sema3F*-driven pruning, we analyzed pruning of corticospinal axons of visual cortex neurons that have been previously shown to be dependent on *Sema3F* signaling. In the early developmental stages, these neurons send their projections not only to the superior colliculus but also to two inappropriate targets, i.e., the inferior colliculus (IC) and the spinal cord. During the third postnatal week, inappropriate axons are eliminated through a pruning process regulated by *Sema3F* [7]. We analyzed the development of the visual cortex projection by the means of Dil anterograde tracing (Fig 4A and B). At P9, before the pruning period, there was no significant difference between WT and  $crmp2^{-/-}$  in the VP index (fluorescence intensity of corticospinal axons after vs. before the branch point). In adult WT mice, though, the inappropriate corticospinal axons were

largely pruned [VP index significantly dropped ( $P < 0.01$ , Fig 4C)], while in  $crmp2^{-/-}$  mice, they were still largely present [the VP indexes were not significantly different between P9 and adult ( $P = 0.24$ ); Fig 4C]. These data demonstrate that CRMP2 participates in postnatal refinement of corticospinal visual axons and is consistent with its role in mediating *Sema3F* signaling.

While, in development, both CNS and PNS projections are refined by pruning, we did not detect changes in the pruning of the peripheral neuromuscular junctions (NMJs) in  $crmp2^{-/-}$  mice using trigonum sterni muscle [the number of double-innervated NMJs was similar in WT and mutant mice at P11 ( $P > 0.99$ , Fig EV3C and D)].

Finally, we asked whether *Sema3F*-dependent axonal guidance is also mediated by CRMP2. Axon guidance is affected in two specific axonal bundles in  $Sema3F^{-/-}$  mice [40]—namely the anterior commissure (AC) and the retroflex fascicle. Immunostaining of P6 and P14 brains with anti-neurofilaments antibody revealed that both structures are present in  $crmp2^{-/-}$  mice (Fig EV4A and D). However, temporal limb of the AC appeared to be hypoplastic. We therefore analyzed morphology of AC in the horizontal sections (Fig EV4B). In knockouts, the diameter of temporal limb was indeed significantly thinner and the olfactory limb defasciculated (Fig EV4B and C). The data thus indicate that CRMP2 also contributes to *Sema3F*-driven axon guidance.

In conclusion, we found significant differences between WT and  $crmp2^{-/-}$  mice in stereotyped pruning in regions controlled by *Sema3F* (visual cortex axons, IPB). In contrast, we found no differences in regions controlled by *Sema3A* (i.e., hippocamposeptal axons) suggesting that CRMP2 mediates *Sema3F*-driven, but not *Sema3A*-driven axon pruning.

**CRMP2 mediates *Sema3F*-dependent axon retraction *in vitro***

In order to directly show that CRMP2 is necessary for *Sema3F*-triggered axon pruning, but dispensable for *Sema3A*-dependent pruning, we tested pruning in an *in vitro* system. We prepared dissociated hippocampal cultures from WT and  $crmp2^{-/-}$  E16.5 embryos and transfected them with EGFP at DIV1 (1 day *in vitro*). At DIV7, we added *Sema3A* or *Sema3F* into the cultures and analyzed the axon behavior in fluorescence microscope by time-lapse imaging. DIV7,

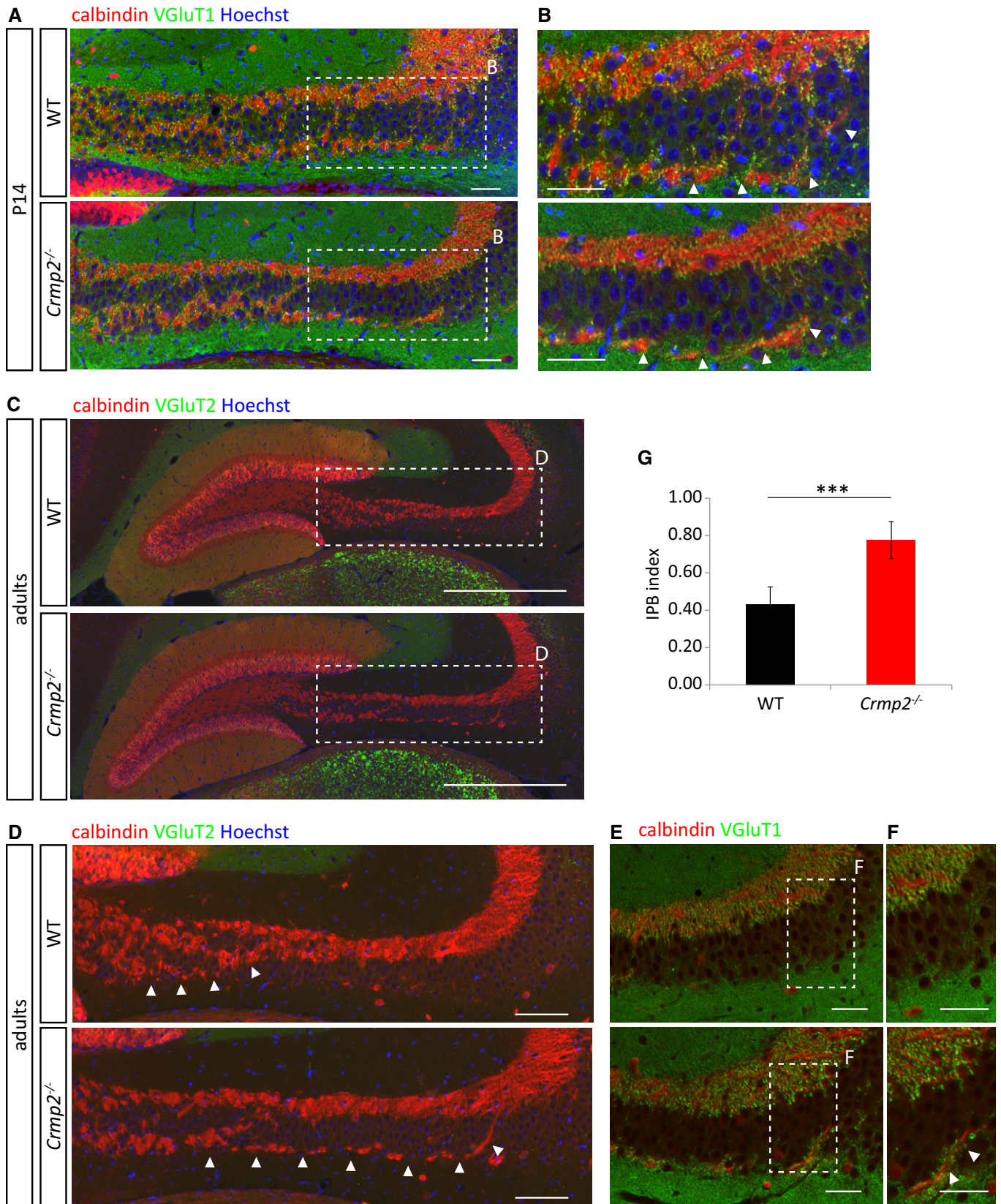


Figure 3.



**Figure 3. Infrapyramidal bundle fails to prune in *crmp2*<sup>-/-</sup> mice.**

- A, B (A) Coronal sections of P14 brains stained for calbindin and VgluT1. Infrapyramidal bundle (IPB) progresses into hippocampal CA3 region in both WT and *crmp2*<sup>-/-</sup> mice. Nuclei are counterstained with Hoechst 33342. (B) Details from depicted regions in (A), arrowheads show the course of IPB. Scale bars: 100  $\mu$ m.
- C, D (C) Staining for calbindin shows unpruned infrapyramidal bundle in adult *crmp2*<sup>-/-</sup> mice. No VgluT2 signal in hippocampal CA3 region is present in WT and *crmp2*<sup>-/-</sup> suggesting mature synapses. Scale bars: 500  $\mu$ m. (D) Details from depicted regions in (C), arrowheads show the course of IPB. Scale bars: 100  $\mu$ m.
- E, F Staining for calbindin and VgluT1 shows mature synapses in the main bundle in both genotypes and in the IPB in *crmp2*<sup>-/-</sup> mice (arrowheads). Scale bars: 100  $\mu$ m.
- G Quantification of IPB index (length of the IPB vs. main bundle, WT  $0.43 \pm 0.05$ , *crmp2*<sup>-/-</sup>  $0.78 \pm 0.05$ ,  $P < 0.001$ ) counted from adult coronal sections (WT  $n = 4$  mice, *crmp2*<sup>-/-</sup>  $n = 5$  mice). Mean  $\pm$  SD, \*\*\* $P < 0.001$ , t-test.

which is an early stage of synapse formation [41], was chosen to facilitate analysis of neurons in still less complex connectivity patterns (Fig 5A and B, Movies EV2 and EV3). We analyzed only stable axon terminals that did not show any movement in 1-h period prior to addition of the guidance cues (45% of all labeled axon terminals). In control conditions in both wild-type and knockout, a small number of the stable axons were spontaneously retracting (WT 13%, KO 20%,  $P = 0.03$ , Fig 5C). After addition of either Semaphorin 3A or Semaphorin 3F into WT culture, we observed a three-fold increase in axon retractions (32% for Semaphorin 3A,  $P < 0.001$ , 41% for Semaphorin 3F,  $P < 0.001$ , Fig 5C). However, in *crmp2*<sup>-/-</sup>, this increase was detectable only after Semaphorin 3A (30%,  $P < 0.05$ ) and not after Semaphorin 3F (22%,  $P > 0.99$ ). These data demonstrate, that in primary neuron cultures undergoing synaptogenesis, CRMP2 is essential to mediate Semaphorin 3F but not Semaphorin 3A signaling. This is in agreement with our *in vivo* findings that stereotyped pruning in *crmp2*<sup>-/-</sup> is affected in Semaphorin 3F-controlled, but not in Semaphorin 3A-controlled regions.

**CRMP2 regulates dendritic spine remodeling in hippocampal granule cells**

Besides triggering axon pruning, Semaphorin 3F regulates also the development of some classes of dendritic spines (e.g., spines of dentate gyrus (DG) granule cells) [42]. In contrast, Semaphorin 3A/Nrp1 signaling seems to be dispensable for dendritic spine morphogenesis [42,43]. In order to test whether CRMP2 participates also in spine development/morphogenesis, we DiO-oligostically labeled DG neurons and analyzed their dendritic spines. Surprisingly, we found significantly increased spine density in *crmp2*<sup>-/-</sup> adult DG granule cells compared to WT (Fig 6B and C,  $P < 0.001$ ). This phenotype was similar to that found in *Sema3F*<sup>-/-</sup> and *Nrp2*<sup>-/-</sup> [42]. Next, we analyzed branching of DG granule cell dendrites. Sholl analysis revealed no differences between WT and *crmp2*<sup>-/-</sup> mice (Fig 6D and E,  $P > 0.99$ ), which is again in line with the phenotype of *Sema3F*<sup>-/-</sup> mice [42].

Higher spine density could be a result of either increased generation of new spines or defective pruning of spines or both. Considering the axon pruning defects we found in Semaphorin 3F-regulated areas in *crmp2*<sup>-/-</sup> mice (see above), and considering that Semaphorin 3F promotes loss of spines *in vitro* [42], we hypothesized that Semaphorin 3F regulates dendritic spine pruning through CRMP2. To test this hypothesis, we labeled and counted DG dendritic spine density in P30 (adolescent) mice when dendritic spines are virtually all formed and the pruning process starts [44,45]. We found no differences in dendritic spine density between WT and mutants at P30 (Fig 6A and C,  $P > 0.99$ ). This indicates that the formation of spines is unaltered in *crmp2*<sup>-/-</sup> mice and that it is

the process of dendritic spine pruning that is defective in these mice. To support this hypothesis, we tested whether the number of excitatory synapses is also increased in DG of adult *crmp2*<sup>-/-</sup> mice using PSD95 and VgluT2 post- and pre-synaptic markers, respectively. We found that in *crmp2*<sup>-/-</sup> mice, the density of colocalized PSD95/VgluT2 puncta was indeed increased in the inner part of the molecular layer (Fig 6F), which is in agreement with DG synaptic pruning deficit. As DG spine morphogenesis is regulated through Semaphorin 3F [42], our findings indicate that CRMP2 mediates Semaphorin 3F-dependent synapse pruning.

Finally, we analyzed the role of CRMP2 in Semaphorin 3F-induced dendritic spine remodeling *in vitro*. We prepared hippocampal cultures, transfected neurons with GFP at DIV14, and analyzed the same dendritic segments at DIV21 and DIV25 (Fig EV5B). We detected significantly decreased spine density at DIV25 in WT neurons consistent with ongoing spine remodeling, but not in *crmp2*<sup>-/-</sup> neurons (Fig EV5C). Importantly, treatment of WT DIV25 neurons with Semaphorin 3F induced elimination of their spines, but no significant effect was detected in CRMP2-deficient neurons (Fig EV5D and E). These observations are in accord with our *in vivo* findings and further support the role of CRMP2 as mediator of Semaphorin 3F-driven spine remodeling.

Defects in the distribution of dendritic spines due to aberrant synapse refinement are one of the key features of both ASD and schizophrenia. Generally, dendritic spine number in ASD patients is higher than in control subjects or variable in different regions, while in schizophrenia patients, it is lower [36]. This applies particularly to some brain regions, e.g., prefrontal cortex (PFC), where excessive spine elimination has been associated with pathogenesis of schizophrenia [46]. Since some phenotypical aspects of conditional *crmp2*<sup>-/-</sup> mice like impaired sensorimotor gating have been related to schizophrenia [17], we asked whether CRMP2 deficiency also leads to spine overpruning and reduced spine density in PFC. At P25, PFC spine density was similar in both WT and mutants (Fig 6F and G,  $P = 0.97$ ) and similar to our findings in the DG. Importantly, unlike in DG, we did not detect any significant difference in PFC spine density between adult WT and *crmp2*<sup>-/-</sup> mice (Fig 6G and H,  $P > 0.99$ ), which is not consistent with schizophrenia-like phenotype.

***Crmp2*<sup>-/-</sup> mice display juvenile sociability defects, memory impairment, and decreased anxiety**

While schizophrenia shares some behavioral symptoms with autism (e.g., cognitive and social deficits), it differs in the onset of the disease, as ASD manifests typically in 3-year-old children while schizophrenia in the adolescence at the earliest [25,37]. This suggests that any changes underlying ASD must be present already

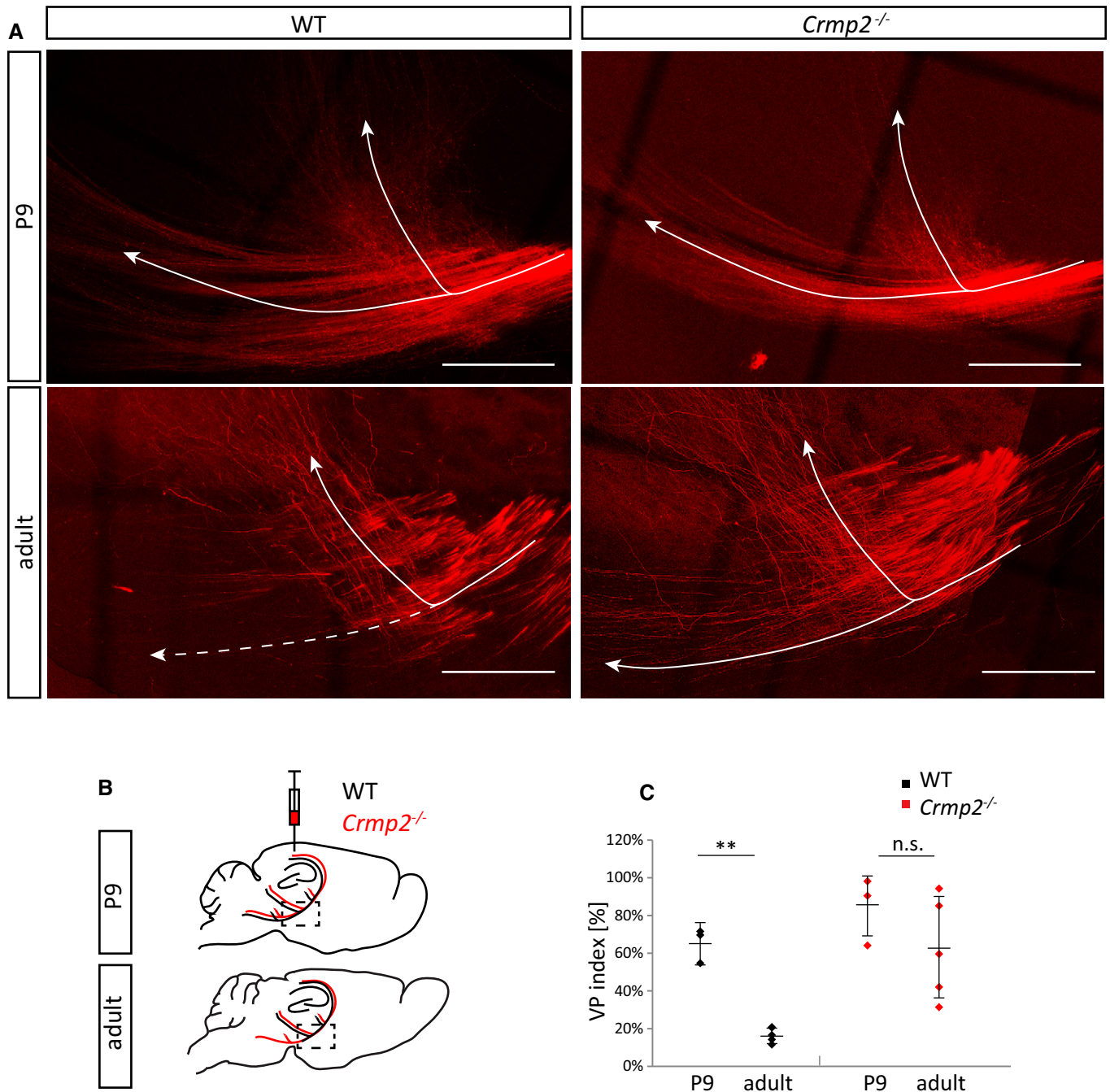


**Figure 4. Defective pruning of corticospinal visual axons in *crmp2*<sup>-/-</sup> mice.**

**A** Upper row: Dil tracing of the visual cortex axons at P9 (before pruning), sagittal sections. Branching point of the tract is shown. Lower row: visual cortex axons in adult mice after pruning period. Note significantly reduced number of axons continuing into pyramidal tract in WT (dashed arrow) (arrows—2 branches of corticospinal visual axons). Maximum projections are shown. Scale bars: 200 μm.

**B** Schematic drawing of Dil injection and axon tracing. Axons that initially enter pyramidal tract fail to prune in *crmp2*<sup>-/-</sup> mice (red line).

**C** Quantification of VP (visual pruning) index (fluorescence intensity of pyramidal axons after vs. before the branch point). In WT animals after the pruning period, only a minor part of axons descends toward the pyramidal tract (WT: P9 0.65 ± 0.09, adults 0.17 ± 0.04, *P* = 0.006). However, in *crmp2*<sup>-/-</sup> mice, corticospinal axons are still largely present, and their VP indexes are not significantly different between adult and P9 stages (*crmp2*<sup>-/-</sup>: P9 0.54 ± 0.18, adults 0.62 ± 0.27, *P* = 0.24). Mean ± SD, \*\**P* < 0.01, 2-way ANOVA with Bonferroni's multiple comparison test. P9: *n* = 3 pups/genotype, adults: *n* = 5 mice/genotype.

very early in postnatal development. To assess this hypothesis, we wanted to see whether CRMP2 deficiency results in juvenile behavioral changes. To this effect, we analyzed ultrasonic

vocalization (USV) in P6, P8, and P12 WT and *crmp2*<sup>-/-</sup> pups as a measure of their sociability [47]. We recorded USVs of WT and mutant pups in 5-min intervals after isolation from their mothers



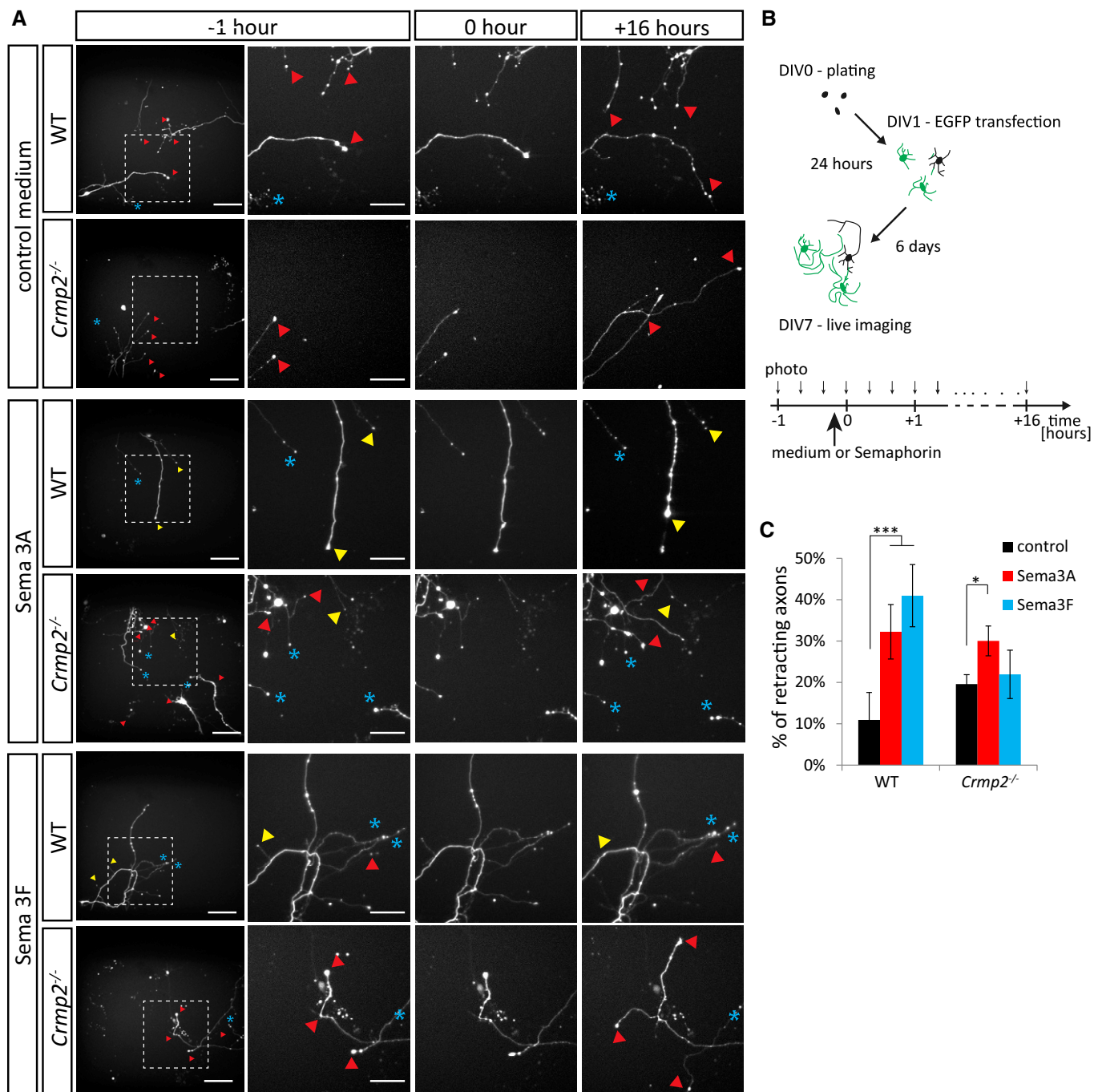


**Figure 5. CRMP2 mediates Sema3F signaling in primary neurons.**

**A** Time-lapse imaging of DIV7 cultured hippocampal neurons before and after semaphorin stimulation. Upper panel: axon growth without semaphorin stimulation. Middle panel: stimulation with Sema3A (0 h) (1 nM,  $n = 669$  axons for WT, 761 axons for knockout) causes retraction of both WT and *crmp2*<sup>-/-</sup> neurons. Lower panel: stimulation with Sema3F (5 nM,  $n = 602$  axons for WT, 955 axons for knockout) causes axon retraction in WT, but not in *crmp2*<sup>-/-</sup> neurons. Red triangles depict growing axons, yellow retracting axons, and blue asterisks indicate steady non-growing axons. See also Movies EV2 and EV3. Scale bars: 100  $\mu$ m (whole image field) and 50  $\mu$ m (magnified).

**B** Schematic drawing of the experimental setup.

**C** Quantification of retracting axons (number of retracting vs. steady axons, three experiments). WT: control  $13.4 \pm 5\%$ , Sema3A  $31.2 \pm 6\%$  ( $P < 0.001$ ), Sema3F  $36.9 \pm 8.7\%$  ( $P < 0.001$ ); *crmp2*<sup>-/-</sup>: control  $19.8 \pm 1.8\%$ , Sema3A  $28.5 \pm 4.4\%$  ( $P < 0.05$ ), Sema3F  $22.4 \pm 4.1\%$  ( $P > 0.99$ ), mean  $\pm$  SD are shown. \*\*\* $P < 0.001$ , \* $P < 0.05$ , 2-way ANOVA with Bonferroni's multiple comparison test.

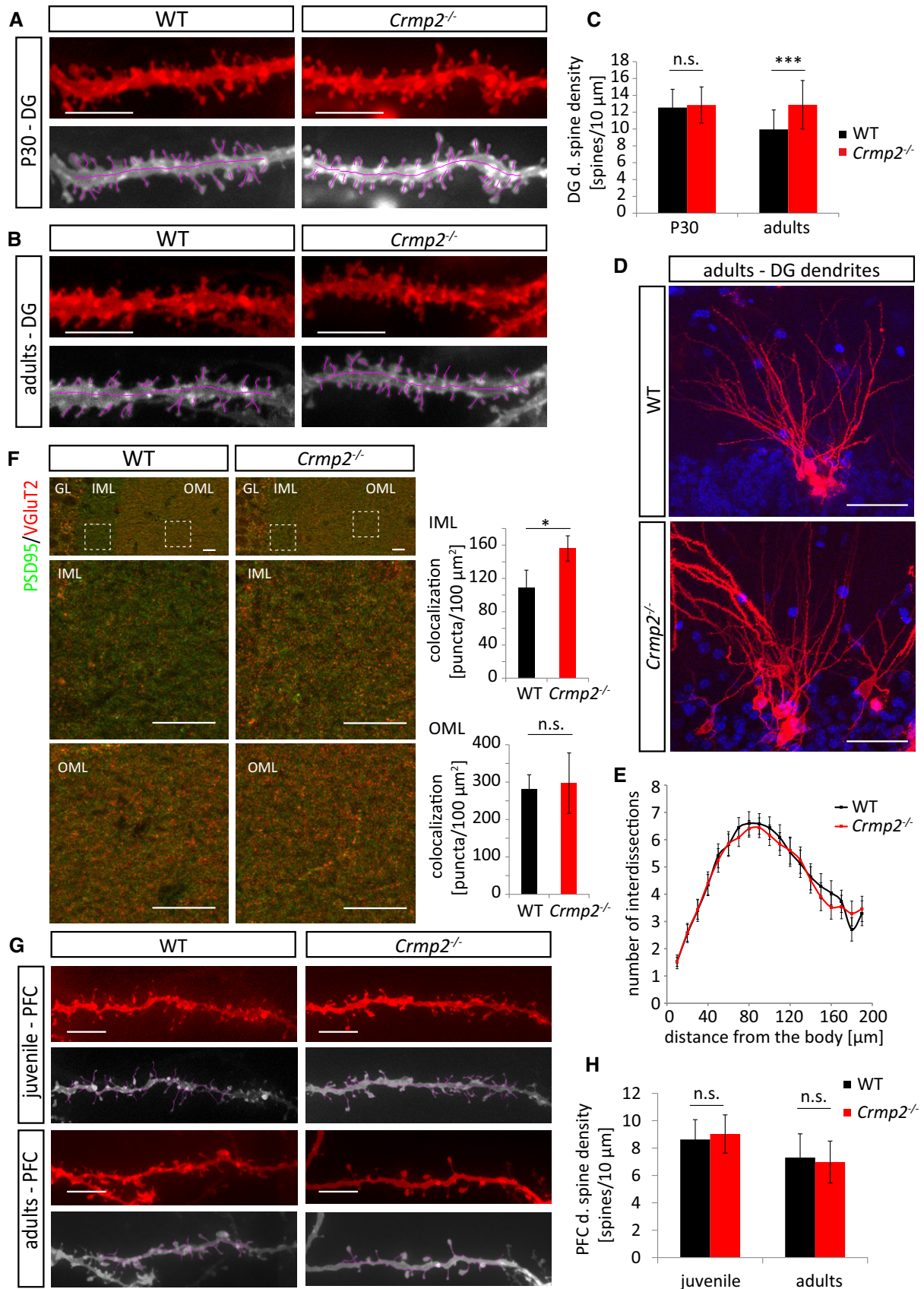


Figure 6.

**Figure 6. CRMP2 regulates dendritic spine refinement in dentate gyrus granule cells.**

- A, B Dendritic spine density in DiOlistically labeled DG granule cells is similar in WT and *crmp2*<sup>-/-</sup> mice at P30. In adults, however, spine density in *crmp2*<sup>-/-</sup> granule cells is increased comparing to WT. Scale bars: 5  $\mu$ m.
- C Quantification of dendritic spine density in DG granule cells in the inner molecular layer (50–100  $\mu$ m away from the soma). WT, P30: 12.5  $\pm$  2.2 spines/10  $\mu$ m, adults: 9.95  $\pm$  2.3; *crmp2*<sup>-/-</sup>, P30: 12.86  $\pm$  2.1 ( $P > 0.99$ ), adults: 12.88  $\pm$  2.9 ( $P < 0.001$ ), mean  $\pm$  SD, \*\*\* $P < 0.001$ , 2-way ANOVA with Bonferroni correction. P30: 3 animals/genotype, WT = 61 dendrites, knockout = 64 dendrites; adults: 3 animals/genotype, WT = 41 dendrites, knockout = 37 dendrites.
- D, E Analysis of branching of DiOlistically labeled DG granule cell dendrites in adult WT and *crmp2*<sup>-/-</sup> mice ( $n = 3$  animals,  $\geq 25$  dendrites). Quantification of granule cell branching by Sholl analysis showed no significant differences ( $P > 0.99$ ). Scale bars: 50  $\mu$ m, mean  $\pm$  SEM, 2-way ANOVA with Bonferroni correction.
- F Defects in synapse elimination in the inner molecular layer revealed by double immunostaining with PSD95 and VGLuT2 antibodies ( $n = 5$  mice/genotype). GL indicates granule cell layer, and IML/OML indicate inner/outer molecular layer, respectively. Density of colocalized PSD95/VGLuT2 puncta was counted. IML: WT 109  $\pm$  21, *crmp2*<sup>-/-</sup> 156  $\pm$  15 ( $P = 0.004$ ). OML: WT 281  $\pm$  38, *crmp2*<sup>-/-</sup> 297  $\pm$  80 ( $P = 0.7$ ). Scale bars: 10  $\mu$ m, mean  $\pm$  SD, \* $P < 0.05$ ,  $t$ -test.
- G Spine density in DiOlistically labeled prefrontal cortex (PFC) is similar in WT and *crmp2*<sup>-/-</sup> mice in both juvenile and adult mice. Scale bars: 5  $\mu$ m.
- H Quantification of dendritic spine density of PFC pyramidal neurons, basal dendrites (WT, juvenile: 8.63  $\pm$  1.44 spines/10  $\mu$ m, adults: 7.3  $\pm$  1.4; *crmp2*<sup>-/-</sup>, juvenile: 9.05  $\pm$  1.73,  $P = 0.97$ , adults: 6.98  $\pm$  1.53,  $P > 0.99$ ), mean  $\pm$  SD, 2-way ANOVA with Bonferroni's multiple comparison test. P25:  $n = 3$ ,  $\geq 50$  dendrites; adults:  $n = 3$ ,  $\geq 50$  dendrites.

and found that at P6 the number of calls was similar between both groups ( $P = 0.73$ ), but decreased significantly in the mutants at P8 ( $P = 0.015$ ; Fig 7A–C). At P12, the mutants were almost completely silent ( $P = 0.002$ ); in fact, only two mutant pups from 13 vocalized at all (10/14 in WT). The duration of the individual calls was also significantly shorter in *crmp2*<sup>-/-</sup> pups in both P8 ( $P = 0.011$ ) and P12 ( $P = 0.003$ ) (Fig 7B). This early onset social behavior defects have been described in numerous mouse models of ASD with dendritic spine pathology [26], some of which also showed dendritic spine pathology later in adults [48–51]. To broaden the analysis of *crmp2*<sup>-/-</sup> social abnormalities also to the adult animals, we performed a three-chamber sociability test. We found disruption of social preference in knockouts since they spent similar time exploring both stranger mice and neutral object, unlike WT, that preferred the mice (WT  $P < 0.001$ , *crmp2*<sup>-/-</sup>  $P = 0.07$ , Fig 7D, Appendix Fig S2A). On the other hand, social novelty seems to be preserved in *crmp2*<sup>-/-</sup> mice, although less expressed than in WT animals (WT  $P < 0.001$ , *crmp2*<sup>-/-</sup>  $P < 0.05$ , Fig 7D, Appendix Fig S2B).

We next asked whether hippocampus-dependent memory functions are affected in *crmp2*<sup>-/-</sup> mice as they exhibit aberrant inputs from DG into CA3 (unpruned mossy fibers) and increased spine density in DG granule cells (input from entorhinal cortex). We tested working memory using Y-maze (a three-arm maze) where WT and mutants showed comparable level of exploratory activity (Fig 7H). However, the ratio of spontaneous arm alternation was significantly lower in *crmp2*<sup>-/-</sup> mice (Fig 7I,  $P = 0.0058$ ) indicating a working memory impairment [17]. In contrast, long-term memory and general behavioral flexibility seem not to be affected in *crmp2*<sup>-/-</sup> mice as revealed by active place avoidance on a rotating arena test (Appendix Fig S2C).

Similar to other CRMP2-deficient mouse models [17,52], we detected anxiety impairment in *crmp2*<sup>-/-</sup> mice using elevated plus maze. In the task, the knockouts also demonstrated increased activity during exploration of the maze (Fig 7E), spent more time in the open arms of the maze ( $P < 0.001$ ), and visited them more often ( $P = 0.0016$ ) than their WT counterparts (Fig 7F and G) suggesting decreased anxiety, or perhaps a more general lack of adequate response to potentially dangerous situations. This phenotype may reflect the hippocampal phenotype of *crmp2*<sup>-/-</sup> mice as lesions in particularly ventral hippocampus have been shown to result in similar decreased anxiety in mouse models [53].

## Discussion

CRMP2 has been long considered an important regulator of semaphorin 3A-mediated axon guidance during embryonic development. Its expression, though, is high even in the early postnatal neurons, but its role in the postnatal development and adult neurons has so far been elusive. In the present study, we demonstrated that CRMP2 is not only mediator of Semaphorin 3A signaling regulating axon guidance in embryonic development, but importantly, that it plays a central role in the postnatal refinement of the nervous system. By generating new *crmp2*<sup>-/-</sup> mice and analyzing their phenotype, we first showed that CRMP2 deficiency *in vivo* leads to axon guidance defects in CNS and PNS that could be attributed to changes of Semaphorin 3A signaling. Strikingly, we demonstrated that CRMP2 mediates also Semaphorin 3F signaling and that CRMP2 deficiency disrupts early postnatal Semaphorin 3F-mediated axon and dendritic spine refinement in multiple areas of the CNS and in hippocampal neuron cultures. Changes in Semaphorin 3F signaling pathway have been considered a risk factor in the pathogenesis of ASD. In accord with that, we showed that *crmp2*<sup>-/-</sup> mice suffer from altered pruning and both early postnatal and adult social interaction defects previously linked to autism. Together, our *in vivo* and *in vitro* data demonstrated a novel function of CRMP2 in postnatal fine-tuning of the nervous system by Semaphorin 3F and showed that its deficiency in mice leads to neurodevelopmental defects associated with pathogenesis of the ASD in human.

### Regulation of axon and dendritic pruning by Semaphorin 3F and CRMP2

Initial growth of axons and dendrites during embryonic and early postnatal period results in an embryonic template that must be later refined to generate a functional healthy nervous system [54]. Stereotyped refinement of nervous system was uncovered in several regions: (i) Infrapyramidal bundle (IPB) axons of hippocampal mossy fibers are retracted between P14 and P30 in mice [55]; (ii) excess of layer 2/3 callosal axons of motor, sensory, and visual cortex is refined until P30 [33]; and (iii) corticospinal axons from layer 5 visual cortex are eliminated between P9 and P25 [7]. In addition, density of dendritic spines in various brain regions in mice and humans peaks between childhood and adolescence [44,45] and its significant portion is eliminated until adulthood. Finally, pruning also occurs in peripheral nervous system—originally polyneuronal innervation of muscle fibers is later in

development refined so that each muscle fiber is innervated by only one motor axon [56,57].

Knockout mouse studies identified extracellular cues and receptors that mediate pruning in rodents. These include *Sema3A* and its receptor complex (*Nrp1/PlxnA4*), and *Sema3F* and its receptors

(*Nrp2/PlxnA3*), ephrin-B3–EphB2 reverse signaling, and C4 component of complement [6,58,59]. Intracellular pathways that translate extracellular signal to cytoskeleton are however poorly understood. Here, we identified CRMP2 as a novel mediator of pruning in rodent brain triggered by *Sema3F*.

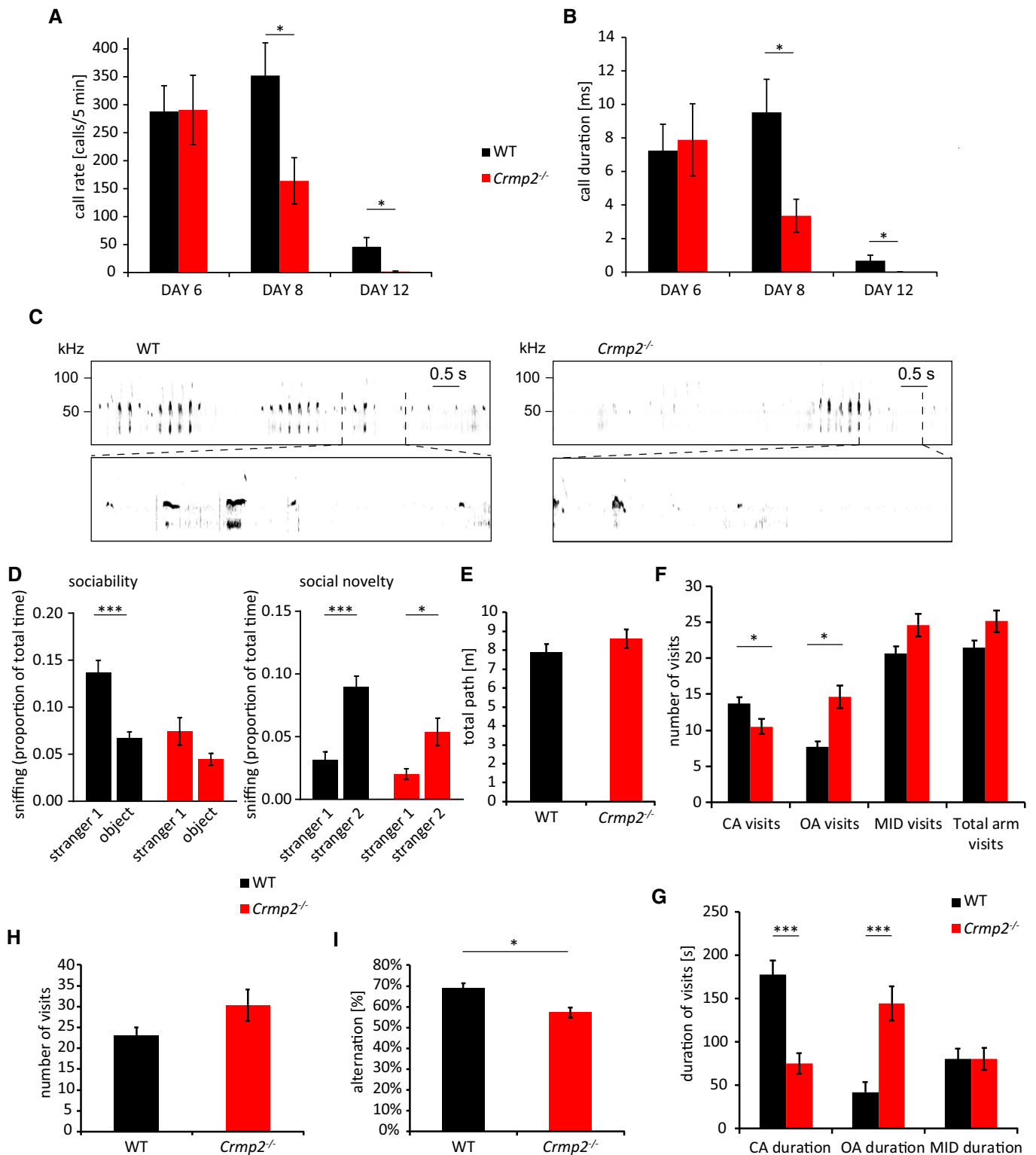


Figure 7.



**Figure 7. Behavioral analysis of *crmp2*<sup>-/-</sup> mice.**

- A, B Ultrasonic vocalization was measured at P6, P8, and P12 (WT *n* = 14 pups, *crmp2*<sup>-/-</sup> *n* = 13 pups). In *crmp2*<sup>-/-</sup> mice, there is a significant decrease in the rate and duration of calls at P8 (call rate, WT 352 ± 58/5 min, *crmp2*<sup>-/-</sup> 164 ± 41/5 min, *P* = 0.015; call duration, WT 9.52 ± 2 ms, *crmp2*<sup>-/-</sup> 3.36 ± 1 ms, *P* = 0.011) and P12 (call rate, WT 46 ± 16/5 min *crmp2*<sup>-/-</sup> 1.54 ± 1.24/5 min, *P* = 0.002; call duration, WT 0.68 ± 0.35 ms, *crmp2*<sup>-/-</sup> 0.007 ± 0.006 ms, *P* = 0.002). Mean ± SEM, \**P* < 0.05, t-test (P6, P8), Mann–Whitney test (P12).
- C Representative sonograms of the P8 mice.
- D 3-chamber test (WT *n* = 11 mice, *crmp2*<sup>-/-</sup> *n* = 13 mice). In sociability phase, WT mice spent significantly more time with a social partner (stranger 1), unlike knockouts [WT—stranger 1: 0.14 ± 0.01, object: 0.07 ± 0.007 (*P* = 0.0001); *crmp2*<sup>-/-</sup>—stranger 1: 0.07 ± 0.01, object: 0.04 ± 0.006 (*P* = 0.07)]. In social novelty phase, when an object was substituted with a second social partner (stranger 2), both WT and knockouts preferred novel mice to known mice [WT—stranger 1: 0.03 ± 0.006, stranger 2: 0.09 ± 0.008 (*P* < 0.0001); *crmp2*<sup>-/-</sup>—stranger 1: 0.02 ± 0.004, stranger 2: 0.05 ± 0.01 (*P* = 0.02)]. Mean ± SEM, \**P* < 0.05, \*\*\**P* < 0.001, t-test.
- E–G Elevated plus maze test (*n* = 10 mice/genotype). (E) Total distance walked is similar in WT and *crmp2*<sup>-/-</sup> (WT 7.9 ± 0.45 m, *crmp2*<sup>-/-</sup> 8.6 ± 0.5 m, *P* = 0.3). (F) Frequency and (G) duration of open arm (OA) visits are increased in *crmp2*<sup>-/-</sup> mice suggesting decreased anxiety. CA denotes closed arms, MID denotes the transition zone between arms, and total arm visits represent a sum of visits in all four arms. (CA frequency: WT 13.7 ± 0.9/5 min, *crmp2*<sup>-/-</sup> 10.5 ± 1.1/5 min, *P* = 0.04; OA frequency: WT 7.7 ± 0.8/5 min, *crmp2*<sup>-/-</sup> 14.6 ± 1.7/5 min, *P* = 0.002; MID frequency: WT 20.6 ± 1/5 min, *crmp2*<sup>-/-</sup> 24.6 ± 1.6/5 min, *P* = 0.06; total arm visits: WT 21.4 ± 1/5 min, *crmp2*<sup>-/-</sup> 25.1 ± 1.5/5 min, *P* = 0.07; CA duration: WT 177 ± 17 s, *crmp2*<sup>-/-</sup> 75.3 ± 12.6 s, *P* < 0.001; OA duration: WT 42 ± 12.6 s, *crmp2*<sup>-/-</sup> 144.4 ± 21 s, *P* < 0.001; MID duration: WT 80.26 ± 11.5 s, *crmp2*<sup>-/-</sup> 80.17 ± 12.6 s, *P* = 0.99), mean ± SEM, \**P* < 0.05, \*\*\**P* < 0.001, t-test.
- H, I Y-maze test (WT *n* = 9 mice, *crmp2*<sup>-/-</sup> *n* = 8 mice). Decreased alternations between arms of the maze indicate impaired working memory (number of visits, WT: 23.1 ± 1.9, *crmp2*<sup>-/-</sup> 30.4 ± 3.8, *P* = 0.12; alternations, WT 68.8 ± 2.5%, *crmp2*<sup>-/-</sup> 57.3 ± 2.5%, *P* = 0.006), mean ± SEM, \**P* < 0.05, t-test.

Sema3F binds preferentially to Nrp2/PlxnA3 receptor complex and is important regulator of neural development. Deficiency of Sema3F, Nrp2, or PlxnA3 results in defects in stereotyped pruning of hippocampal infrapyramidal bundle, distribution of DG dendritic spines, or anterior commissures, [42,55]. Moreover, *PlxnA3/A4*<sup>-/-</sup> mice display defects in pruning of visual axons. Similarly, in our *crmp2*<sup>-/-</sup> mice, we found all: IPB pruning defect, alteration of DG spine density (Figs 3 and 6), and defects in pruning of visual cortex axons (Fig 4). Moreover, our *in vitro* assays (Figs 5 and EV5) showed Sema3F is unable to induce axon and dendritic spine retraction in hippocampal neurons isolated from *crmp2*<sup>-/-</sup> embryos. In addition to Sema3F, IPB is also regulated by ephrin-B3 reverse signaling. It is possible to speculate that CRMP2, and in particular CRMP2A isoform, which is expressed in mossy fibers, conveys signaling of both Sema3F and ephrin-B3. Further studies will assess this hypothesis in more detail.

Sema3A has been shown to orchestrate pruning of, e.g., CA1 hippocamposeptal or callosal axons [3,33]. As CRMP2 has originally been identified as a mediator of Sema3A [8], we hypothesized that CRMP2 is involved also in Sema3A-triggered pruning. However, we did not find any evidence that would support this hypothesis. We did not detect DiI-positive CA1 neuron bodies by retrograde tracing from medial septum after the pruning period in *crmp2*<sup>-/-</sup> pups [6] (Fig EV3B). In callosal axons, we found significant differences in axon guidance between WT and *crmp2*<sup>-/-</sup> mice in P6–P9 mice (Fig 2), but the significance was lost in adult mice (Appendix Fig S1C–E), which could be due to the presence of effective Sema3A-dependent axon pruning. In line with these *in vivo* data, we found that Sema3A (but not Sema3F) was able to partially induce axon retraction of the stalling *crmp2*<sup>-/-</sup> axons in 1-week-old hippocampal neuron cultures (Fig 6). Relatively high variability in this experiment could be due to different sensitivity of individual synapses to semaphorin stimulation.

Importantly, we also did not find any defect in the pruning of neuromuscular junctions (NMJs) in *crmp2*<sup>-/-</sup> mice (Fig EV3C and D). At the end of the embryonic development, each synapse is innervated by up to 10 axon branches of different motor units [56]. During the first two postnatal weeks, all except one terminal branch are pruned back establishing singly innervated NMJs [60]. While the exact molecular cascade regulating motor axon pruning is not

known, Sema3A seems to play a role in the process as its receptor, Nrp1, is expressed in pre-synaptic axon terminals [61]. Moreover, Sema3A secreted from Schwann cells participates in NMJ remodeling [62]. Sema3F signaling has so far not been linked to motor axon pruning.

Dendritic spine density changes dynamically during childhood and adolescence. In mice, spine density peaks around 1 month and then decreases to reach stable levels around 2 months [45]. It has been shown that distribution of dendritic spines is regulated by class 3 semaphorins [42]. Previous *in vitro* experiments showed that Sema3F, but not Sema3A, decreases PSD-95-positive puncta in dissociated DG neurons [42]. Accordingly, Sema3F-treated cortical neurons displayed decrease in apical dendrite spine density [42]. Adult *Sema3F*<sup>-/-</sup>, *Nrp2*<sup>-/-</sup>, and *PlxnA3*<sup>-/-</sup> mice show increased spine density in several brain regions, in particular DG dendrites [42,63]. *Crmp2*<sup>-/-</sup> mice partially mimic this phenotype as we also found increased spine density in adult, but not in P30 DG granule cells (Fig 6). Interestingly, in *Sema3F*<sup>-/-</sup> mice, increased DG spine density is detectable already during spine generation (P21) and is largely retained into adulthood, while in WT, they are subsequently pruned [42]. In *crmp2*<sup>-/-</sup> mice, we did not find increased DG spine density in the pre-pruning period (P30, Fig 6A), but similar to *Sema3F*<sup>-/-</sup> mice, we did find defects in DG spine pruning. Before pruning, spines also tended to be relatively enlarged in *crmp2*<sup>-/-</sup> mice (Fig EV5A). Similar observations were found in Sema3F- and Nrp2-deficient mice using electron microscopy [42]. Aberrant spine size could reflect disruption in actin dynamic. *In vitro* analysis of dendritic spine remodeling further supports our *in vivo* findings (Fig EV5). Together, these data suggest that while Sema3F signaling regulates both spine generation and pruning, CRMP2 contributes mainly to spine pruning.

**CRMP2 in axonal growth *in vivo***

As demonstrated in knockout lines of Sema3A and its downstream targets (*Sema3A*<sup>-/-</sup>, *Nrp1*<sup>-/-</sup>, and *PlxnA4*<sup>-/-</sup> mice), Sema3A signaling is an essential regulator of the development of rodent trigeminal nerve, facial nerve, DRGs projection, olfactory bulb, hippocampal formation, and corpus callosum [27,28,33,34,64–67]. Surprisingly, although Sema3A or Nrp1 deletion causes strong

overgrowth of some peripheral nerves (e.g., trigeminal and spinal axons) [27,28], we found only a mild overgrowth and increased branching of these axons upon deletion of its downstream mediator CRMP2 in *crmp2*<sup>-/-</sup> mice (Figs 1 and EV2). This could be due to a partial rescue of *Sema3A* signaling in these neurons by other CRMP family members as mentioned before. Indeed, we and others [52] found that full CRMP2 deficiency *in vivo* is associated with increase of CRMP1 and CRMP4 levels (Fig EV2). CRMP1 and CRMP4 are sequentially and functionally close to CRMP2, and their expression pattern partially overlaps [68,69]. Moreover, CRMP4 (Fig EV2) and CRMP1 [70] are expressed in peripheral nerves suggesting that their elevation could rescue the reduced axon growth caused by acute CRMP2 deficiency. Increased expression of CRMP1 or CRMP4 could partially compensate for CRMP2 deficiency not only in *Sema3A*-dependent axon guidance but also in pruning, as we did not detect significant defects in *Sema3A*-dependent axon pruning in *crmp2*<sup>-/-</sup> neurons *in vivo* or *in vitro* (Figs 5 and EV3).

Previous *in vitro* studies demonstrated axon growth-promoting effect of CRMP2, while we did not detect any axon growth reduction in *crmp2*<sup>-/-</sup> mice. This may be because the role of CRMP2 in regulation of axon growth, neuron polarization, and migration has so far been studied *in vitro* using an acute knockdown of CRMP2 rather than *in vivo* in full knockout mice, which we used in our experiments and where the CRMP2 deficiency may be better compensated by other genes (e.g., CRMP1 or CRMP4).

Electroporation studies of *Sema3A*<sup>-/-</sup> or *Nrp1*<sup>floxed/floxed</sup> brains demonstrated their role in the development of corpus callosum, with mispositioned axons in callosal midline and axonal mistargeting in contralateral cortex at P8 [33]. Defects in axon pruning of this region were also suggested [33]. Using the *in utero* electroporation and DiI tracing in *crmp2*<sup>-/-</sup> mice, we also found defective guidance of callosal axons in the contralateral cortex and their altered orientation in the midline in the rostral-caudal axis (Fig 2).

Notably, *Sema3F* signaling is essential also for guidance of specific cranial nerves and was related to the development of limbic system and anterior commissure [40,71]. From these, we only detected partial malformation of AC in *crmp2*<sup>-/-</sup> mice (AC is missing in *Sema3F*<sup>-/-</sup> or *Nrp2*<sup>-/-</sup> mice) suggesting CRMP2 may participate also in *Sema3F*-mediated axon guidance (Fig EV4).

Previous *in vitro* and *in vivo* experiments suggested that CRMP2 also regulates neuronal migration [72]. However, using the *in utero* electroporation, we found no significant changes in neuron distribution in the developing WT and mutant cortical plates at E17.5 (Fig EV1F). This likely reflects different experimental paradigms used in the studies (somatic knockdown vs. full knockout) [72].

### CRMP2 involvement in pathogenesis of neurodevelopmental disorders

Deregulation of CRMP2 has been linked to several neurodevelopmental disorders (*SFARI* Gene database, <https://gene.sfari.org/database/human-gene/DPYSL2>). Recently published analysis of conditional brain-specific [17] and full *crmp2* knockout mice [52] showed multiple behavioral defects associated with CRMP2 deficiency. Notably, conditional knockout mice revealed hyperactivity and prepulsed inhibition (PPI) deficit together with social behavior impairment. PPI is a test for evaluating sensorimotor gating—the phenomenon that is often altered in schizophrenia patients. In

addition, clozapine (an antipsychotic drug) treatment was capable to reduce hyperactivity in conditional *crmp2*<sup>-/-</sup> mice. Furthermore, morphological analysis showed increased volume of brain ventricles and impaired dendritic development in hippocampal CA1 and DG neurons, which is associated with schizophrenia, but also other neurodevelopmental disorders [17]. Importantly, the analysis of the full and conditional CRMP2 knockout mice revealed also their significant differences. In particular, while PPI was reduced in the conditional mice and in the full *crmp2*<sup>-/-</sup> mice, it was not significantly different to WT [17,52]. This suggests that even a minor difference in the spatio-temporal inactivation of CRMP2 during development can have a major impact on the development and severity of the resulting neurodevelopmental defects. In the full CRMP2 knockout mice, we generated, we found several phenotypical defects present in the published conditional and full CRMP2 knockout mice (e.g., ventriculomegaly, spine density changes in DG, working memory defects, or hyperactivity) [17,73]. We also found brain sizes comparable in both WTs and *crmp2*<sup>-/-</sup> mice, similar as reported in the CRMP2 knockout mice [17,73], although we detected a non-significant tendency for a thinner cortex in the knockout mice (not shown) in agreement with the hypoplastic corpus callosum and anterior commissure. Changes in interhemispheric connectivity have recently been linked to ASD and schizophrenia through CYFIP1, a CRMP2 binding partner [74,75]. Importantly, we demonstrate that CRMP2 knockout leads to defects in axonal pruning and dendritic spine remodeling compatible with ASD rather than schizophrenia [25] (Figs 3, 4 and 6). Similar to other ASD mouse models [49], also in *crmp2*<sup>-/-</sup> mice the dendritic spine pruning deficiency is not present in all brain regions [e.g., we did not detect it in the prefrontal cortex (Fig 6F and G) or CA1 neurons (Fig EV5F and G)]. This may reflect specific spatio-temporal combinations of expression of CRMP2 (and its isoforms) and semaphorins in different brain regions (of note, there is a strong expression of CRMP2A isoform specifically in the inner molecular layer of DG (Fig EV1A), where we detected the pruning deficiency). The detail role of CRMP2 isoforms in axon pruning will be analyzed in future studies.

Morphological changes were accompanied by altered social communication in early postnatal (P8 and P12) mutants and decreased sociability in adults (Fig 7) further corroborating the role of CRMP2 in the pathogenesis of ASD. Defects in early postnatal USVs followed by dendritic spine pathology have been previously observed in several mouse models of ASD [49–51]. The connection between early postnatal altered sociability and impairment of stereotyped axon pruning is much less clear. Nevertheless, defects in stereotyped axon pruning have been associated with social interaction deficit and ASD in humans and mice, e.g., through functional variants and knockouts of *Otx-1* gene [76,77].

Importantly, *Sema3F* signaling has been also implicated in the pathogenesis of ASD. *Sema3F*- or *NRP2*-deficient mice show both behavioral and neuropathological aspects of ASD [78], and *Sema3F* interacts with multiple ASD-related genes, e.g., fragile X mental retardation protein or *MECP2* [79]. Thus, by linking *Sema3F* and CRMP2 signaling and comparing the histological as well as behavioral effects of their deficiency, our data strongly implicate that the *Sema3F*-CRMP2 signaling plays an important role in ASD pathogenesis. Since previously CRMP2 has been linked with pathogenesis of schizophrenia, it may serve as a

molecular link connecting class 3 semaphorin signaling defects to both ASD and schizophrenia.

## Materials and Methods

### Animals

All animal studies were ethically reviewed and performed in accordance with European directive 2010/63/EU and were approved by the Czech Central Commission for Animal Welfare. Mice, all in C57BL6/N background, were housed and handled according to the institutional committee guidelines with free access to food and water. Unless stated otherwise, adult mice used for experiments were 12–16 weeks old. See Appendix Table S1 for number of animals used in experiments.

### *Crmp2*<sup>-/-</sup> mice generation

We used TALEN mutagenesis (transcription activator-like effector nucleases) to generate *crmp2*<sup>-/-</sup> mice. Two TALEN pairs targeting sequences 185–150 bp 5' of *crmp2* exon 2 and 183–218 bp 3' of exon 3 (Fig 1A) were designed using TAL Effector Nucleotide Targeter 2.0 (<https://tale-nt.cac.cornell.edu/>) [80,81], assembled using the Golden Gate Cloning system [80], and cloned into the ELD-KKR backbone plasmid. DNA-binding domains of TALENs specific for the desired target sites within the *crmp2* locus consisted of following repeats: HD-HD-NN-HD-HD-HD-NG-NI-NN-HD-NG-NN-NN-NI-NG-HD-NG (5' TALEN-*crmp2*-ex1), NN-HD-NI NI-NG-HD-HD-NG-HD-NG-NN-NG-HD-NG-HD-NG-NG (3' TALEN-*crmp2*-ex1), HD-HD-NI-NI-NN-NI-NN-NG-HD-NI-HD-NG-NN-NI-NN-HD-NG-NG (5' TALEN-*crmp2*-ex2), and NN-HD-NI-HD-NI-NG-NG-HD-NG-NI-HD-HD-NI-NI-NN-NG (3' TALEN-*crmp2*-ex2). All TALEN plasmids were used for production of TALEN encoding mRNA as described previously [82]. TALEN mRNAs (with total RNA concentration of 40 ng/μl) were microinjected into C57BL6/N-derived zygotes. Genomic DNA isolated from tail biopsies of newborn mice was screened by PCR for deletion of exons 1 and 2 (3,673 bp) (primers F1: 5'-ATATCCCACGATTCTGACCAATCA-3' and R1: 5'-CCAAATAACTGCAGTGTAGCTAT-3'), and deletion was confirmed by locus sequencing and mice used as founders of *crmp2*<sup>-/-</sup> line. The mouse line was genotyped by PCR using locus-specific primers: R1: ACTTACCGTGATGCGTGGAA, F1: TCACCCTCCCGGACGAT, and R2: TCTACCAATGTTACAACACAGA.

### Antibodies, cell dyes, and plasmids

Primary antibodies used in this study are as follows: mouse anti-CRMP2 and hamster anti-CRMP1 (WAKO, IHC 1:200, WB 1:5,000), rabbit anti-TUC4 (CRMP4, Millipore, IHC 1:400, WB 1:5,000), rabbit affinity purified anti-CRMP2A (IHC 1:75) [14], rabbit anti-CRMP2A (WB, 1:30,000) [14], mouse anti-neurofilaments (2H3 antigen, DSHB Iowa, 1:150), rabbit anti-MAP2 (Abcam, 1:300), rabbit anti-calbindin (Swant, 1:600), mouse anti-Vglut2 and anti-Vglut1 (Millipore, 1:400), goat anti-PSD95 (Millipore, 1:200), mouse anti-tau (Abcam, 1:500), mouse anti-βIII-Tubulin conjugated to Alexa 488 (BioLegend, 1:200), mouse anti-actin (Sigma, 1:500), and rabbit anti-βIII-Tubulin (Sigma, 1:500). Secondary fluorescent antibodies

were conjugated with various Alexa Fluor dyes: anti-mouse (Alexa 488 or 594), anti-rabbit (Alexa 594), and anti-goat (Alexa 488), diluted 1:400. Hoechst 33342 (1 μg/ml) was used to counterstain cell nuclei. In some cases, ABC kit (Vector Laboratories) was used for detection. For whole-mount immunostaining, secondary anti-mouse antibody conjugated with HRP was used (1:1,000). For Western blots, secondary anti-mouse, anti-rabbit, or anti-hamster conjugated with HRP was used (1:10,000). Cholera toxin subunit B conjugated to Alexa 647, DiI, and DiO was purchased from Thermo Fisher. α-Bungarotoxin conjugated to Alexa 594 was purchased from Invitrogen (50 μg/ml; 1:50). EGFP was cloned into pCAGGS vector.

### Histology, immunohistochemistry, and biochemistry

Mice were perfused transcardially with PBS and ice-cold 4% paraformaldehyde (PFA) in PBS. Brains were isolated and postfixed overnight at 4°C in 4% PFA/PBS. Subsequently, brains were washed in PBS and processed as described previously [14,83]. Seven-μm-thick paraffin sections were created. Immunohistochemistry was done as described previously [14]. Sections were deparaffinated as follows: 2 × 10 min 100% xylene, 2 × 10 min 100% ethanol, 3 min 90% EtOH, 3 min 70% EtOH, 3 min 50% EtOH, and PBS. Antigen retrieval was performed in some cases using citrate-based antigen retrieval solution (Vector) diluted 1:100 in water. Slices were blocked in 1% BSA/0.2% Tween/PBS (PBST) and incubated with primary antibodies overnight at 4°C. Next, slices were washed 3 × 5 min in PBST and incubated with secondary antibodies conjugated with Alexa Fluors, 2 h at RT. Then, slices were washed 3 × 5 min in PBST and mounted in Mowiol with Hoechst (1:1,000). For bright-field microscopy, slices were pretreated 15 min in 3% H<sub>2</sub>O<sub>2</sub> prior to blocking and ABC kit (Vector) was used according to the manufacturer's instructions. HRP activity was detected with 0.05% DAB. Subsequently, slices were dehydrated in ethanol-xylene and embedded into Eukitt. Brain protein isolation, SDS-PAGE, and Western blotting were done as described previously [14].

### Whole-mount immunohistochemistry

Whole-mount immunohistochemistry was performed as described previously [14] with some modifications. E10.5–E12.5 embryos were isolated from time-pregnant mothers. WT and knockouts from the same litter were compared. Embryos were fixed in 4% PFA/PBS overnight, 4°C. Next day, they were washed with PBS and unmasked in 1:100 diluted antigen retrieval solution (Vector). Embryos were then washed again in PBS for 10 min (RT) followed 30 min in Dent fixative (20% DMSO/methanol) at 4°C. Subsequently, all samples were bleached overnight at 4°C in 5% H<sub>2</sub>O<sub>2</sub>/20% DMSO/methanol. Next, embryos were blocked overnight in 10% FBS/20% DMSO/PBS at 4°C and then incubated in anti-neurofilaments antibody clone 2H3 for 4 days (dilution 1:100 in blocking solution) followed by secondary HRP-conjugated antibody (1:1,000) for 24 h. Then, embryos were washed in 20% DMSO/PBS and incubated in 0.6% Tween/PBS overnight. Finally, samples were washed in PBS and incubated in 0.05% DAB for 2 h. H<sub>2</sub>O<sub>2</sub> was then used as a substrate. Labeled embryos were washed in PBS and cleared in ascending glycerol concentration (20, 40, 60, and 80%). They were stored in 80% glycerol at 4°C. Images were captured using Nikon

SMZ18 stereomicroscope and post-processed in Helicon focus to create sharp images. Surface area occupied by a given nerve was measured in ImageJ. Axons were traced in NeuroLucida 360.

### DiOlistics and DiI tracing

We used DiOlistic approach using Gene Gun helium-powered system from Bio-Rad. Bullets were prepared as described [84], and tubing was coated with 10 mg/ml polyvinylpyrrolidone (PVP). We mixed 100 mg Tungsten beads and 2.5 mg DiI or DiO (dissolved in  $\text{CH}_2\text{Cl}_2$ ). After  $\text{CH}_2\text{Cl}_2$  evaporation, resulted powder was transferred into aluminum-wrapped falcon tube and 3 ml  $\text{H}_2\text{O}$  was added. Solution was sonicated at 4°C until no clumps were visible (30–45 min). Then, solution was sucked into tubing in prep station, beads were able to settle down, and water was removed. Tubing was rotated 1 h during continuous drying with nitrogen (2–3 l/min). Finally, 1.3-cm bullets were cut from tubing and stored in 4°C with silica gel beads to prevent rehydration.

Slices for DiOlistics were prepared as follows: Mice were perfused with 20 ml 4% PFA/PBS, and brains were isolated and postfixed 30 min in 4% PFA/PBS. Then, brains were washed 1–3 h in PBS and 20 min in 15% sucrose/PBS following another 20 min in 30% sucrose/PBS. 250  $\mu\text{m}$  coronal slices were prepared using vibratome Leica 2000S. Prior to shooting, slices were treated 5 min in 15% sucrose and 5 min in 30% sucrose. Dye was carried using pressure 120 Psi and modified filter as described [84]. After shooting, slices were washed 3 $\times$  in PBS quickly and dye was let to diffuse 40 min at 4°C. Slices were then mounted onto glass slide in 0.5% n-propyl gallate/90% glycerol/PBS (NPG) and imaged by CARV II/Nikon Ti-E spinning disk.

For carbocyanine dye tracing, mice were perfused transcardially with PBS and fixed with 4% PFA/PBS. Next, either small DiI crystal was placed or 0.1  $\mu\text{l}$  of DiI solution was injected into target area. We used 2.5 mg/100  $\mu\text{l}$  concentration, and DiI was dissolved in DMSO. Slices were prepared in vibratome and scanned by Leica TCS SP8. Details are as follows.

### Corpus callosum tracing

DiI solution was injected into superficial layers of cortex. Brains were maintained in 4% PFA/PBS in 37°C for 3–4 weeks. Then, brains were cut in oblique (horizontal + 20°) direction (Appendix Fig S1A), 150- $\mu\text{m}$ -thick sections were prepared. Slices with traced axons were mounted onto glass slide in NPG mounting solution.

### Hippocamposeptal axon tracing

After fixation, brains were trimmed to expose septum. DiI crystals were inserted into the medial septum and brains were maintained in 4% PFA/PBS for 1–2 weeks. 100  $\mu\text{m}$  (P0–1) or 150  $\mu\text{m}$  (P8) coronal slices were prepared. We found a strong labeling of septohippocampal projections (e.g., axons arising from the septum entering the hippocampus) and also subicular neurons projecting to the medial septum in both WT and knockouts. We screened for retrogradely labeled CA1 neuron bodies in the hippocampus, whose presence at P8 indicates incomplete pruning.

### Visual corticospinal axon tracing

DiI solution was injected into primary visual area. After 2–3 weeks, brains were cut sagittally to 150–180- $\mu\text{m}$  slices that were

mounted in NPG with Hoechst. The tracing pattern was compared with data from Allen brain atlas connectivity studies to ensure that we targeted correct area. We observed two axon branches in the diencephalon: first branch growing into pyramidal tract (corticospinal axons) and second to superior colliculus (collicular axons). To quantify the axonal growth into the pyramidal tract, we compared fluorescence intensity of corticospinal axons vs. intensity of axons before branching. We refer to this ratio as visual pruning index (VP index), with its lower values indicating the presence of refinement.

### In utero electroporations

*In utero* electroporations were done as previously described [85]. Briefly, pregnant mice were anaesthetized by 2.5% isoflurane. Anesthesia was maintained by 2% isoflurane. We injected pCAGGS-EGFP plasmid (3  $\mu\text{g}/\mu\text{l}$ ) into ventricles of E14.5 embryos (migration assay, analysis at E17.5) or E15.5 embryos (callosal axons, analyzed at P6). Electroporation was carried out by small paddle electrodes (35 V, five pulses, 950-ms interval) to target sensory cortex. For migration assays, embryos were harvested at E17.5, and brains were fixed in 4% PFA/PBS, sliced (150- $\mu\text{m}$  vibratome sections), counterstained with Hoechst, and scanned by Leica TCS SP8. In this case only, both WT and *crmp2*<sup>+/-</sup> embryos were used as controls. Callosal axons were analyzed at P6. After birth, pups were nurtured by a foster mother. At P6, mice were sacrificed, and brains were fixed in 4% PFA/PBS, sliced (150  $\mu\text{m}$  vibratome sections), and analyzed by CARV II/Nikon Ti-E spinning disk.

### Semaphorin assays and live imaging

Mouse E16.5 hippocampal neurons were prepared and cultured as described [14]. Briefly, pregnant mice were sacrificed, and embryos isolated and decapitated in cold HBSS with 10 mM Hepes. Hippocampi were isolated, moved to Neurobasal medium (Neurobasal (Gibco) with 2.5% B27 supplement (Gibco), 2.5 mM glutamine, and 1% penicillin/streptomycin solution), and triturated. Subsequently, solution was strained through a 40- $\mu\text{m}$  strainer (Biologix) and spun down (300 g, 2 min, 4°C). The supernatant was removed, and the remaining cells were resuspended in a fresh Neurobasal medium and counted. Neurons were plated into 24-glass bottom plates (100,000 cells/well) coated with laminin (1  $\mu\text{g}/\text{ml}$ ) and poly-D-lysine (50  $\mu\text{g}/\text{ml}$ ) and cultured in Neurobasal medium that was refreshed every 2–3 days. Neurons were transfected with pCAGGS-EGFP using Lipofectamine 2000 (Invitrogen), 24 h after plating (axon retraction assay) or at DIV14 (dendritic spine analysis). Mouse semaphorin 3A and 3F (carrier free) or control Fc were purchased from R&D systems and were diluted to 1 mg/ml stock concentration. For axon retraction assay at DIV 7, medium volume was adjusted to 300  $\mu\text{l}$  in each well. Neurons were photographed three times (with 20 min gaps), and then, 50  $\mu\text{l}$  of fresh medium with Fc or Sema3A (final concentration 1 nM) or Sema3F (final concentration 5 nM) was added. Subsequently, neurons were imaged every 20 min for 16 h by Leica DMI6000 equipped with a heating box and  $\text{CO}_2$  atmosphere. For analysis of dendritic spines, the same segments were photographed at DIV21 and DIV25. At DIV25, neurons were stimulated with Sema3F (5 nM) for 3 h and photographed again.



### Microfluidic chambers and DRG collapse assay

Microfluidic chambers were prepared as described before [31,86]. E11.5–E12.5 spinal cord explants were dissected in cold HBSS and placed into laminin (3 µg/ml)- and poly-L-ornithine (1.5 µg/ml)-coated proximal well. After 3–4 days, axons entered the distal compartment. Then, explants were labeled by Alexa 647-conjugated cholera toxin subunit B. 5 nM Sema3A of control Fc was applied distally, and axons were photographed by Leica DMI6000 microscope every 10 min during 14-h interval. Axons growing at least 50 µm were analyzed. Growth cone collapse was analyzed in DRG explants isolated at E11.5–E12.5. DRGs were plated on coverslips coated with laminin (1 µg/ml) and poly-D-lysine (50 µg/ml) and cultured in Neurobasal medium supplemented with NGF (R&D systems, 25 ng/ml). The day after plating, explants were stimulated with various Sema3A concentrations for 30 min, fixed, and stained with antibodies against actin (to label growth cones) and β-3 tubulin (to label axons). DRGs were imaged by Nikon spinning disk.

### Analysis of developmental motor axon pruning

WT and *crmp2*<sup>-/-</sup> pups (both sexes) were sacrificed on P11, and the thorax was excised as previously described [87–90] and fixed in 4% PFA in 0.1 M phosphate buffer (PB) for 1 h on ice. The triangularis sterni muscle was dissected and incubated overnight (4°C) in anti-βIII-tubulin antibody conjugated to Alexa 488 (BioLegend 801203; 1:200)- and Alexa 594-conjugated α-bungarotoxin (Invitrogen B13423; 50 µg/ml; 1:50) in blocking solution (5% BSA, 0.5% Triton X-100 in 0.1 M PB). Muscles were then washed in 0.1 M PB and mounted in Vectashield (Vector Laboratories). Z-stacks were recorded using a confocal microscope (FV1000, Olympus) equipped with a 20×/0.8 N.A. oil-immersion objective and analyzed for the percentage of doubly innervated NMJs using Fiji (cell counter plugin) [91].

### Behavioral tests

- 1 Ultrasonic vocalizations were recorded from P6, P8, and P12 pups (WT *n* = 14, *crmp2*<sup>-/-</sup> *n* = 13). Each pup was taken from its home cage, put into Styrofoam box, and recorded for 5 min with microphone (Dodotronic Ultramic 250K, Italy) placed at the top of the box. Audacity software (freely available) was used for recordings with sampling frequency set to 250 kHz. The vocalizations were analyzed automatically using Avisoft-SASLab Pro; however, the automatic analysis was checked and manually corrected if necessary. Main parameters measured were number of vocalizations and its total length.
- 2 Sociability and social novelty preference were tested in three-chambered apparatus (54 × 20 × 33 cm) made from clear plexiglass. The chambers were divided by transparent walls with squared openings (5 × 5 cm) and sliding doors. Each mouse (WT *n* = 11, *crmp2*<sup>-/-</sup> *n* = 13) was first placed in the middle compartment for 10 min. After the habituation, unknown male mice (stranger 1) were enclosed in a little wire cage and placed in either left or right compartment. Black plug (4.5 cm in diameter) was used as an object and placed in the opposite compartment inside identical wire cage. The position

of stranger mouse and object was counterbalanced between trials, and stranger mice were previously habituated to the cage. Sliding doors were then opened, and the test mouse was allowed to freely explore the apparatus for 10 min. After end of this part of experiment, the object was removed and another unknown mouse (stranger 2) was put inside the same chamber. The test mouse was then allowed to explore all chambers for another 5 min. The behavior was recorded by a camera placed above the apparatus. Time spent in each chamber and time spent sniffing the wire cages were analyzed manually in BORIS software.

- 3 The elevated plus maze (EPM) is a cross-shaped maze elevated 40 cm above the floor level, with all four arms (30 cm long, 5 cm wide, 16 cm high) accessible from the central platform. Two opposite arms were enclosed by opaque walls (closed arms), while the other two were without walls (open arms). The test assesses spontaneous and anxiety-like behaviors of the animals. The closed arms are perceived as safer by the animals, as they are darker, more protected, and without risk of falling. Anxious animals are expected to spend most of the time in the closed arms, while less anxious and more explorative individuals explore the open arms more often. The behavior of the animals during each 5-min session was recorded by a web camera placed above the apparatus. Locomotor activity (total distance) and time spent in different compartments were analyzed offline by digital tracking software (EthoVision, Noldus). Numbers of animals: *n* = 10 for both WT and knockouts, aged 31–44 weeks.
- 4 Spontaneous alternation was tested in three-armed maze (Y-maze), with each arm 35 cm long, 6 cm wide, and 18 cm high. The mice were left free to explore the empty apparatus for 8 min. Between trials, the apparatus was cleaned by ethanol and then wiped clean and dry to erase any scent marks. Number of arm visits was counted, indicating the exploratory activity (a visit was counted if the mouse placed all paws into the arm). Spontaneous alternation was measured as the ratio of actual triads (three different arms entered in three subsequent visits) to potential triads (theoretical maximum performance). In the Y-maze task, 17 male mice (9 WT, 8 KO), aged 31–44 weeks, were tested.
- 5 The active place avoidance task, or AAPA [92,93] (for review, see Ref. [94]), is a rodent cognitive task testing hippocampal functions, including spatial navigation, cognitive coordination, and flexibility. As a dry-arena task, it is more suitable for mice than the Morris water maze, as mice are worse swimmers than rats and tend to be overtly stressed by water immersion [95]. We used a carousel maze (circular arena 56 cm in diameter) with electrified grid floor, surrounded by a transparent plexiglass wall, rotating at approximately 1 rotation per minute. The apparatus was located in a dimly lit room with abundant extramaze cues, with an additional, highly contrast cue card in close proximity (1.5 m) of the arena. A computer-based tracking system (Tracker, Biosignal Group, USA) recorded the positions of the mouse and the arena at a sampling rate of 25 Hz. A 60-degree unmarked-to-be-avoided sector was defined in the coordinate frame of the room by tracking software. Each entrance into the sector was punished by mild electric foot shocks (scrambled; 100 Hz alternating current; 40–80 V) delivered by the tracking system into the grid floor. Each shock lasted 0.5 s and was

repeated after 0.9 s if the mouse failed to escape the to-be-avoided sector in time. Intensity of the shock was individualized for each mouse (0.2–0.4 mA), to ensure escape reaction while avoiding excessive pain. The training schedule consisted of five acquisition sessions and four reversal sessions, where the sector position was changed by 180°. Two 10-min sessions were scheduled for each experimental day, separated by approximately 3 h of rest in the home cage. The arena rotated while the sector remained fixed in the reference frame of the room; therefore, the mice had to move actively away from the sector in the direction opposite to arena rotation; otherwise, they would be carried into the sector. For successful avoidance, the animal had to separate the distant room-frame cues, which could be used to locate and avoid the sector, from the irrelevant, arena-frame cues. Selection of the correct spatial cues and achievement of the correct behavioral strategy requires segregation of spatial frames, a skill that is considered equivalent of human cognitive coordination [96]. Furthermore, cognitive flexibility was tested in reversal sessions, to adjust the behavioral response to reversed sector location. The trajectory of the mice was analyzed offline using the custom-made and freely available Carousel Maze Manager 4.0 [97]. Total distance walked, a measure of locomotor activity of the mouse, and the number of entrances, a measure of its ability to avoid entering the to-be-avoided sector, were used as the most important output parameters. Active place avoidance performance was evaluated by two consecutive RM-ANOVA analyses, with sessions taken as repeated measures, and genotype as a between-subject factor. In this task, 21 male mice (11 KO, 10 WT), 12–14 weeks old, were tested.

### Light microscopy

Five types of microscopes were used in this study: (i) Leica TCS SP8 confocal equipped with 405-nm laser (Hoechst), 488-nm laser (DiO, EGFP excitation), 552-nm laser (DiI excitation), 10×/0.3 dry, and 25×/0.75 immerse-oil objectives (Figs 2G, 4, 6D, F, EV1F, EV3B, and EV5B, D, Appendix Fig S1C). (ii) Inverted fluorescent microscope Leica DMI6000 equipped with 20×/0.4 dry objective, 37°C incubator, and CO<sub>2</sub> chamber for live imaging (Figs 1F and 5). (iii) CARV II/Nikon Ti-E spinning disk equipped with 20×/0.5 dry, 40×/1.3, and 100×/1.4 immerse-oil objectives (Figs 1B, 2C, D, 3, 6A, B, F, EV1A, F, EV2G, EV3A, EV4A, D, and EV5A, F). (iv) Olympus FV1000 confocal microscope equipped with 20×/0.8 objective (Fig EV3C). (v) Nikon SMZ18 stereomicroscope for microdissections and whole-mount analysis equipped with 1× and 2× SHR Plan Apo objectives (Figs 1C, 2A, EV1C, D, EV2A, B, E, F, and EV4B). Microscopy images from Figs 1–4 and EV1, EV3, and EV4 are compositions of more fields automatically generated by Leica LAS X software or NIS elements software. Maximum projections were generated in ImageJ.

### Image processing and statistics

We used NeuroLucida 360 software to reconstruct callosal axons from both *in utero* electroporation and DiI-tracing experiments. In case of oblique sections, we picked only midline regions (approximately 100 μm from midline to each side) and traced axons

semi-automatically using AutoNeuron algorithm. To display overall axon growth direction, polar histograms and fan-in diagrams were generated using NeuroLucida explorer. Polar histograms show total axon length in a specific degree range. We counted lengths in each 20° of histogram. Fan-in diagrams represent the same in another graphical view when all traced axons rise from a single point. Dendrites and dendritic spines were analyzed either with NeuroLucida360 or with NeuronJ plugin in ImageJ. Spine head diameter was measured after 3D reconstruction of spines in NeuroLucida 360. Images from whole-mount preparations were processed in Helicon focus to create sharp projections. Growth of peripheral nerves and all data from time-lapse imaging series were analyzed in ImageJ. Neuron migration was analyzed in ImageJ using cell counter plugin. Measurements of axon pruning from immunohistochemistry and DiI-tracing experiments were done in ImageJ. In all figures, different channels of image series were combined in pseudo-color using the “screen” function in Adobe Photoshop and adjusted to enhance low-intensity objects. GraphPad Prism was used for statistical analysis. For comparison of two independent groups, unpaired *t*-test was used unless stated otherwise. Multiple comparisons were performed using two-way ANOVA. Data from behavioral experiments were analyzed by unpaired *t*-test (P6, P8 vocalization, sociability, Y-maze, EPM), ANOVA (AAPA), or Mann–Whitney test (P12 vocalization). All data are presented as means ± SD, unless stated otherwise.

**Expanded View** for this article is available online.

### Acknowledgements

The work of MB, JZ, MJ, TP, BP, and AS was supported by Czech Health Research Council grant no. NV18-04-00085. MB, RW, BP, JZ, and MK were supported by Czech Science Foundation grant no. 16-15915S. The work of JZ, RW, and BP was supported by Grant Agency of the Charles University grant nos. 682217, 524218, and 1062216, respectively. MJ, TP, and AS were supported by Czech Science Foundation grant no. 19-03016S and Czech Health Research Council grant no 17-30833A. MW, MSB, and TM were supported by the ERC (FP/2007-2013; ERC Grant Agreement No. 616791), the German-Israeli Foundation, SFB 870, DFG grant CRC870-A11, and the Munich Cluster for Systems Neurology (SyNergy; EXC2145). RS was supported by RVO 68378050 by Academy of Sciences of the Czech Republic. Czech Centre for Phenogenomics infrastructure, used during the project, was supported by grants LM2015040, CZ.1.05/2.1.00/19.0395, and CZ.1.05/1.1.00/02.0109 funded by the Ministry of Education, Youth and Sports and the European Regional Development Fund. We are grateful to Dr. Jan Krůšek from the Department of Cellular Neurophysiology, Institute of Physiology, CAS, Prague, for his help with preparation of glass micropipettes. We acknowledge the Microscopy Centre—Light Microscopy Core Facility, IMG ASCR, Prague, Czech Republic, supported by MEYS (LM2015062), OPPK (CZ.2.16/3.1.00/21547) and (LO1419), and Light Microscopy Core Facility, IPHYS ASCR, Prague, Czech Republic, supported by MEYS (LM2015062 Czech-BioImaging) for their support with confocal and live imaging.

### Author contributions

Study design: MB, JZ; data acquisition and analysis: JZ, MB, RW, KJ, MJ, RM, TP, BP, MW, MSB, MK, PK, XZ; supervision: MB, EP, AS, RS, TM, GA-B; writing—original draft: JZ, MB, MSB; writing—review and editing: JZ, MB, GA-B, TM, RM, AS, TP, MSB; project administration: MB.

### Conflict of interest

The authors declare that they have no conflict of interest.

## References

- Riccomagno MM, Kolodkin AL (2015) Sculpting neural circuits by axon and dendrite pruning. *Annu Rev Cell Dev Biol* 31: 779–805
- Johnston MV (2004) Clinical disorders of brain plasticity. *Brain Dev* 26: 73–80
- Vanderhaeghen P, Cheng HJ (2010) Guidance molecules in axon pruning and cell death. *Cold Spring Harb Perspect Biol* 2: a001859
- Van Battum EY, Brignani S, Pasterkamp RJ (2015) Axon guidance proteins in neurological disorders. *Lancet Neurol* 14: 532–546
- Yu F, Schuldiner O (2014) Axon and dendrite pruning in *Drosophila*. *Curr Opin Neurobiol* 27: 192–198
- Bagri A, Cheng HJ, Yaron A, Pleasure SJ, Tessier-Lavigne M (2003) Stereotyped pruning of long hippocampal axon branches triggered by retraction inducers of the semaphorin family. *Cell* 113: 285–299
- Low LK, Liu XB, Faulkner RL, Coble J, Cheng HJ (2008) Plexin signaling selectively regulates the stereotyped pruning of corticospinal axons from visual cortex. *Proc Natl Acad Sci USA* 105: 8136–8141
- Goshima Y, Nakamura F, Strittmatter P, Strittmatter SM (1995) Collapsin-induced growth cone collapse mediated by an intracellular protein related to UNC-33. *Nature* 376: 509–514
- Byk T, Dobransky T, Cifuentes-Diaz C, Sobel A (1996) Identification and molecular characterization of Unc-33-like phosphoprotein (Ulip), a putative mammalian homolog of the axonal guidance-associated unc-33 gene product. *J Neurosci* 16: 688–701
- Minturn JE, Fryer HJ, Geschwind DH, Hockfield S (1995) TOAD-64, a gene expressed early in neuronal differentiation in the rat, is related to unc-33, a *C. elegans* gene involved in axon outgrowth. *J Neurosci* 15: 6757–6766
- Fukata Y, Itoh TJ, Kimura T, Menager C, Nishimura T, Shiromizu T, Watanabe H, Inagaki N, Iwamatsu A, Hotani H et al (2002) CRMP-2 binds to tubulin heterodimers to promote microtubule assembly. *Nat Cell Biol* 4: 583–591
- Uchida Y, Ohshima T, Sasaki Y, Suzuki H, Yanai S, Yamashita N, Nakamura F, Takei K, Ihara Y, Mikoshiba K et al (2005) Semaphorin3A signalling is mediated via sequential Cdk5 and GSK3beta phosphorylation of CRMP2: implication of common phosphorylating mechanism underlying axon guidance and Alzheimer's disease. *Genes Cells* 10: 165–179
- Yuasa-Kawada J, Suzuki R, Kano F, Ohkawara T, Murata M, Noda M (2003) Axonal morphogenesis controlled by antagonistic roles of two CRMP subtypes in microtubule organization. *Eur J Neurosci* 17: 2329–2343
- Balastik M, Zhou XZ, Alberich-Jorda M, Weissova R, Ziak J, Pazyra-Murphy MF, Cosker KE, Machonova O, Kozmikova I, Chen CH et al (2015) Prolyl isomerase Pin1 regulates axon guidance by stabilizing CRMP2A selectively in distal axons. *Cell Rep* 13: 812–828
- Yoshimura T, Kawano Y, Arimura N, Kawabata S, Kikuchi A, Kaibuchi K (2005) GSK-3beta regulates phosphorylation of CRMP-2 and neuronal polarity. *Cell* 120: 137–149
- Arimura N, Menager C, Kawano Y, Yoshimura T, Kawabata S, Hattori A, Fukata Y, Amano M, Goshima Y, Inagaki M et al (2005) Phosphorylation by Rho kinase regulates CRMP-2 activity in growth cones. *Mol Cell Biol* 25: 9973–9984
- Zhang H, Kang E, Wang Y, Yang C, Yu H, Wang Q, Chen Z, Zhang C, Christian KM, Song H et al (2016) Brain-specific Crmp2 deletion leads to neuronal development deficits and behavioural impairments in mice. *Nat Commun* 7: 11773
- Makihara H, Nakai S, Ohkubo W, Yamashita N, Nakamura F, Kiyonari H, Shioi G, Jitsuki-Takahashi A, Nakamura H, Tanaka F et al (2016) CRMP1 and CRMP2 have synergistic but distinct roles in dendritic development. *Genes Cells* 21: 994–1005
- Nakata K, Ujike H, Sakai A, Takaki M, Imamura T, Tanaka Y, Kuroda S (2003) The human dihydropyrimidinase-related protein 2 gene on chromosome 8p21 is associated with paranoid-type schizophrenia. *Biol Psychiatry* 53: 571–576
- Liu Y, Pham X, Zhang L, Chen PL, Burzynski G, McGaughey DM, He S, McGrath JA, Wolyniec P, Fallin MD et al (2014) Functional variants in DPYSL2 sequence increase risk of schizophrenia and suggest a link to mTOR signaling. *G3 (Bethesda)* 5: 61–72
- Clark D, Dedova I, Cordwell S, Matsumoto I (2006) A proteome analysis of the anterior cingulate cortex gray matter in schizophrenia. *Mol Psychiatry* 11: 459–470, 423
- Quach TT, Honnorat J, Kolattukudy PE, Khanna R, Duchemin AM (2015) CRMPs: critical molecules for neurite morphogenesis and neuropsychiatric diseases. *Mol Psychiatry* 20: 1037–1045
- Braunschweig D, Krakowiak P, Duncanson P, Boyce R, Hansen RL, Ashwood P, Hertz-Picciotto I, Pessah IN, Van de Water J (2013) Autism-specific maternal autoantibodies recognize critical proteins in developing brain. *Transl Psychiatry* 3: e277.
- De Rubeis S, He X, Goldberg AP, Poultney CS, Samocha K, Cicek AE, Kou Y, Liu L, Fromer M, Walker S et al (2014) Synaptic, transcriptional and chromatin genes disrupted in autism. *Nature* 515: 209–215
- Lord C, Elsabbagh M, Baird G, Veenstra-Vanderweele J (2018) Autism spectrum disorder. *Lancet* 392: 508–520
- Bourgeron T (2015) From the genetic architecture to synaptic plasticity in autism spectrum disorder. *Nat Rev Neurosci* 16: 551–563
- Kitsukawa T, Shimizu M, Sanbo M, Hirata T, Taniguchi M, Bekku Y, Yagi T, Fujisawa H (1997) Neuropilin-semaphorin III/D-mediated chemorepulsive signals play a crucial role in peripheral nerve projection in mice. *Neuron* 19: 995–1005
- Taniguchi M, Yuasa S, Fujisawa H, Naruse I, Saga S, Mishina M, Yagi T (1997) Disruption of semaphorin III/D gene causes severe abnormality in peripheral nerve projection. *Neuron* 19: 519–530
- Chen H, Bagri A, Zupicich JA, Zou Y, Stoeckli E, Pleasure SJ, Lowenstein DH, Skarnes WC, Chedotal A, Tessier-Lavigne M (2000) Neuropilin-2 regulates the development of selective cranial and sensory nerves and hippocampal mossy fiber projections. *Neuron* 25: 43–56
- Cheng HJ, Bagri A, Yaron A, Stein E, Pleasure SJ, Tessier-Lavigne M (2001) Plexin-A3 mediates semaphorin signaling and regulates the development of hippocampal axonal projections. *Neuron* 32: 249–263
- Maimon R, Ionescu A, Bonnie A, Sweetat S, Wald-Altman S, Inbar S, Gradus T, Trotti D, Weil M, Behar O et al (2018) miR126-5p downregulation facilitates axon degeneration and NMJ disruption via a non-cell-autonomous mechanism in ALS. *J Neurosci* 38: 5478–5494
- Brown M, Jacobs T, Eickholt B, Ferrari G, Teo M, Monfries C, Qi RZ, Leung T, Lim L, Hall C (2004) Alpha2-chimaerin, cyclin-dependent Kinase 5/p35, and its target collapsin response mediator protein-2 are essential components in semaphorin 3A-induced growth-cone collapse. *J Neurosci* 24: 8994–9004
- Zhou J, Wen Y, She L, Sui YN, Liu L, Richards LJ, Poo MM (2013) Axon position within the corpus callosum determines contralateral cortical projection. *Proc Natl Acad Sci USA* 110: E2714–E2723
- Wu KY, He M, Hou QQ, Sheng AL, Yuan L, Liu F, Liu WW, Li G, Jiang XY, Luo ZG (2014) Semaphorin 3A activates the guanosine triphosphatase

- Rab5 to promote growth cone collapse and organize callosal axon projections. *Sci Signal* 7: ra81
35. Wang CL, Zhang L, Zhou Y, Zhou J, Yang XJ, Duan SM, Xiong ZQ, Ding YQ (2007) Activity-dependent development of callosal projections in the somatosensory cortex. *J Neurosci* 27: 11334–11342
  36. Penzes P, Cahill ME, Jones KA, VanLeeuwen JE, Woolfrey KM (2011) Dendritic spine pathology in neuropsychiatric disorders. *Nat Neurosci* 14: 285–293
  37. Garey L (2010) When cortical development goes wrong: schizophrenia as a neurodevelopmental disease of microcircuits. *J Anat* 217: 324–333
  38. Liu XB, Low LK, Jones EG, Cheng HJ (2005) Stereotyped axon pruning via plexin signaling is associated with synaptic complex elimination in the hippocampus. *J Neurosci* 25: 9124–9134
  39. Linke R, Pabst T, Frotscher M (1995) Development of the hippocamposeptal projection in the rat. *J Comp Neurol* 351: 602–616
  40. Sahay A, Molliver ME, Ginty DD, Kolodkin AL (2003) Semaphorin 3F is critical for development of limbic system circuitry and is required in neurons for selective CNS axon guidance events. *J Neurosci* 23: 6671–6680
  41. Basarsky TA, Parpura V, Haydon PG (1994) Hippocampal synaptogenesis in cell culture: developmental time course of synapse formation, calcium influx, and synaptic protein distribution. *J Neurosci* 14: 6402–6411
  42. Tran TS, Rubio ME, Clem RL, Johnson D, Case L, Tessier-Lavigne M, Huganir RL, Ginty DD, Kolodkin AL (2009) Secreted semaphorins control spine distribution and morphogenesis in the postnatal CNS. *Nature* 462: 1065–1069
  43. Yamashita N, Morita A, Uchida Y, Nakamura F, Usui H, Ohshima T, Taniguchi M, Honnorat J, Thomasset N, Takei K et al (2007) Regulation of spine development by semaphorin3A through cyclin-dependent kinase 5 phosphorylation of collapsin response mediator protein 1. *J Neurosci* 27: 12546–12554
  44. Petanjek Z, Judas M, Simic G, Rasin MR, Uylings HB, Rakic P, Kostovic I (2011) Extraordinary neoteny of synaptic spines in the human prefrontal cortex. *Proc Natl Acad Sci USA* 108: 13281–13286
  45. Bian WJ, Miao WY, He SJ, Qiu Z, Yu X (2015) Coordinated spine pruning and maturation mediated by inter-spine competition for cadherin/catenin complexes. *Cell* 162: 808–822
  46. Garey LJ, Ong WY, Patel TS, Kanani M, Davis A, Mortimer AM, Barnes TR, Hirsch SR (1998) Reduced dendritic spine density on cerebral cortical pyramidal neurons in schizophrenia. *J Neurol Neurosurg Psychiatry* 65: 446–453
  47. Ey E, Torquet N, Le Sourd AM, Leblond CS, Boeckers TM, Faure P, Bourgeron T (2013) The Autism ProSAP1/Shank2 mouse model displays quantitative and structural abnormalities in ultrasonic vocalisations. *Behav Brain Res* 256: 677–689
  48. Hung AY, Futai K, Sala C, Valtschanoff JG, Ryu J, Woodworth MA, Kidd FL, Sung CC, Miyakawa T, Bear MF et al (2008) Smaller dendritic spines, weaker synaptic transmission, but enhanced spatial learning in mice lacking Shank1. *J Neurosci* 28: 1697–1708
  49. Schmeisser MJ, Ey E, Wegener S, Bockmann J, Stempel AV, Kuebler A, Janssen AL, Udvardi PT, Shibani E, Spilker C et al (2012) Autistic-like behaviours and hyperactivity in mice lacking ProSAP1/Shank2. *Nature* 486: 256–260
  50. Binder MS, Lugo JN (2017) NS-Pten knockout mice show sex- and age-specific differences in ultrasonic vocalizations. *Brain Behav* 7: e00857
  51. Reynolds CD, Nolan SO, Jefferson T, Lugo JN (2016) Sex-specific and genotype-specific differences in vocalization development in FMR1 knockout mice. *NeuroReport* 27: 1331–1335
  52. Nakamura H, Yamashita N, Kimura A, Kimura Y, Hirano H, Makihara H, Kawamoto Y, Yitsuki-Takahashi A, Yonezaki K, Takase K et al (2016) Comprehensive behavioral study and proteomic analyses of CRMP2-deficient mice. *Genes Cells* 21: 1059–1079
  53. Kjelstrup KG, Tuvnes FA, Steffenach HA, Murison R, Moser EI, Moser MB (2002) Reduced fear expression after lesions of the ventral hippocampus. *Proc Natl Acad Sci USA* 99: 10825–10830
  54. Luo L, O'Leary DD (2005) Axon retraction and degeneration in development and disease. *Annu Rev Neurosci* 28: 127–156
  55. Riccomagno MM, Hurtado A, Wang H, Macopson JG, Griner EM, Betz A, Brose N, Kazanietz MG, Kolodkin AL (2012) The RacGAP beta2-Chimaerin selectively mediates axonal pruning in the hippocampus. *Cell* 149: 1594–1606
  56. Tapia JC, Wylie JD, Kasthuri N, Hayworth KJ, Schalek R, Berger DR, Guatimosim C, Seung HS, Lichtman JW (2012) Pervasive synaptic branch removal in the mammalian neuromuscular system at birth. *Neuron* 74: 816–829
  57. Brill MS, Kleele T, Ruschkies L, Wang M, Marahori NA, Reuter MS, Hausrat TJ, Weigand E, Fisher M, Ahles A et al (2016) Branch-specific microtubule destabilization mediates axon branch loss during neuromuscular synapse elimination. *Neuron* 92: 845–856
  58. Xu NJ, Henkemeyer M (2009) Ephrin-B3 reverse signaling through Grb4 and cytoskeletal regulators mediates axon pruning. *Nat Neurosci* 12: 268–276
  59. Cocchi E, Drago A, Serretti A (2016) Hippocampal pruning as a new theory of schizophrenia etiopathogenesis. *Mol Neurobiol* 53: 2065–2081
  60. Sanes JR, Lichtman JW (1999) Development of the vertebrate neuromuscular junction. *Annu Rev Neurosci* 22: 389–442
  61. Venkova K, Christov A, Kamaluddin Z, Kobalka P, Siddiqui S, Hensley K (2014) Semaphorin 3A signaling through neuropilin-1 is an early trigger for distal axonopathy in the SOD1G93A mouse model of amyotrophic lateral sclerosis. *J Neuropathol Exp Neurol* 73: 702–713
  62. De Winter F, Vo T, Stam FJ, Wisman LA, Bar PR, Niclou SP, van Muiswinkel FL, Verhaagen J (2006) The expression of the chemorepellent Semaphorin 3A is selectively induced in terminal Schwann cells of a subset of neuromuscular synapses that display limited anatomical plasticity and enhanced vulnerability in motor neuron disease. *Mol Cell Neurosci* 32: 102–117
  63. Demyanenko GP, Mohan V, Zhang X, Brennaman LH, Dharbal KE, Tran TS, Manis PB, Maness PF (2014) Neural cell adhesion molecule NrCAM regulates Semaphorin 3F-induced dendritic spine remodeling. *J Neurosci* 34: 11274–11287
  64. Schwarting GA, Kostek C, Ahmad N, Dibble C, Pays L, Puschel AW (2000) Semaphorin 3A is required for guidance of olfactory axons in mice. *J Neurosci* 20: 7691–7697
  65. Friedel RH, Plump A, Lu X, Spilker K, Jolicoeur C, Wong K, Venkatesh TR, Yaron A, Hynes M, Chen B et al (2005) Gene targeting using a promoterless gene trap vector (“targeted trapping”) is an efficient method to mutate a large fraction of genes. *Proc Natl Acad Sci USA* 102: 13188–13193
  66. Pozas E, Pascual M, Nguyen Ba-Charvet KT, Guijarro P, Sotelo C, Chedotal A, Del Rio JA, Soriano E (2001) Age-dependent effects of secreted Semaphorins 3A, 3F, and 3E on developing hippocampal axons: *in vitro* effects and phenotype of Semaphorin 3A (-/-) mice. *Mol Cell Neurosci* 18: 26–43
  67. Schwarz Q, Waimey KE, Golding M, Takamatsu H, Kumanogoh A, Fujisawa H, Cheng HJ, Ruhrberg C (2008) Plexin A3 and plexin A4 convey semaphorin signals during facial nerve development. *Dev Biol* 324: 1–9



68. Bretin S, Reibel S, Charrier E, Maus-Moatti M, Auvergnon N, Thevenoux A, Glowinski J, Rogemond V, Premont J, Honnorat J et al (2005) Differential expression of CRMP1, CRMP2A, CRMP2B, and CRMP5 in axons or dendrites of distinct neurons in the mouse brain. *J Comp Neurol* 486: 1–17
69. Niisato E, Nagai J, Yamashita N, Abe T, Kiyonari H, Goshima Y, Ohshima T (2012) CRMP4 suppresses apical dendrite bifurcation of CA1 pyramidal neurons in the mouse hippocampus. *Dev Neurobiol* 72: 1447–1457
70. Yamane M, Yamashita N, Hida T, Kamiya Y, Nakamura F, Kolattukudy P, Goshima Y (2017) A functional coupling between CRMP1 and Nav1.7 for retrograde propagation of Semaphorin3A signaling. *J Cell Sci* 130: 1393–1403
71. Giger RJ, Cloutier JF, Sahay A, Prinjha RK, Levensgood DV, Moore SE, Pickering S, Simmons D, Rastan S, Walsh FS et al (2000) Neuropilin-2 is required *in vivo* for selective axon guidance responses to secreted semaphorins. *Neuron* 25: 29–41
72. Ip JP, Fu AK, Ip NY (2014) CRMP2: functional roles in neural development and therapeutic potential in neurological diseases. *Neuroscientist* 20: 589–598
73. Tobe BT, Crain AM, Winquist AM, Calabrese B, Makihara H, Zhao WN, Lalonde J, Nakamura H, Konopaske G, Sidor M et al (2017) Probing the lithium-response pathway in hiPSCs implicates the phosphoregulatory set-point for a cytoskeletal modulator in bipolar pathogenesis. *Proc Natl Acad Sci USA* 114: E4462–E4471
74. Dominguez-Iturza N, Lo AC, Shah D, Armendariz M, Vannelli A, Mercaldo V, Trusel M, Li KW, Gastaldo D, Santos AR et al (2019) The autism- and schizophrenia-associated protein CYFIP1 regulates bilateral brain connectivity and behaviour. *Nat Commun* 10: 3454
75. Silva AI, Haddon JE, Ahmed Syed Y, Trent S, Lin TE, Patel Y, Carter J, Haan N, Honey RC, Humby T et al (2019) Cyfip1 haploinsufficient rats show white matter changes, myelin thinning, abnormal oligodendrocytes and behavioural inflexibility. *Nat Commun* 10: 3455
76. Liu X, Malenfant P, Reesor C, Lee A, Hudson ML, Harvard C, Qiao Y, Persico AM, Cohen IL, Chudley AE et al (2011) 2p15-p16.1 microdeletion syndrome: molecular characterization and association of the OTX1 and XPO1 genes with autism spectrum disorders. *Eur J Hum Genet* 19: 1264–1270
77. Weimann JM, Zhang YA, Levin ME, Devine WP, Brulet P, McConnell SK (1999) Cortical neurons require Otx1 for the refinement of exuberant axonal projections to subcortical targets. *Neuron* 24: 819–831
78. Li Z, Jagadapillai R, Gozal E, Barnes G (2019) Deletion of semaphorin 3F in interneurons is associated with decreased GABAergic neurons, autism-like behavior, and increased oxidative stress cascades. *Mol Neurobiol* 56: 5520–5538
79. Degano AL, Pasterkamp RJ, Ronnett GV (2009) McCP2 deficiency disrupts axonal guidance, fasciculation, and targeting by altering Semaphorin 3F function. *Mol Cell Neurosci* 42: 243–254
80. Cermak T, Doyle EL, Christian M, Wang L, Zhang Y, Schmidt C, Baller JA, Somia NV, Bogdanove AJ, Voytas DF (2011) Efficient design and assembly of custom TALEN and other TAL effector-based constructs for DNA targeting. *Nucleic Acids Res* 39: e82
81. Doyle EL, Booher NJ, Standage DS, Voytas DF, Brendel VP, Vandyk JK, Bogdanove AJ (2012) TAL Effector-Nucleotide Targeter (TALE-NT) 2.0: tools for TAL effector design and target prediction. *Nucleic Acids Res* 40: W117–W122
82. Kasperek P, Krausova M, Haneckova R, Kriz V, Zbodakova O, Korinek V, Sedlacek R (2014) Efficient gene targeting of the Rosa26 locus in mouse zygotes using TALE nucleases. *FEBS Lett* 588: 3982–3988
83. Magiera MM, Bodakuntla S, Ziak J, Lacomme S, Marques Sousa P, Leboucher S, Hausrat TJ, Bosc C, Andrieux A, Kneussel M et al (2018) Excessive tubulin polyglutamylation causes neurodegeneration and perturbs neuronal transport. *EMBO J* 37: e100440
84. Sherazee N, Alvarez VA (2013) DiOlistics: delivery of fluorescent dyes into cells. *Methods Mol Biol* 940: 391–400
85. Haddad-Tovoli R, Szabo NE, Zhou X, Alvarez-Bolado G (2013) Genetic manipulation of the mouse developing hypothalamus through *in utero* electroporation. *J Vis Exp* e50412
86. Ionescu A, Zahavi EE, Gradus T, Ben-Yaakov K, Perlson E (2016) Compartmental microfluidic system for studying muscle-neuron communication and neuromuscular junction maintenance. *Eur J Cell Biol* 95: 69–88
87. Kleele T, Marinkovic P, Williams PR, Stern S, Weigand EE, Engerer P, Naumann R, Hartmann J, Karl RM, Bradke F et al (2014) An assay to image neuronal microtubule dynamics in mice. *Nat Commun* 5: 4827
88. Brill MS, Marinkovic P, Misgeld T (2013) Sequential photo-bleaching to delineate single Schwann cells at the neuromuscular junction. *J Vis Exp* e4460
89. Marinkovic P, Godinho L, Misgeld T (2015) Imaging acute neuromuscular explants from Thy1 mouse lines. *Cold Spring Harb Protoc* 2015: pdb prot087692
90. Kerschensteiner M, Reuter MS, Lichtman JW, Misgeld T (2008) *Ex vivo* imaging of motor axon dynamics in murine triangularis sterni explants. *Nat Protoc* 3: 1645–1653
91. Schindelin J, Arganda-Carreras I, Frise E, Kaynig V, Longair M, Pietzsch T, Preibisch S, Rueden C, Saalfeld S, Schmid B et al (2012) Fiji: an open-source platform for biological-image analysis. *Nat Methods* 9: 676–682
92. Bures J, Fenton AA, Kaminsky Y, Zinyuk L (1997) Place cells and place navigation. *Proc Natl Acad Sci USA* 94: 343–350
93. Burghardt NS, Park EH, Hen R, Fenton AA (2012) Adult-born hippocampal neurons promote cognitive flexibility in mice. *Hippocampus* 22: 1795–1808
94. Stuchlik A, Petrasek T, Prokopova I, Holubova K, Hatalova H, Vales K, Kubik S, Dockery C, Wesierska M (2013) Place avoidance tasks as tools in the behavioral neuroscience of learning and memory. *Physiol Res* 62 (Suppl 1): S1–S19
95. D'Hooge R, De Deyn PP (2001) Applications of the Morris water maze in the study of learning and memory. *Brain Res Brain Res Rev* 36: 60–90
96. Wesierska M, Dockery C, Fenton AA (2005) Beyond memory, navigation, and inhibition: behavioral evidence for hippocampus-dependent cognitive coordination in the rat. *J Neurosci* 25: 2413–2419
97. Bahnik Š (2014) *Carousel Maze Manager (Version 0.4.0)* Software. Retrieved from [https://github.com/bahniks/CM\\_Manager\\_0\\_4\\_0](https://github.com/bahniks/CM_Manager_0_4_0)